Thesis- Masters of Science

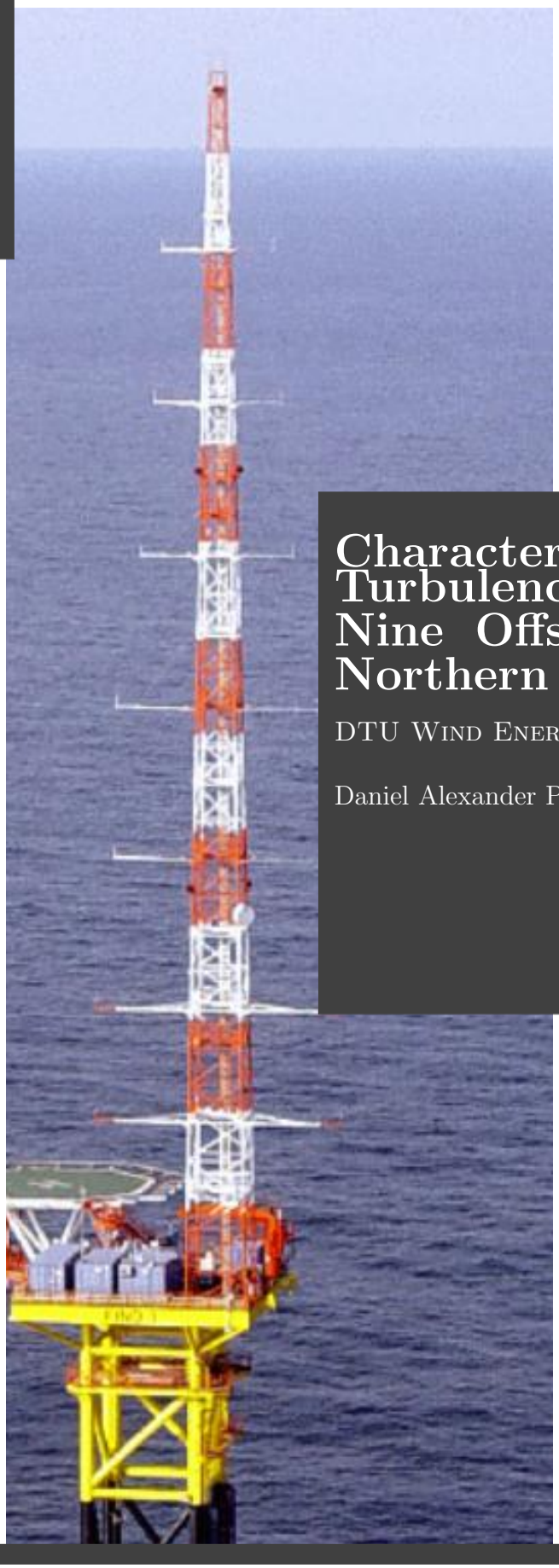

Characterization of Ambient Offshore Turbulence Intensity from Analysis of Nine Offshore Meteorological Masts in Northern Europe

DTU Wind Energy Master Thesis M-0056

Daniel Alexander Pollak

8/3/2014

DONG energy

EWEM TU Delft Delft University of Technology DTU CARL VON OSSIETZKY universität OLDENBURG NTNU European Commission ERASMUS MUNDUS

European Wind Energy Masters Program - EWEM- Wind Physics Track

Characterization of Ambient Offshore Turbulence Intensity from Analysis of Nine Offshore Meteorological Masts in Northern Europe

DTU Wind Energy Master Thesis M-0056

Master of Science Thesis

For obtaining a Masters of Science in Wind Energy Engineering at the Technical University of Denmark and in Engineering Physics (Wind Physics focus) at the University of Oldenburg (Germany)

Daniel Alexander Pollak

8/3/2014

European Wind Energy Masters Program - EWEM
DTU - Technical University of Denmark
UO - University of Oldenburg, Germany

European Wind Energy Masters Program - EWEM
Of
Wind Physics Track

The undersigned hereby certify that they have read and recommend to the European Wind Energy Masters Program - EWEM , acceptance of the thesis titled **"Characterization of Ambient Offshore Turbulence Intensity from Analysis of Nine Offshore Meteorological Masts in Northern Europe"** by **Daniel Alexander Pollak** in fulfillment of the requirements for the dual **Masters of Science** degrees.

Dated: 8/3/2014

Supervisor: _____
Rozenn Wagner of DTU -Risø

Supervisor: _____
Martin Kuhn of UO

Reader: _____
Ameya Sathe of DTU -Risø

Reader: _____
Detlev Heinemann of UO

Reader: _____
Nicolai Nygaard of DONG Energy

Reader: _____
Miriam Jimemez of DONG Energy

Abstract

Offshore wind offers a vast and inexhaustible energy source with minimal greenhouse gas emissions. To maximize offshore wind energy generation it is critical to have a comprehensive understanding of all atmospheric and oceanic parameters that could affect any part of the wind turbine system, prime of which is ambient turbulence intensity (TI); a measure of the degree of fluctuations within the three dimensional wind field (σ_U, wind speed standard deviation). The research undertaken in this thesis is helping to unravel the complex and intricate dependencies of offshore ambient turbulence intensity, specifically on wind speed($\overline{U}$), height(z), wind direction(θ) and fetch. To probe into these characteristics, data from nine meteorological towers located between 7 and 111 kilometers offshore in the Irish and North Seas are investigated. This study is pioneering in that never before has data from this many meteorological masts been examined simultaneously for this purpose. In preparation for analysis, some basic filters were applied and mast shadow effects were recognized and corrected for.

The average turbulence intensity at 50m ranged from 6.32% to 7.44%, with TI decreasing with distance from the coast until 40-50 kilometers after which TI interestingly began to increase again. In fact, when examining TI as a function of wind direction, TI was largest in sectors with fetch greater than 100-200 km and least in land sectors. Additional factors that influenced the TI - θ dependency, especially in the sites with reduced fetch, were coastal orientation, inland topography and atmospheric stability.

Dissimilar to the relationships indicated in the IEC 61400-3 standards, σ_U is not linear, and TI not monotonically decreasing as a function of wind speed. Instead there is a height-dependent wind speed bin, between 8-14 m/s, where the transition from thermally- to mechanically-generated turbulence occurs. When comparing plots of σ_U and TI versus $\overline{U}$ for all of the masts at various heights, it can be seen, remarkably so, that seven of the masts show near ubiquitous agreement. This implies that when averaging over all wind directions, these relationships are universal throughout Northern Europe. This is not the case for the remaining two masts: M8 & M2. The deviation at M8 is a result of the narrow sector analyzed while at M2, the deviation is suspected to be a result of climate variability or systematic errors.

The vertical profiles of σ_U and TI are highly susceptible to different wind regimes. At low wind speeds σ_U and TI are nearly uniform with height as a result of the well-mixed nature of thermally-driven turbulence. At high wind speeds a strong, nearly linear, decrease with height is realized resulting from the air-sea interface that generates the mechanically-driven turbulence. Strong similarities exist in these vertical profiles and directional dependency plots between masts within similar geographic regions.

Acknowledgements

I would first like to thank my advisers at DONG Energy, Nicolai Nygaard and Miriam Marchante Jimmez for helping me throughout the thesis and for providing the opportunity to work with this fantastic set of data. It has been an honor to work on my thesis within the Wind Assessment & Layout team at DONG and it has been a pleasure getting to know each and every one of you. Next I would like to thank my university advisers Ameya Sathe, Rozenn Wagner, and Detlev Heinemann for their insight into my project and help in navigating the logistics of the two degree-awarding universities, the Technical University of Denmark and the University of Oldenburg. I would also like to thank Linda Gaffel and Zarah Glaap from the EWEM office for their moral support and help in navigating requirements between both universities. Besides these individuals, there are many others who have made my experience in Denmark and Germany a delightful one, and to them I say tak!

Contents

Chapter 1

Introduction

1.1 Motivation

Wind offers an inexhaustible local energy source with minimal greenhouse gas emissions and is a resource that is vast, free and is overhead, ready for exploitation. Energy demand is expected to increase by 56% between 2010 and 2040 [1]. Given the finite quantity of conventional fossil fuels in tandem with the current and amplifying effect of anthropogenic climate change caused by burning of these fuels, it is imperative that wind energy be one of a growing portfolio of renewable energy sources that can grow to fill these energy voids.

Offshore wind energy generation has grown substantially over the last few years expanding from a cumulative installed capacity of 2073 MegaWatts (MW) in 2009 to 6562 MW in 2013, a 316% increase [2]. It is predicted that the industry will continue expanding at a fast rate as many countries are developing offshore wind farms to meet their growing energy needs with the least amount of emitted carbon [3].

The continued interest and growth in the offshore wind energy industry can be attributed to the numerous factors that make it more advantageous over onshore wind energy. Some of these factors include:

- Expansive regions with fewer siting restrictions from noise and visual pollution. Additionally, many of the best places onshore to put turbines have been exhausted.
- Higher and more persistent wind speeds that result in higher energy densities (recall that generated power is a function of the wind speed cubed). Most wind turbines reach rated power at around 12 m/s [4], so if mean annual wind speeds are higher offshore, they are likely to be much closer to this value yielding higher capacity factors. These capacity factors are higher than onshore locations, except for mountainous areas with large orographic speed-up effects.
- Lower turbulence intensity which allows for the turbines to harvest the energy more efficiently. Additionally, fatigue loads on the entire wind turbine structure are re-

duced [5][6], potentially saving money by reduced maintenance costs and through expansion of the turbine lifetime.

- Proximity of the offshore regions to the large electrical loads of cities. This is especially important because as according to the United Nations, half of the global population lives within 60 km or 37 miles from the coast. [7]
- Shallower surface layer depths in the marine atmospheric boundary layer (MABL) versus the onshore atmospheric boundary layer (ABL) and thus less wind shear over the rotor plane of the turbine. As a result, higher wind speeds can be reached at lower heights and less fatigue will be experienced on the structure.

Despite these advantages, some challenges remain that are hindering offshore wind energy development. One of particular interest is the incomplete understanding of offshore wind characteristics. This led the International Electrotechnical Commission (IEC) to establish its offshore wind turbine design standards (IEC 61400-3 [8]) based on the onshore standards (IEC 61400-1 [9]) despite these standards not being representative of the offshore wind climate.

Many studies have questioned the suitability of the onshore wind model prescribed by the IEC for offshore conditions and provided insight on how to adjust the model so that it is more fitting to reality [10][11][12]. This thesis does not focus on these models, but instead provides a large scale analysis of observational data that can in later studies be compared with, and be used to improve these models of ambient offshore turbulence characteristics.

The main parameter under analysis in this thesis is the turbulence intensity which is defined as the average fluctuations of the horizontal wind speed, or standard deviation (σ_U)) during a 10-minute period divided by the mean wind speed ($\overline{U}$) for the same period:

$$TI = \frac{\sigma_U}{\overline{U}} \tag{1.1}$$

Having a clear understanding of the ambient offshore turbulence intensity is imperative for wind energy companies to have in order to be competitive and design robust wind turbine structures that are optimized for the localized climate. Complete understanding of TI assists in the estimation of fatigue loads on wind turbine structures and thus indicates the necessary design. Additionally, this understanding can help improve wind turbine wake models because they use ambient turbulence intensity as an input. This in turn would help improve and optimize the spacing and layout of future wind farms.

1.2 A Groundbreaking Opportunity

This thesis work is groundbreaking and unique because never before has such a large dataset of high quality offshore meteorological mast observations been examined together for the purpose of characterizing turbulence characteristics in the offshore environment. Additionally, other than Turk et al[11], most of the previous studies were based on data from coastal sites (within 40 km of coast) and on masts with limited observational heights

and vertical resolution. The vast amount of data available for analysis in this thesis provides a fantastic opportunity to examine the various dependencies of turbulence intensity and its deriving components.

This work herein examines nine different meteorological masts with great vertical data coverage and in locations that vary from as close as 7 kilometers (km) from the coast to as far as 110 km. All of the sites are in the North Sea and Irish Sea, helping to paint a picture of these characteristics throughout the offshore areas of Northern Europe.

1.3 Thesis Research Questions

The offshore wind climate is dictated by the conditions in the marine atmospheric boundary layer (MABL), discussed in Chapter 2. There are a myriad of factors and intricate relationships that influence the nature of turbulence intensity in the MABL including wind speed, wind direction, fetch, height, the coastal discontinuity, humidity fluxes, seasons, time of day and climatic variability just to name a few.

It was not possible to examine all of these in the short time frame of this thesis, so the specific research questions within this thesis are as follows:

- How do the wind speed standard deviation (σ_U) and ambient offshore turbulence intensity (TI) vary with wind speed($\overline{U}$), height (z) and wind direction (θ) at the nine different sites?
- Likewise, how do the standard deviations of σ_U (σ_{σ_U}) and TI (σ_{TI}) vary with these same parameters.
- Are these relationships universal, regional or strictly site dependent?
- How do the found trends compare with previous studies at other locations and the IEC 61400-3 standards for offshore wind turbine design?
- How do these relationships vary with fetch, or proximity to the coast?

The background information required to understand the material presented when answering these questions is provided in Chapter 2. Chapter 3 presents information on the various sites and data used, and additionally goes over the quality control measures that were adopted in order to use data of the highest quality in the analysis. Chapter 4 presents a comprehensive view of the results while Chapter 5 summarizes the key findings and suggests future work. In addition to the plots and figures that appear within the main body of text, numerous appendices are appended to the thesis that give readers the opportunity to examine results from each of the individual masts and heights.

Chapter 2

The Marine Atmospheric Boundary Layer (MABL) and IEC Standards

2.1 Characteristic of Wind

The characteristics of wind are defined by the physics behind it which occur on a variety of space and time scales. Broadly, wind is generated by pressure differences derived from differential heating of the Earth's surface by the sun. The resulting large scale Polar, Hadley and Ferrel atmospheric cells then in turn drive synoptic weather fronts that drive the wind and weather conditions in a region. The mid-latitudes, which includes Northern Europe, are dominated by Westerly winds westward moving synoptic weather systems. On the smaller mesoscale, land-sea breezes and mountain-valley density currents can lead to significant changes in the wind climate. These various phenomena vary over periods of hours, days and seasons [4].

2.2 Atmospheric Boundary Layer

The atmospheric boundary layer (ABL) is the lowest part of the atmosphere and consequently the part that is in contact with, and influenced by the Earth's surface. The bottom 10% of the ABL is called the surface or Prandtl layer and is the region where wind speed increases the most rapidly due to the no-slip conditions at the surface. As a result, it is also the layer in which wind shear, or the difference in wind speed with height, is the largest. The remaining 90% is called the Ekman layer and is strongly influenced by the Coriolis force which causes a turning of the wind with height. Winds in this region still increase with height but not nearly as rapidly as within the surface layer; therefore there is less vertical wind shear. The depth of the boundary layer can be as low as 100 meters at night, but due to strong convection from radiative heating of the surface during the day, it can reach depths of 2 to 3 kilometers [13][14].

2.3 Marine Atmopsheric Boundary Layer (MABL) and Monin-Obukhov Similarity Theory

The marine atmospheric boundary layer (MABL) denotes the boundary layer over water surfaces. While similar to the ABL, there are some unique differences, prime of which is the dynamic nature of water. Unlike on land where the wind velocity at the land-atmosphere interface must be zero, the wind velocity at the ocean-atmospheric interface can vary as the water surface moves in three dimensions under the influence of this wind forcing. A diagram of the layers of the MABL is provided in figure 2.1, taken from Emeis' Wind Energy Meteorology textbook [14].

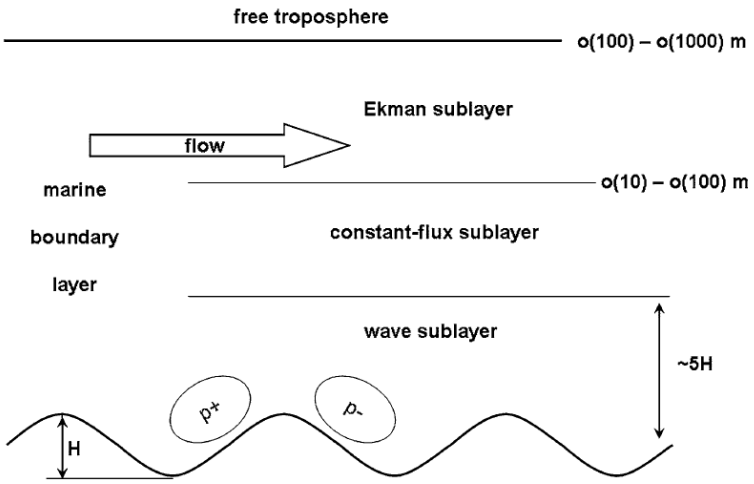

Figure 2.1: *A representation of the layers in the marine atmospheric boundary layer. Modern offshore wind farms have blades that can reach up to 200 m in height, into the Ekman sublayer. This figure was taken from the textbook Wind Energy Meteorology [14]*

The lowest layer is the wave sublayer and is the layer in direct contact with the waves, where the mechanical generation of turbulence occurs. As with the ABL, the layer above is the constant flux or Prandtl layer and is the region where wind speed increases the most rapidly with height. The depth of this layer is often much shallower than on land; as low as 10 meters (m) in stable conditions and with low to moderate wind speeds [13][14]. This characteristic is highly advantageous for the building of offshore wind farms because higher wind speeds can be achieved at lower heights.

As is inferred by its name, the constant flux layer is characterized by momentum and heat fluxes that are nearly constant with height, an assumption upon which the Monin-Obukhov theory is based. While the theory was developed through measurements onshore, it is believed to be applicable in marine environments [15]. With the assumptions of homogeneous and stationary flow, the theory predicts the wind profile in the constant flux layer to be log-linear giving the wind speed U at any height z as [16]:

$$U(z) = \frac{u_*}{\kappa}[ln(\frac{z}{z_0}) - \Psi_m(\frac{z}{L})] \tag{2.1}$$

where u_* is the friction velocity, z_0 is the roughness length, L is the Obukhov length, κ is the von Karman constant taken as 0.4 and lastly where Ψ is a universal stability function. This equation reveals the that vertical wind profile in the MABL is dependent on the roughness length and the Obukhov length.

The Obukhov length, a proxy parameter for atmospheric stability, can be derived through three methods, namely the sonic, gradient and bulk methods [16]. Because this thesis does not examine stability, these various methods are not discussed. In neutral conditions the Obukhov length approaches 0 and the second term in equation 2.1 drops out, resulting in the logarithmic wind profile, as is discussed in the next section.

2.4 Wind Shear

Wind shear describes the change in wind speed with height and is a constant source of cyclic loading and thus fatigue on all components of the wind turbine [5][17]. The larger the wind shear, the larger the loading and fatigue on the turbine. Wind shear is calculated by extrapolating measurements from lower heights to higher heights via the logarithmic law equation:

$$U(z) = \frac{u_*}{\kappa}[log(\frac{z}{z_0})] \tag{2.2}$$

Additionally it can be given by the power law:

$$U(z) = U_{ref}(\frac{z}{z_{ref}})^{\alpha} \tag{2.3}$$

where alpha is the shear or power law coefficient. The IEC standards dictate a constant coefficient of 0.2 for onshore turbines and 0.14 for offshore turbines [8][9].

Often times, the logarithmic wind profile is used when extrapolating measurements vertically. This proves to be problematic given that the profile is only valid in near-neutral conditions. As will be discussed in the next section, near-neutral conditions are not extremely commonplace in the offshore environment [18][19][20].

2.5 Atmospheric Stability in the MABL

One of the biggest differences between conditions onshore and offshore is the constant existence of upward latent heat fluxes offshore[21]. These latent heat fluxes when combined with the stability driven sensible heat fluxes enhance the presence of non-neutral stability in offshore environments; leading to either very stable or very unstable conditions.

Due to the large heat capacity of water, the sea surface temperature (SST) does not vary significantly diurnally and generally lags behind seasonal changes in air temperature by about a month [13][14]. Since atmospheric stability offshore depends on the difference in temperature between the sea surface and the overlying air, the seasons that see the most profound non-neutral stability are the autumn and spring.

In the spring, when the wind blows offshore, the daytime air temperature of the land is often much higher than that of the sea, often leading to stable conditions and a decoupling of the flow at the surface and aloft (inversion). Conversely, in the autumn cooler air temperatures over land are advected over the warmer water surface, leading to prevalence of unstable conditions [18][19][22][23].

2.6 Sea Surface Roughness

In contrast to land surfaces where the roughness length is assumed constant, offshore the sea surface roughness is dependent on wind speed. Specifically the roughness is governed by the exchange of momentum between wind and waves which depends on factors such as wind speed, water depth and distance to shore [24]. Larger wind speeds will generate larger waves which will in turn increase the roughness. This being said, the typical roughness lengths offshore of below one millimeter are profoundly lower than those onshore which are on the order of centimeters to meters.

As was indicated in equation 2.3 and in the logarithmic law, roughness is the most influential term in dictating the wind speed at various heights, when assuming neutral stability. The roughness also strongly impacts the turbulence intensity as rougher surfaces will generate more turbulence. This is the prime reason why turbulence intensity is lower offshore than onshore.

At low wind speeds (less than 3 m/s) the sea surface is considered to be aerodyanmically smooth and an inverse function of the friction velocity. But as the wind speed increases, the sea surface roughness increases [25]. Under these special offshore conditions, Charnock proposed the sea surface roughness length to be proportional to the square of the friction velocity as given by the Charnock equation [26]:

$$z_0 = \alpha \frac{u_*^2}{g} \tag{2.4}$$

where α is the Charnock parameter. With this relation, Charnock assumed that the winds were blowing steadily and long enough for the wave-wind interface to be in complete equilibrium, therefore independent of fetch. There has been research done that indicates otherwise and proposes different parameterizations for the Charnock parameter and equation. A variety of different values for α have been proposed, ranging from 0.016 for moderately rough sea surfaces and 0.072 fir a very rough surface [14][27].

Wave age and height has been shown [10][33] to be very influential in the relationship between turbulence intensity and wind direction as a result of the different roughness lengths associated with different wave ages. Wave age describes the interaction between the wind and wave field. Young waves are wind-driven waves where the wind speed is larger than the wave phase speed. Old waves are those that are present once the wind has died down, commonly known as swell. In the case of swell, it is possible that wave's phase speed is larger than the wind speed, leading the surface wind to be driven by the waves. This therefore causes an upward flux of momentum leading to the failure of Monin Obukhov theory, which assumes constant fluxes [14].

2.7 Fetch & Proximity to Coast

Fetch and the coastal discontinuity are discussed throughout this thesis. Fetch is defined as the distance to the coastline in a specific wind direction sector. Because the roughness lengths onshore and offshore are very different, this difference in roughness creates an internal boundary layer where the transition from the ABL to MABL occurs. Within this coastal discontinuity zone, turbulence intensity decreases with increasing fetch due to the significant reduction in roughness. In previous studies this decrease has been found to level out to a nearly constant value after about 20-40 km from the coast [28][29][30].

Although these land effects are felt mostly within 15-20 km from the coast, they can still be detected at further distances, especially under very stable conditions where mixing is suppressed [28][29][30]. [30] indicated that this coastal discontinuity could be felt as far as 40km from the coast while [31] and [32] stated that this effect could influence the flow at distances of up to 100-200 km.

Even though this thesis does not go into the depths of examining stability and waves, due to the lack of such data at all of the sites, it is important to keep these concepts in mind when progressing through the thesis. The next section provides background on the IEC standards in which the data presented here are compared to.

2.8 IEC 61400-3 Offshore Wind Energy Standards

It is common knowledge within the wind energy meteorology community that the International Electrotechnical Commission's (IEC) 61400-3 standards and recommendations for offshore wind turbines are not representative for such locations, as they are simply the same onshore standards, save a few minor changes, just now applied offshore. These standards outline the minimum design requirements for offshore wind turbines and use the normal turbulence model as its basis [8][9].

In IEC 61400-3, σ_U is considered to be unchanging with height and log-normally distributed within a specific wind speed bin. For σ_U in a specific wind speed bin, the IEC 61400-3 defines it as a linear function of wind speed described by the equation:

$$\overline{\sigma} = (\beta_1 I_{ref})V + \beta_0 I_{ref} \tag{2.5}$$

where $\beta_1 I_{ref}$=0.75 & $\beta_1 I_{ref}$=3.75 $\frac{m}{s}$. As will be profoundly evident in the result of this thesis, σ_U is not a linear function of wind speed (Refer to section 4.1.1)

The standard deviation of σ_U is denoted here as σ_{σ_U} and is considered constant with wind speed. This is also not found in the real data (see Section 4.1.2). Its equation is as follows:

$$\sigma_{\sigma_U} = (1.44\frac{m}{s})I_{ref} \tag{2.6}$$

In both of the above equations, the variable I_{ref} represents a reference turbulence intensity for a wind speed of 15 m/s at wind turbine hub height. Within the IEC 61400-3, three wind speed classes are designated:

- $I_{ref} = 0.16$ (Class A)
- $I_{ref} = 0.14$ (Class B)
- $I_{ref} = 0.12$ (Class C)

where higher numbers indicate higher turbulence. To characterize the turbulence characteristics at a site the IEC recommends using the 90th percentile of TI so that some extent of the more extreme winds are incorporated into the standards. The 90th percentile IEC reference turbulence intensity (TI_{IEC}) is written as:

$$TI_{IEC} = I_{ref}(0.75V + \frac{5.6\frac{m}{s}}{V}) \tag{2.7}$$

In section 4.1.3, the TI_{IEC} lines for Class A, B, and C are plotted alongside the observational data for the 9 sites. As will be seen, the real measurements do not follow the monotonically decreasing nature of the above equation and begin to deviate after about speeds of 8-14 m/s (value depends on height). This is due to the influence of growing wave heights, and thus roughness, at higher wind speeds. [8][9]

Chapter 3

Data Quality Control

3.1 Overview of Data

3.1.1 Locations

Data from nine met masts in the Irish Sea and North Sea are analyzed in this research. The locations of these masts are displayed on the map below (Figure 3.1).

For easy identification and labeling, each of the masts was given a two or three letter abbreviation in addition to a specific color. In all forthcoming figures and plots these abbreviations and colors are used when representing their specific mast. They are as follows:

- F1 - [BLACK] FINO1 (North Sea)
- F3 - [GREEN] FINO3 (North Sea)
- HO - [RED] Hornsea (North Sea)
- HU - [PINK] Humber Gateway (North Sea)
- LA - [PURPLE] London Array (North Sea)
- M2 - [TURQUOISE] Horns Rev M2 (North Sea)
- M8 - [BLUE] Horns Rev M8 (North Sea)
- SF1 - [YELLOW] Shell Flats 1 (Irish Sea)
- SF2 - [ORANGE] Shell Flats 2 (Irish Sea)

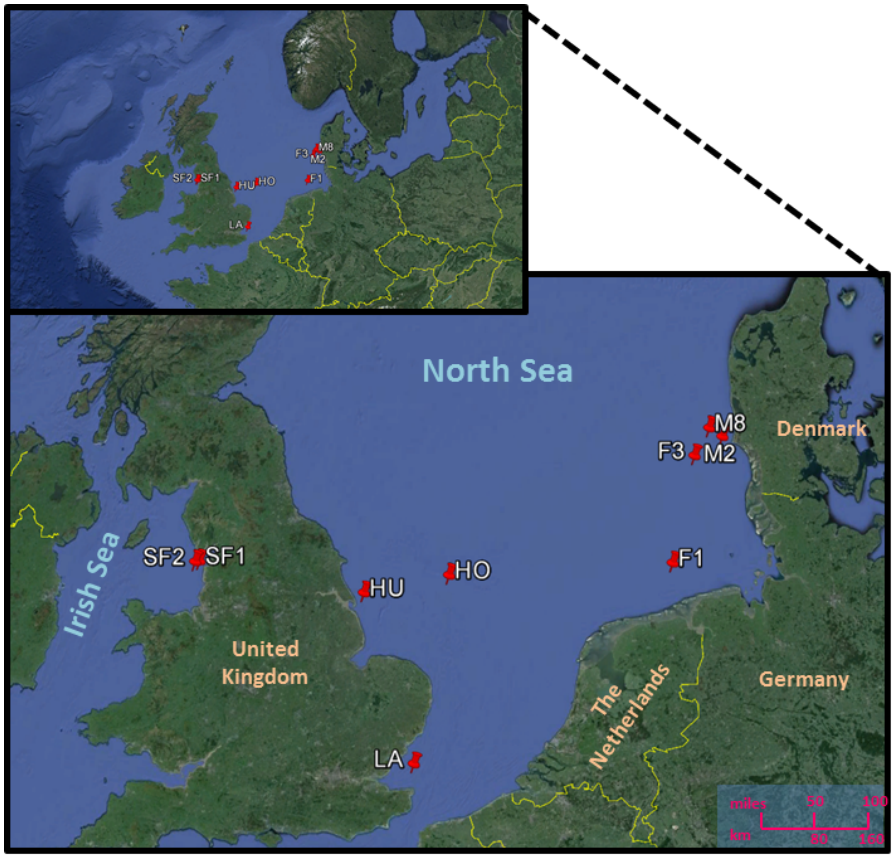

Figure 3.1: *Map of all of the mast locations in the North and Irish Sea (Google Maps)*

3.1.2 Mast Orientations & Instrumentation

A wealth of data were used for the analysis forthcoming in this thesis. Each mast has its own unique features and instrumentation layouts. The metadata include information on the mast structure and boom orientations, the types of instruments and data loggers used to collect data and lastly provides notation of any changes that may have been made over time to the said features. Knowing details of the mast structure and the equipment used is important and could help to tailor analyses between different datasets (some require different filtering criteria). It is critical to know these details to potentially help explicate trends noticed between masts that have no other explanation.

Additionally, not all of the masts listed their measurement heights in the same coordinate system and thus for a few (SF1, SF2, LA) the listed measurement heights had to be converted to height above mean sea level (AMSL). Some were listed in HAT, highest astronomical tide or LAT, lowest astronomical tide.

A list of all of the instrumentation each mast is detailed in appendix A. Mash schematics may also be located in this appendix.

3.1.3 Key Parameters & Measurement Heights

Data from a variety of parameters are available across many heights at each mast. The parameters of prime importance in this research are wind speed ($\overline{U}$), wind speed standard deviation (σ_U), and wind direction (θ) as they are essential in characterizing and deriving turbulence intensity (TI). This includes describing how turbulence intensity varies with wind speed, wind direction, height and fetch for example.

All data has a temporal resolution of 10 minutes where for each 10 minute period the mean wind speed($\overline{U}$), standard deviation of the wind speed (σ_U) and minimum and maximum wind speed are given.

Including all nine masts, there are in total 74 datasets of wind speed and 26 datasets of wind direction, a remarkable amount of offshore measurements. A detailed list of heights in which these parameters are available is summarized in the table in figure 3.2. Note that while all 74 datasets of wind speed are used in this thesis, only one wind direction dataset per mast is used, as signified by the height listed in red (Figure 3.2). The general rule of thumb is to use the highest wind vane observation, though this rule was not used in the case of HO, as is discussed in section 3.2.1.

	Wind Speed (AMSL)	Wind Direction
F1	100^{L}, 90^{s}, 80^{s}, 70^{s}, 60^{s}, 50^{s}, 40^{s}, 33^{s}	90, 80, 70, 60, 50, 40, 33
F3	106^{L}, 90^{tri}, 70^{tri}, 50^{tri}	100, 60
HO	101, 96^{b}, 91^{b}, 86^{b}, 66^{b}, 46^{b}, 26^{b}	94, 83, 63, 43
HU	90^{L}, 88^{tri}, 70^{b}, 52^{b}, 34^{b}	86, 68
LA	82, 80^{o}, 57^{b}, 32^{b}, 20^{b}	78, 29
M2	62, 45^{b},30^{b},15^{b}	60, 43, 28
M8	107^{s}, 97^{s}, 87^{s}, 77^{s}, 67^{s}, 47^{s}, 37^{s}, 27^{s}	105, 65, 35
SF1	87^{L}, 85^{o}, 75^{b}, 55^{b}	83
SF2	57^{L}, 55^{o}, 45^{b}	53

Figure 3.2: *Lists the heights of wind speed and wind direction observations. The wind directions used for the analysis are highlighted in red. The superscripts indicate the type of mast effect correction needed, if needed.*

The five superscripts used in the table represent either the number of observations that are available at each height or indicate that a special sector was used for analysis. In the case of the former, this provides indication of the type of mast shadow correction required and performed. Definitions of the superscripts are as follows:

- *b* - or both, indicates that there are observations on both sides of the mast, requiring a mast shadow correction where the upwind anemometer is used when the other is waked.
- *tri* - signifies that there are three measurements available at this height and thus all three measurements are used for different sectors. No explicit correction is used (Triangular Mast)
- *o* - or one, signifies that there is data from one side of mast. When this anemometer is in wake, a relationship between itself and one of the surrounding heights (already corrected using 'b' method) is determined and used as correction.
- *s* - or sector, means that a hard directional filter was applied. For F1 all of the anemometers are located on the southeast (SE) side of the mast and thus only flow from 0-280 degrees were considered (Figure 3.12). For M8, due to effects of Horns Rev, only the 255-285 degree sector was used. No robust mast shadow correction is possible.
- *L* - or lightning, indicates a top measurement height surrounded or influenced by a lightning rod or cage. These directions are corrected using a relationship between the next height down during periods without this interaction (Chapter 3.5).

The following drawing (figure 3.3) provides example mast structure with examples of all of the superscripts described above except for the triangular mast.

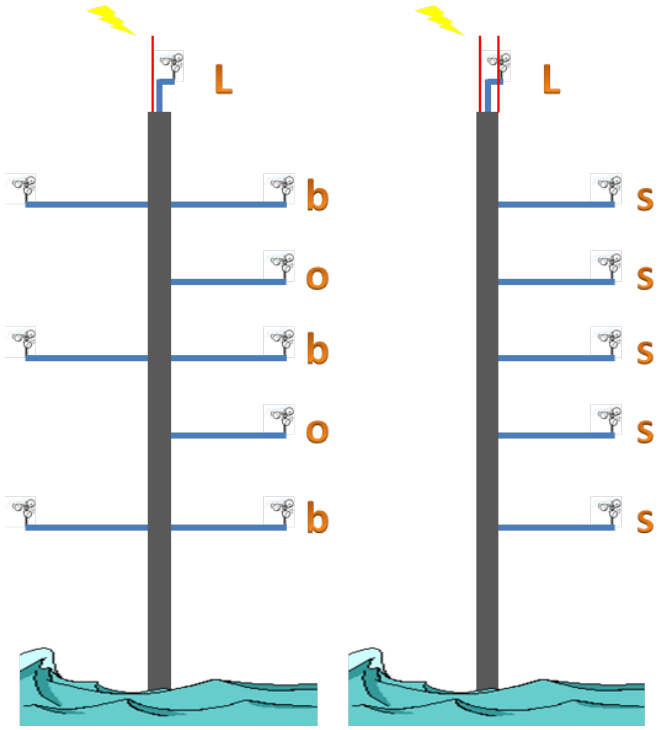

Figure 3.3: *A example mast schematic demonstrating the different orientations and setups as listed above.*

3.1.4 Temporal Availability

All of the data used for analysis are 10 minute averages. The table in Figure 3.4 depicts the start and end dates of measurements for each mast in addition to the total number of years that data was available. Data gaps are included and for this reason the last column displays the percentage of data missing.

	Start Date (Used)	End Date (Used)	Length (years)	% Missing Data
F1	2005-04-01	2009-03-31	4.00	3-10% Missing 20% sector filt
F3	2010-05-01	2013-04-30	4.00	~10%
HO	2012-02-01	2012-10-31	0.75	4-22%
HU	2009-10-20	2011-10-19	1.00	2.51%
LA	2008-12-23	2010-12-13	1.97	0%
M2	1999-05-15	2001-05-14	1.00	1.66%
M8	2011-08-01	2012-07-25	0.98	11% missing 78% sector filt
SF1	2011-08-01	2012-07-31	1.00	0.61%
SF2	2011-08-01	2012-07-31	1.00	0.58%

Figure 3.4: *Start and end dates of data used for analysis along with total time period. The last column quantifies the percentage of this time period with missing data.*

At certain masts and heights the missing data rate was as high as 22%. This is important to keep in mind, especially during speculations on seasonal effects, depending on when the missing data occurred.

A graphical representation of this temporal data availability is also displayed below (Figure 3.5).

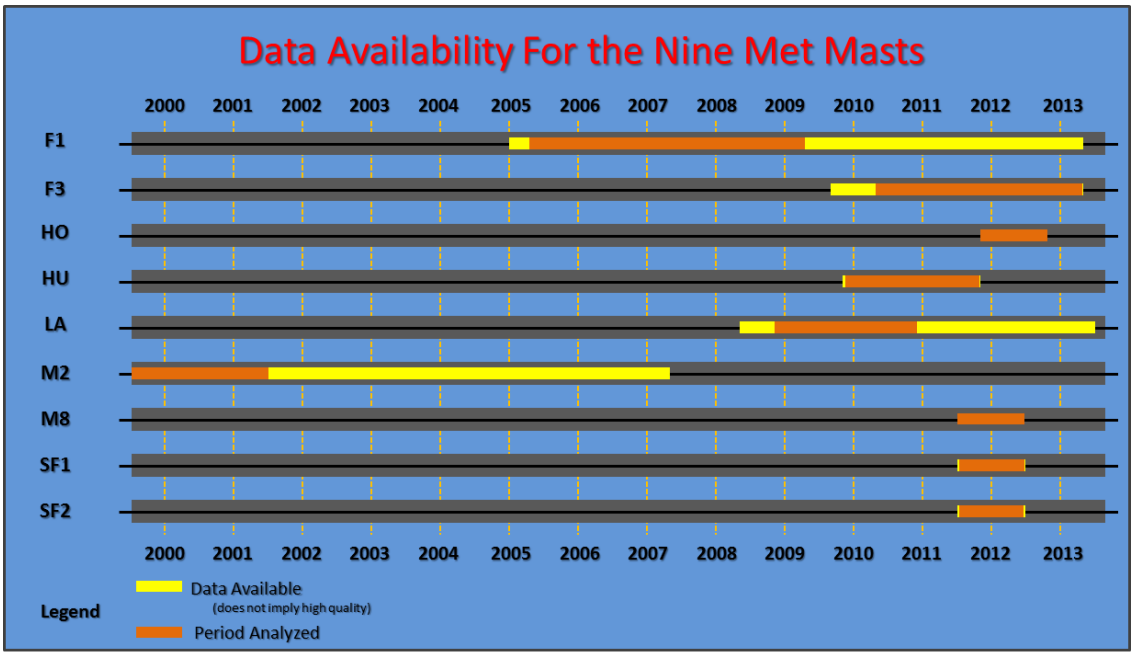

Figure 3.5: *Visual representation of years in which data were collected at each mast. The yellow bar indicates when data was available and the orange represents the time periods used for analysis (as close to an even year)*

As represented in figure 3.5 the yellow bar represents available data, whereas the orange bar indicates the actual periods of analysis. There are two reasons why not all of the available data were used for analysis. The first applies to all of the masts, and is that in order to avoid introduction of seasonal biases, data were selected for analysis in yearly increments (or as close to as possible) [10][18][33]. Note that only 9 months of data at HO were available, with the winter months being those that were missing.

The second reason applies to M2, LA, and F1 in which latter periods of the time series are not selected for analysis due to the building of the Horns Rev 2, London Array and Alpha Ventus wind farms respectively. Because M8 was only in operation after the Horns Rev II wind farm was operational, only the free-stream sector was used for analysis. This research is focused solely on ambient offshore turbulence intensity and thus it is important not to introduce any wake or disturbance effects from the wind turbines themselves.

3.1.5 Vertical Wind Profile & Region Demarcation

The vertical wind profile for each of the masts is plotted (all wind directions included) in figure 3.6 and shows the variety of wind climates present between the masts as seen by the 2 m/s range between the profiles (except M8). Because the data were taken in different years, it is important to note that some of these differences could be due to inter-annual variability in general atmospheric flow and conditions across the region. One of the largest

influences to inter-annual variability in Europe is the North Atlantic Oscillation (NAO) teleconnection. Its fluctuations should be taken into consideration

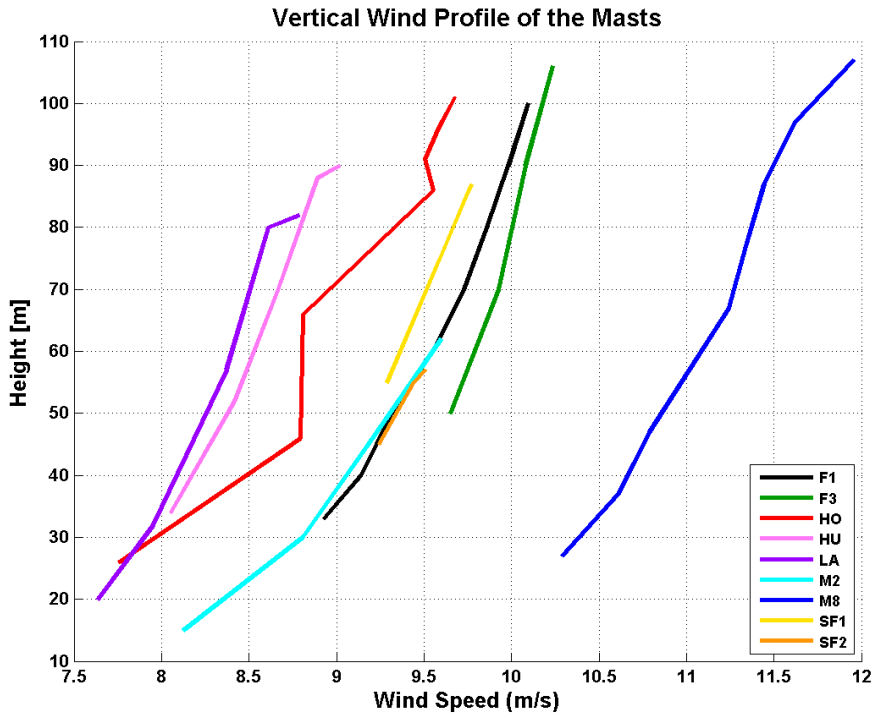

Figure 3.6: *The average vertical wind profile for all of the masts. Note the similarities between the masts within similar geographic areas*

For masts located in similar geographic areas, the profiles have some similarities. It is for this reason that when examining the dependence of turbulence intensity on wind direction (Chapter 4.3) the masts are discussed in four distinct regions:

- North Sea - Far Offshore: greater than 40 km (F1, F3, HO)
- East Coast of the United Kingdom (LA & HU)
- Irish Sea - West Coast of United Kingdom (SF1 & SF2)
- North Sea West of Denmark (F3, M2, M8)

The profiles of LA and HU off the east coast of the UK are very similar, as are the SF1 and SF2 off the west coast of the UK. On the other hand, the far offshore masts are quite varied in their profiles as is visible by the large difference between HO, F1, and F3. HO's slower profile is likely due to the data gap in the winter, when winds are usually at their strongest.

For M2 and F3, which are located about 50 km apart have similar profiles. The profile for M8 is much larger than the others, but can be attributed to the fact that the 30 degree sector used is a solely ocean fetch, therefore higher wind speeds can be expected.

Figure 3.7 displays the vertical wind profile for each of the masts with a logarithmic vertical axis. With the exception of HO, most of the profiles are linear meaning that the logarithmic law approximation of wind speed change with height is a good fit in offshore Northern Europe.

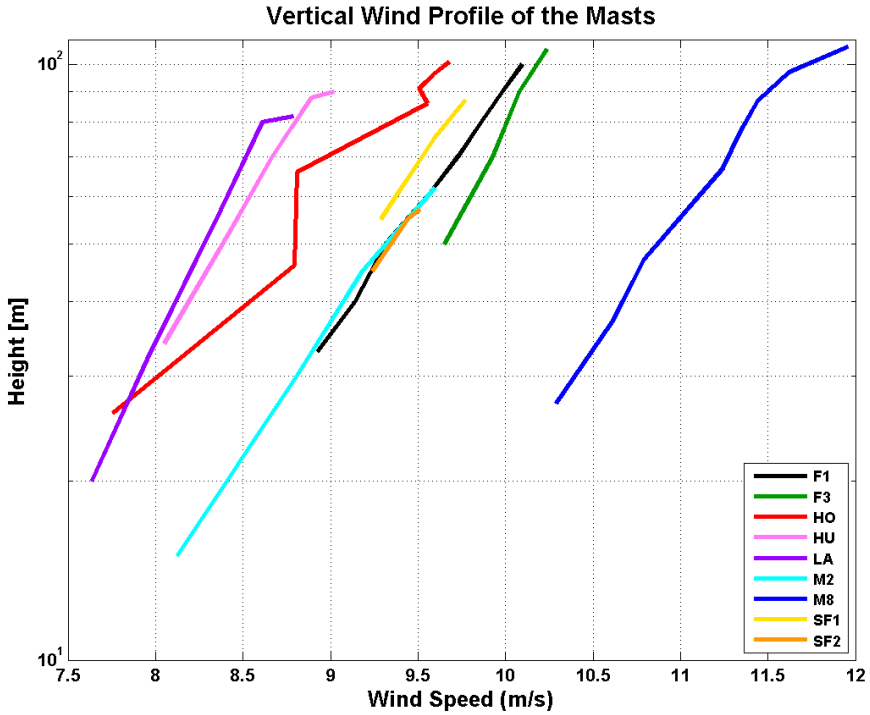

Figure 3.7: *The average vertical wind profile for all of the masts with a semilog height axis*

3.1.6 Proximity to Shore

One of the key differentiable features between the masts is their location and proximity to shore. The meteorological conditions and thus ambient turbulence that is observed at each site could be highly variable depending on three factors:

1. Distance of the closest land (and entire coastline) [km]
2. Bearing of this landmass [degrees]
3. Prevailing wind direction [degrees] ie. prevailing wind from land or sea

Different values of these three factors could dictate the prevailing meteorological regime and help clarify any similarities or differences seen in the forthcoming analysis. The table below in figure 3.8 displays the most critical information with respect to the landform surrounding each site.

Proximity of Land to Masts - Land Sectors Based On Distances									
Mast Name	**HO**	**LA**	**HU**	**F1**	**F3**	**M2**	**M8**	**SF1**	**SF2**
Latitude (deg)	53.88	51.59	53.63	54	55.2	55.52013	55.63179	53.87358	53.857056
Longitude (deg)	1.99	1.39	0.26	6.6	7.2	7.786672	7.514	-3.201028	-3.293194
Nearest Land (km)	**111**	**20**	**7.3**	**40-45**	**67**	**18.6**	**36**	**11**	**15.5**
Bearing to Land (deg)	**204**	**175**	**225 - 275**	**145 - 170**	**54**	**76**	**103**	**62 - 122**	**96**
Fetch < 10 km	X	X	**242 - 290**	X	X	X	X	X	X
Fetch 0 - 25 km	X	**170 - 210**	**184 - 314**	X	X	**59 - 87**	X	**0 - 19 43 - 145 349 - 360**	**65 - 125**
Fetch 0 - 50 km	X	**0 - 4 170 - 360**	**170 - 323**	**130 - 175**	X	**26 - 115**	**53 - 108**	**0 - 172 342 - 360**	**0 - 162 350 - 360**
Fetch 0 - 100 km	X	**0 - 14 100 - 360**	**140 - 337**	**106 - 230**	**36 - 131**	**12 - 161**	**22 - 151**	**0 - 240 280 - 310 335 - 360**	**0 - 240 282 - 312 342 - 360**
Fetch 0 - 200 km	**185 - 290**	**0 - 14 74 - 360**	**136 - 337**	**30 - 235**	**19 - 198**	**10 - 186**	**19 - 156**	Land Within	Land Within
Fetch > 200 km	**0 - 185 290-360**	**14 - 74**	**0 - 136 337 - 360**	**0 - 30 235-360**	**0 - 19 198 - 360**	**0 - 10 186 - 360**	**0 - 19 156-360**	Land Within	Land Within
Additional Fetches & Bearing to Other Masts	**110 - 135 km:** 185-223 233-267	**20 - 35 km:** 170-225 262-345			**M2** 52km (45 deg) **M8** 53km (22.5 deg) **F1** - 140km (196.5 deg) **67 - 80km**= 47-120	**M8** 21.2km (306 deg) **F3** 51 km (226 deg)	**35-40km:** 82-104	**SF1** & **SF2** are 6.5 km from each other	

Figure 3.8: *Table summarizing the location of the masts and their proximity to shore*

In the blue rows at the top of the table, the latitude and longitude of each site is given. The following green rows indicate the distance to the nearest landmass (km) in addition to the bearing (degrees) of this nearest point. Having just the nearest point and bearing is not sufficient enough and thus the following rows indicate the sectors (degree ranges) in which there is land within the specific fetches listed. Boxes that have a red 'X' indicate that no landmass is located within that specific distance. In all cases except for SF1 and SF2 there are always sectors in which the nearest landmass is located beyond 200 km. This analysis was performed using some of the measurement tools on Google Earth (All Rights Reserved).

The third factor mentioned in the list above is the prevailing wind direction. This can be deduced by examining the wind roses for each of the sites (Figure 3.9). As was discussed in Chapter 2, the clear prevalence of westerly winds in this region is clear.

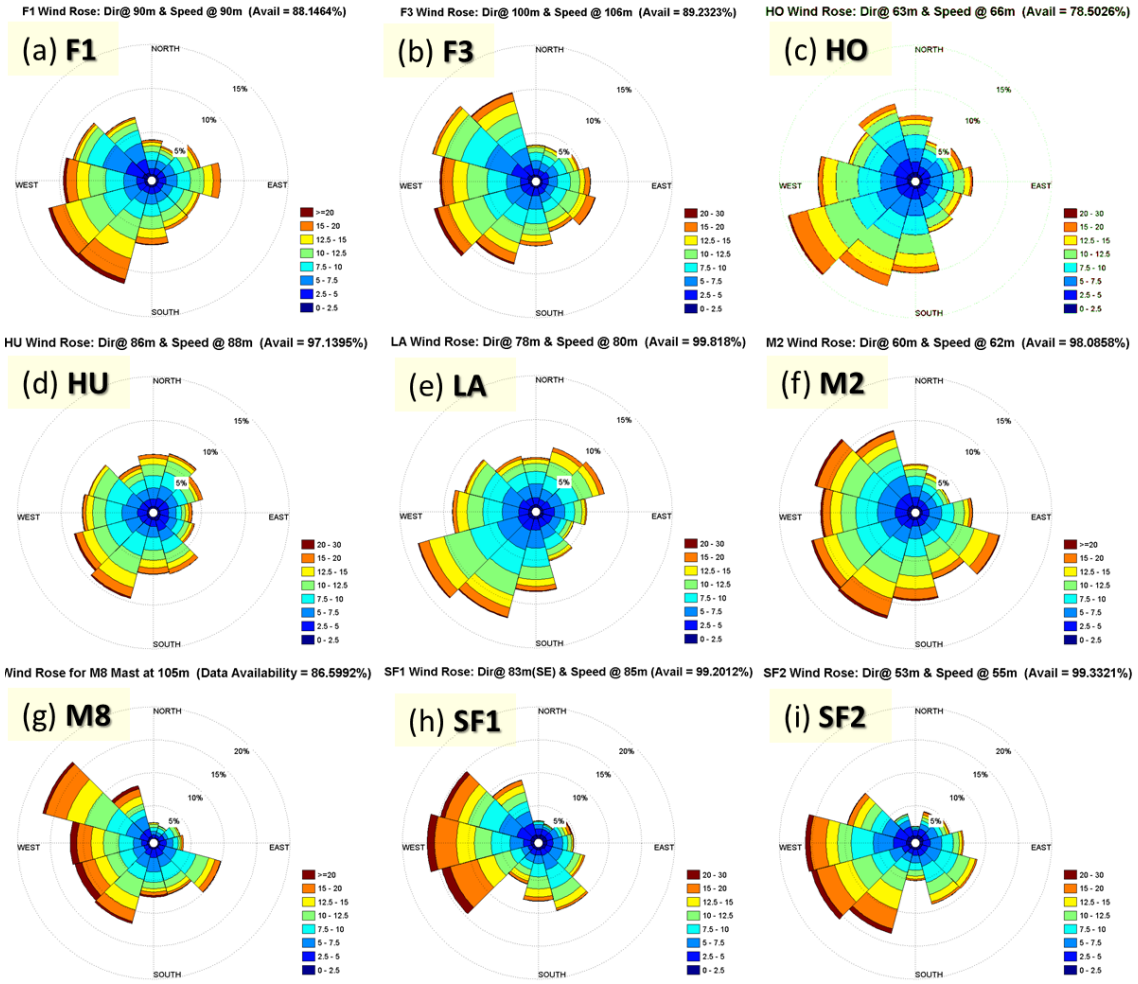

Figure 3.9: *Wind roses for all of the sites. The name of the mast as well as the height it represents are listed in the titles on each plot*

3.2 Preparing Raw Data for Analysis

The vast quantity of data available for this analysis vitalizes the process of data preparation. This scrupulous approach entails gathering all mast metadata, plotting raw time series and their probability density functions (pdf), developing well-founded filtering criteria and lastly, describing appropriate methods for implementation of these filters.

3.2.1 Examining Time Series of Raw Data

The first step was to examine the metadata (as detailed in the previous section) and plot all of the raw data in time series form. While cumbersome, it is essential in order to gain insight into the data, eyeball any outliers and notate key differences between masts and among heights.

In addition to plotting the raw time series, histograms and probability density functions (pdf) of each variable at each height are charted. A normal or Weibull distribution in the histogram ensures that the data distribution is not something out of the ordinary. For example, in figure 3.10, the raw time series from SF2's northwest(NW) oriented wind vane at 53 m (panel a), does not seem too out of the ordinary in that it ranges between 0 and 360 degrees. Though, it does seem to fluctuate a lot between these bounds. The flat histogram (panel b) reveals that the changes seen are too rapid and non-physical and that the southeast (SE)-oriented wind vane must be used for all analyses (panels c and d).

This initial analysis is important because it assists in the decision of which datasets to use for which analyses. For example, it became apparent that it is not always ideal to choose the highest wind direction measurement height for use in the analysis. On the HO mast (Figure 3.11) , the 94m wind direction data (panel a) had a non-physical signal for a couple of months and at 83m (panel b) and 43m (panel d), during this same period, there were no data at all. Therefore the 63m wind direction (panel c) was selected as the dataset to be used in analysis (see figure 3.11).

These initial analyses additionally provided insight into the different types of criteria that are necessary and were applied as filters in order to create a robust data set for analysis.

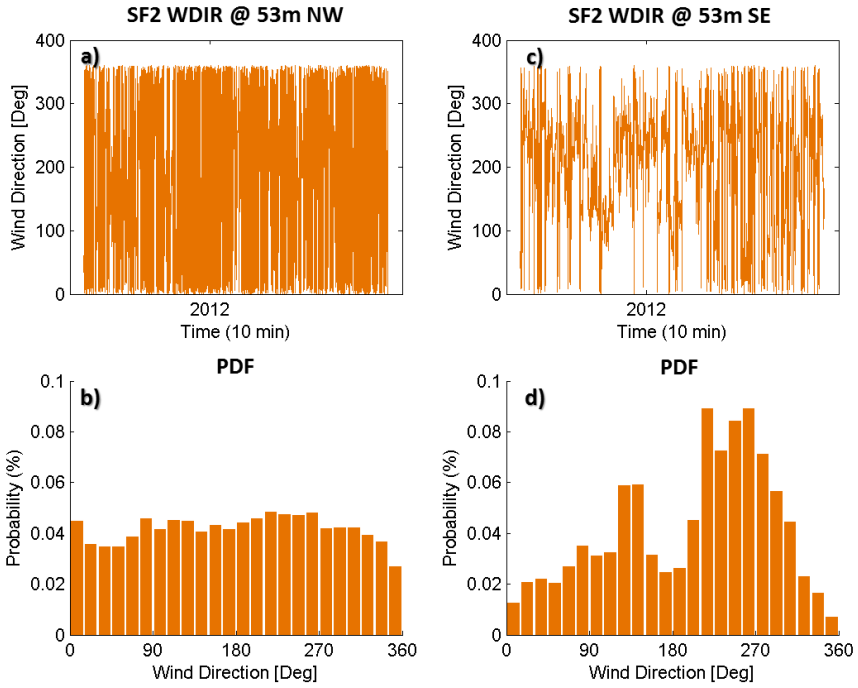

Figure 3.10: *Raw wind direction time series and probability density functions at SF2 for wind direction on oppositely-oriented booms. Clearly the data on the NW side is in error given the pdf.*

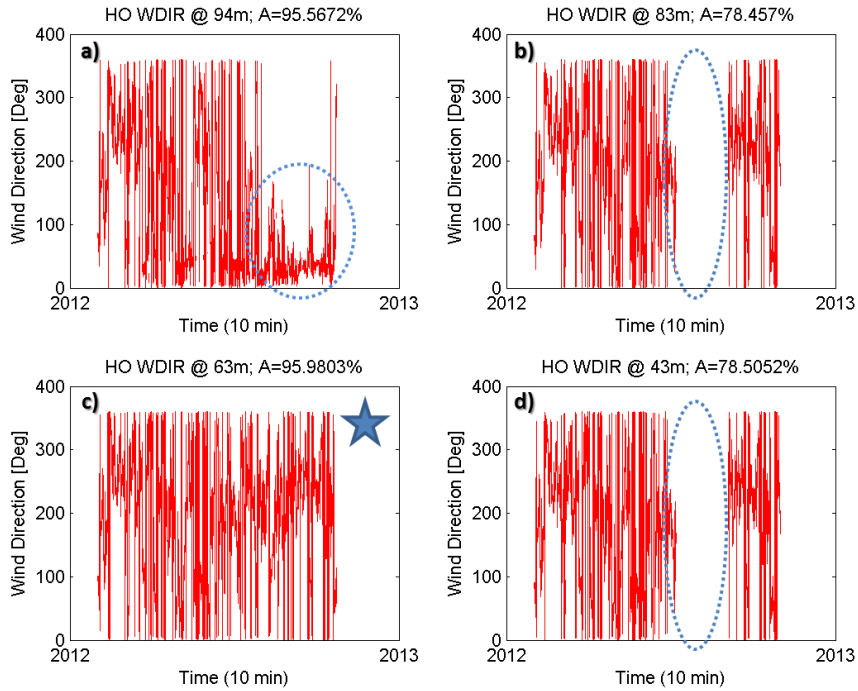

Figure 3.11: *Raw wind direction time series from HO depicting the reasoning why the 63m height was picked to represent wind direction at the site*

3.3 Filter Criteria Applied

Conclusions made through data analysis are only robust if the data used in the analysis is of high quality. One preventative step that can be taken to ensure utmost data quality is that the data collection instruments are calibrated correctly and regularly maintained and serviced. Such initiatives are not always taken and cannot be assured so in the case of this work it is necessary to post-process and rigorously examine the data to remove or correct biased data. A large chunk of this projects' work was devoted to developing a robust filtering technique that could be used for each of the masts. While this standard was applied to all of the masts, some tweaking of these filters were made based on the individual masts' orientation and the site's meteorological conditions.

3.3.1 Wind Speed Filters

Four criteria were used to filter raw wind speed data and corresponding times of the wind direction data. Data were excluded when one of the following conditions were exceeded:

- $V < 0.1 \ \frac{m}{s}$
- $V > 100 \ \frac{m}{s}$
- $V_{max} = V_{min}$
- $\sigma_V > 3 \ \sigma_{V,AllData}$

The first filter ensures that null or very low winds speeds are not considered as they are insignificant. Additionally, for some of the masts (F1&F3), the flag for missing data is -999, and thus it is this filter that removes such points. The second filter removes all non-physical values. Wind speeds higher than 100 m/s are only seen in strong tornadoes which do not occur in this region.

All of the masts report a minimum and maximum wind speed for each 10 minute data period. It is assumed that it is highly unlikely, given the accuracy of modern cup anemometers, that there would be no variation in wind speed during a ten minute period. Therefore, data in which the minimum and maximum speeds are recorded as the same are removed.

The last criterion is implemented to detect periods with anomalously high turbulence; turbulence that is beyond the expected value given a certain site. Data are removed if the standard deviation of a specific ten minute period is larger than three times the standard deviation of all of the data. Some potential instances when this threshold is passed could be when a helicopter lands at the met mast for servicing, or if anomalously high and also nonphysical wind speeds are recorded (wind speeds that are below 100 m/s threshold but still nonphysical). [20]

3.3.2 Wind Direction Filters

Three criteria were used to filter raw wind direction data:

- $\theta < 0^o$
- $\theta > 360^o$
- $\sigma_\theta > 40$

The first two criteria are obvious but were sometimes altered depending on the mast. For example, the M8 mast is located on the edge of the Horns Rev wind farm and thus only one 30 degree sector [255 to 285 degrees] had an inflow free of influences by the farm and thus is used for analysis. For F1, the anemometers are only on the southeast side of the mast which means that the wind speed reported from flow from between 280 and 360 degrees is in the masts shadow, artificially reducing wind speeds and increasing the turbulence. The enormous mast shadow effect is clearly evident by the more than doubling of the turbulence intensity in wind speed sectors of larger than 280 degrees (Figure 3.12). Additionally, you can see the effect of the lightning rod on the top anemometer by the mini peaks seen between Northwest(315 degrees) and Northeast (45 degrees).

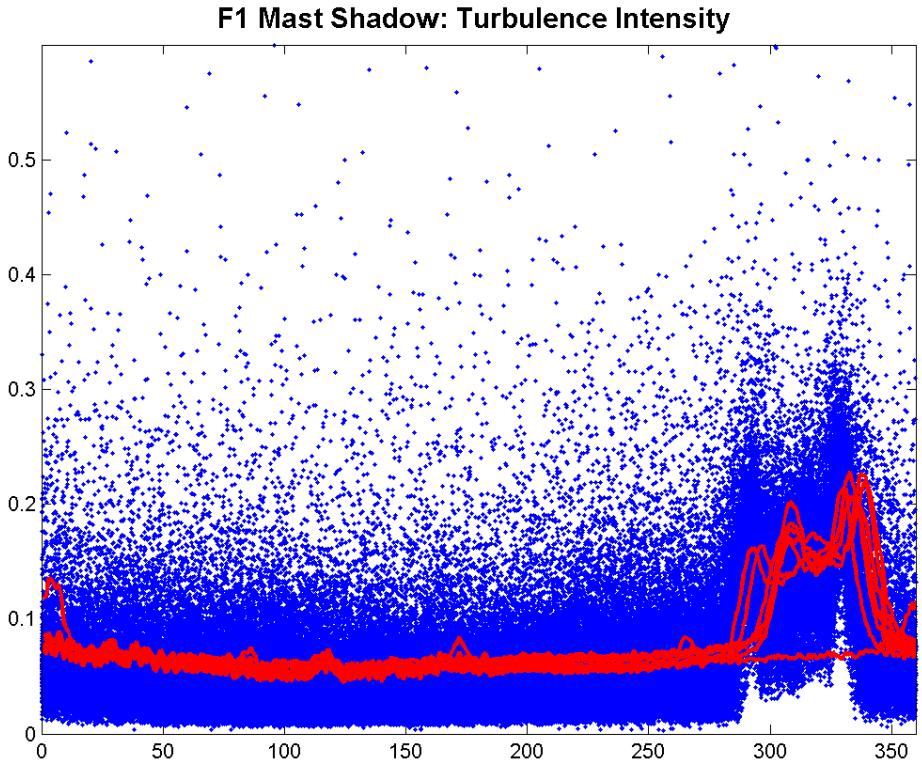

Figure 3.12: *Indication of where the F1 mast shadow is located by plotting turbulence intensity at all heights versus wind direction.*

3.3.3 Temperature Filters

At the beginning of the project, temperature filters were implemented to ensure that data taken during any potential icing events were removed. Frozen instruments do not record values that reflect real conditions. Temperature filters removed between 5-15% of the data even though very few icing events were observed. It was decided that it would not be justifiable to remove such large portions of the data for a few anomalous points. Additionally it would be reasonable to expect that the other filters could remove some of these anomalous points. An example of a time in which icing occured is visible in figure 3.17 within the mast shadow section (3.4).

3.3.4 Total Data Filtered

Tabs were kept of all of the data points that were removed for each aforementioned criteria to provide clear insight into where, when and why data were filtered out. Figure 3.13 displays an example of a summarizing table of the number of points that were filtered out per criteria at each height here for the LA mast.

LA

Wind Speed Height		TOTAL (103,824 points)			High Speed		Low Speed Filter	
		Avail %	Pts Removed	% Removed	Count	%	Count	%
80	TT	91.38	8950	8.620	0	0	0	0
77	SE	99.35	672	0.647	0	0	0	0
55	NW	99.32	709	0.683	0	0	0	0
55	SE	99.32	703	0.677	0	0	0	0
30	NW	99.26	773	0.745	0	0	0	0
30	SE	99.31	717	0.691	0	0	0	0
16	NW	99.36	666	0.641	0	0	0	0
16	SE	99.35	678	0.653	0	0	0	0

Min = Max WPSD		3 Sigma Speed STD		No Temp		High Wind Direction		Low Wind Direction		Wind Dir Std >40		Missing Times	
Count	%	Count	%	Ct	%	Count	%	Count	%	Count	%	Count	%
8351	8.04	1	~0	-	-	0	0	0	0	81	0.08	1	~0
73	0.07	1	~0	-	-	0	0	0	0	114	0.11	1	~0
114	0.11	1	~0	-	-	0	0	0	0	110	0.11	1	~0
109	0.10	1	~0	-	-	0	0	0	0	110	0.11	1	~0
181	0.17	1	~0	-	-	0	0	0	0	112	0.11	1	~0
126	0.12	1	~0	-	-	0	0	0	0	113	0.11	1	~0
75	0.07	1	~0	-	-	0	0	0	0	114	0.11	1	~0
87	0.08	1	~0	-	-	0	0	0	0	114	0.11	1	~0

Figure 3.13: *An example of the amount of data that were removed or filtered based on the different criteria specified above. Example is for LA.*

Using the criteria listed above, the average amount of data removed for each data set was around 0.5%. This value excludes any periods of missing data which varied by mast from 0 to as much as 22%. Figure 3.14 summarizes the percentage of data removed by each filter. The numbers in parentheses indicate the range of the data removed.

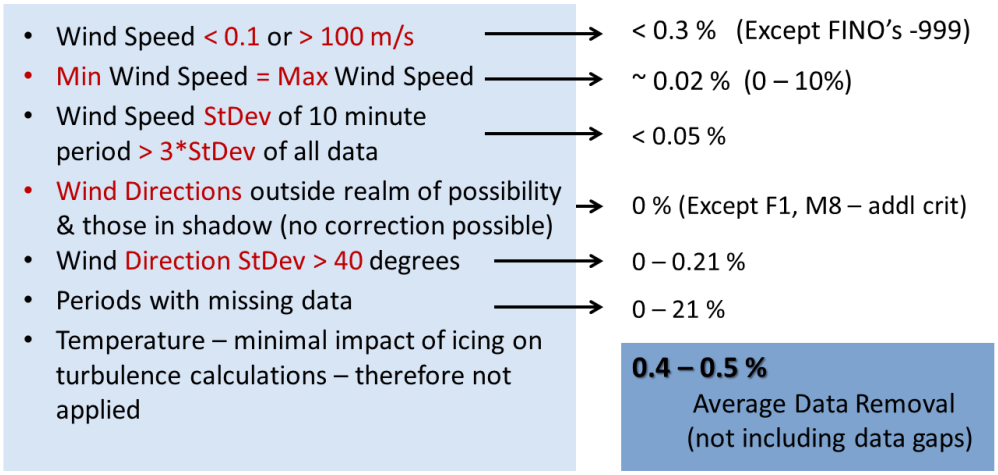

Figure 3.14: *Displays the most common amount of data that were filtered per filter criteria (excluding periods of missing data)*

Figure 3.15 displays an overview of the percentage of each masts' time period (given in figure 3.5) in which data was available or passed through the filters and thus are used in the upcoming analysis.

The low percentages for F1 and M8 are the result of sectoral filters applied to remove mast shadow effects and wind farm effects respectively which do not reflect on the data quality but on the conditions necessary to assess true ambient turbulence intensity. When these effects are not considered then the amount of data available for analysis is around 88%.

Mast	Height	% Avail	Mast	Height	% Avail
F1 (~88%)	100	68.5%	LA	80	91.9%
	90	68.4%		77	99.8%
	80	66.8%		55	99.8%
	70	68.5%		30	99.7%
	60	68.5%		16	99.8%
	50	65.8%	M2	62	99.7%
	40	64.6%		45	99.6%
	33	62.8%		30	99.7%
F3	106	89.1%		15	95.9%
	90	85.0%	M8 (~88%)	107	12.1%
	70	86.8%		97	12.1%
	50	89.2%		87	12.1%
HO	101	75.8%		77	12.1%
	96	76.1%		67	12.1%
	91	76.2%		47	12.1%
	86	78.5%		37	12.1%
	66	95.9%		27	12.1%
	46	78.5%	SF1	82	99.2%
	26	95.9%		80	99.2%
HU	90	76.1%		70	99.2%
	88	97.0%		50	99.2%
	70	87.1%	SF2	52	99.3%
	52	97.1%		50	99.3%
	34	97.2%		40	99.3%

Figure 3.15: *Percentage of data available for analysis*

3.4 Mast Shadow Correction

After application of the general filter, a mast shadow correction is implemented. Each dataset must be corrected for flow distortion due to mast shadow, with the exception of the top cup anemometers which instead need a correction for the lightning rod or cage, if present on the mast (Discussed in Section 3.5). Four types of mast shadow correction were utilized depending on the characteristics of each individual dataset (refer back to figure 3.2). Each dataset can be classified into one of these four categories:

1. *b* - Two datasets at the same measurement height, on opposite sides of the mast
2. *tri* - Three datasets at the same measurement height, each 120 degrees apart
3. *o* - One dataset available at specific height, but on mast where other heights have two datasets
4. *s* - Only one dataset available per measurement height for the entire mast

Each of these four has a distinguishable method for mast shadow correction, the specifics of which are discussed in the subsequent subsections.

3.4.1 Two Datasets at Same Height

In this instance there are 2 instruments taking measurements on opposite sides of the mast (ex. Northwest and Southeast-oriented instruments at the same height). To determine the wind directions in which mast shadow correction is required, a ratio of wind speeds (also σ_U) between the two sides versus wind direction is plotted.

The resulting curve is analyzed to pinpoint wind directions where mast shadow is present and has a slight sinusoidal dependence on wind direction. Shadow is considered present whenever there is a deviation of the ratio from unity. In the areas in which there is no mast shadow (sinusoidal curve about 1), measurements from the cups on both sides are averaged. When mast shadow is present, then the upwind anemometer is used.

Figure 3.16 displays plots of the ratios between the wind speeds and wind speed standard deviations of the oppositely-oriented anemometers.

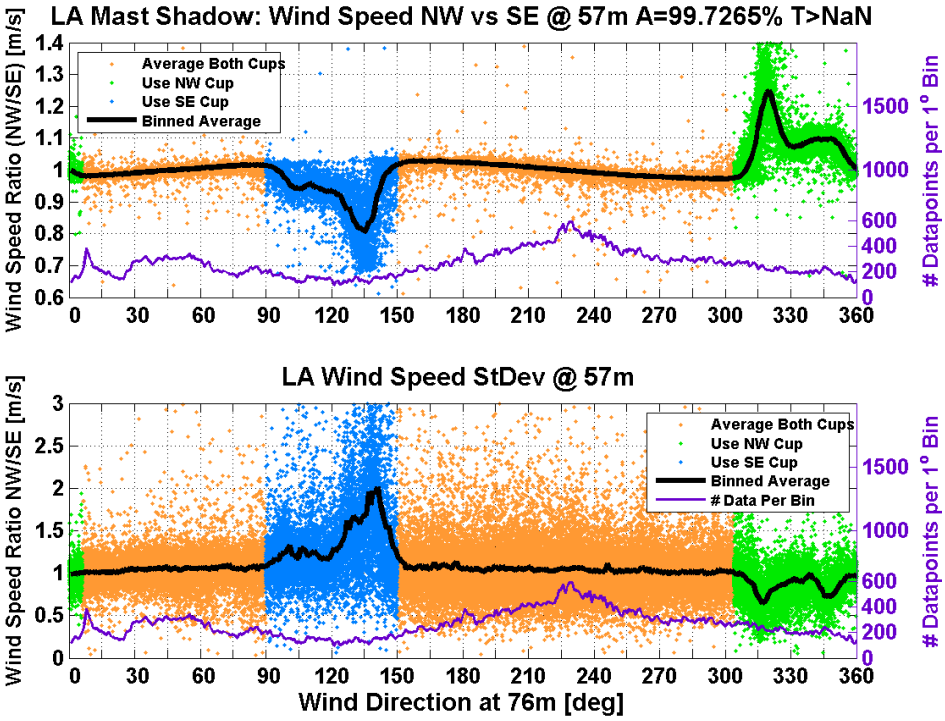

Figure 3.16: *Mast shadow plot of $\overline{U}$ and σ_U for LA. The upstream cups are used when there is mast shadow present and at other times, in orange, both measurements are averaged.*

Each specific scatter point on the top plot dictates the wind speed ratio and its representative wind direction. The black line is the average ratio value within each 1 degree bin. The secondary y-axis on the right and the line on the plot in purple signify the number of these scatter points per 1 degree bin. It is evident that the northwest cup is in the

mast's shadow between about 90 and 150 degrees due to the dip in the ratio well below one. This means that the southeast cup reports wind speeds of about 25% larger than the northwest cup. The opposite is visible at wind directions of between 300 and 360 degrees.

The bottom plot displays the ratio of the wind speed standard deviations. There is much larger scatter in this plot, but the average is completely centered around 1 (as opposed to the sinusoidal trend seen in $\overline{U}$). The flow distortion from the mast has the opposite effect as the wind speed, where the wind speed standard deviation ratio is increased when the specific cup is in the shadow. This makes intuitive sense, because if the cup is in the shadow, there are more turbulent vorticies and eddies generated and thus the standard deviation would in fact be larger.

A similar plot for M2 displayed in figure 3.17, is very similar in explanation, though there is one interesting feature that must be noted. When examining the ratio at approximately 27 degrees, you notice a vertical line of observations. This signal is cause by icing of the wind vane and at least one of the cups. To prove that this was in fact an incident of icing, a low temperature filter of 0.5 degrees was applied. The resulting plots of these ratios, seen in figure 3.18, show no indication of this icing-caused anomalous signal. Despite this, no sweeping temperature filter was applied because such icing incidents were rare and do not justify removal of up to 15 percent of the data.

The mast shadow plots for all of the other masts can be accessed in the Appendix B. For the purposes of saving space, only one height is shown per mast.

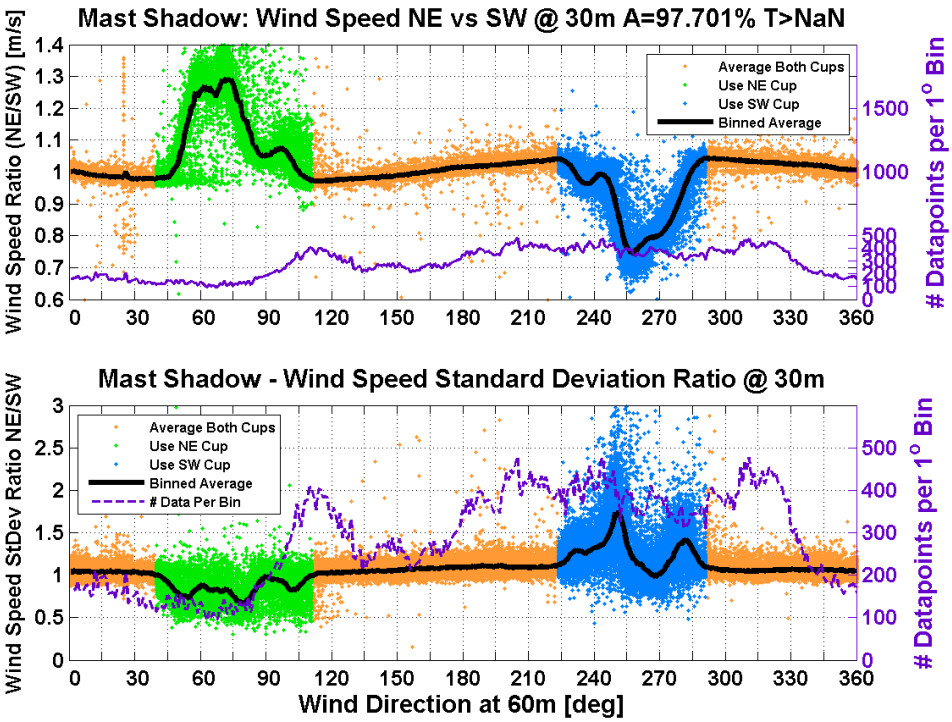

Figure 3.17: *M2: Mast shadow plot without a temperature filter*

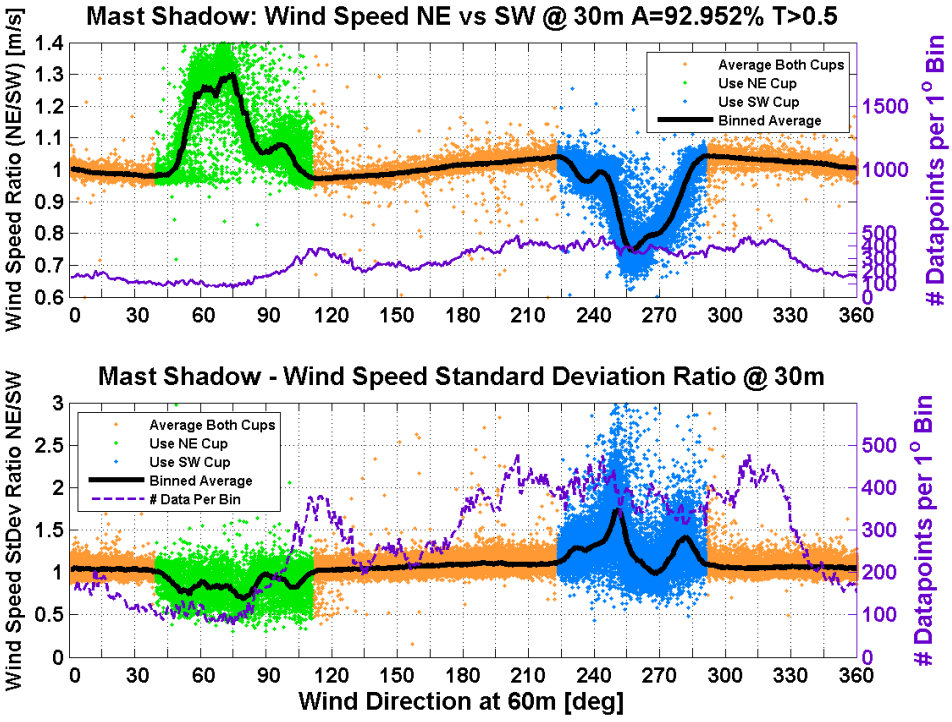

Figure 3.18: *M2: Mast shadow plot with a low temperature filter of 0.5 degrees C*

3.4.2 Three Datasets at Same Height

This case, where there are data from three orientations, each 120 degrees apart, only occurs at F3. As was recommended in a presentation by Detlef Stein of DNV GL, no averaging of the observations is performed [35]. Instead, each anemometer is used for a 120 degree sector in which the anemometer is most perpendicular to the flow (to avoid mast shadow and speed-up effects). For example, a cup oriented at 225 degrees is used when the wind direction is between 105 and 165 degrees and 285 and 345 degrees. Since F3 is the only triangular-shaped mast, the below figure and sectors used are specific solely to this mast.

- 105^o oriented mast [345^o to 45^o] & [165^o to 225^o] sectors
- 225^o oriented mast [105^o to 165^o] & [285^o to 345^o] sectors
- 345^o oriented mast [45^o to 105^o] & [225^o to 285^o] sectors

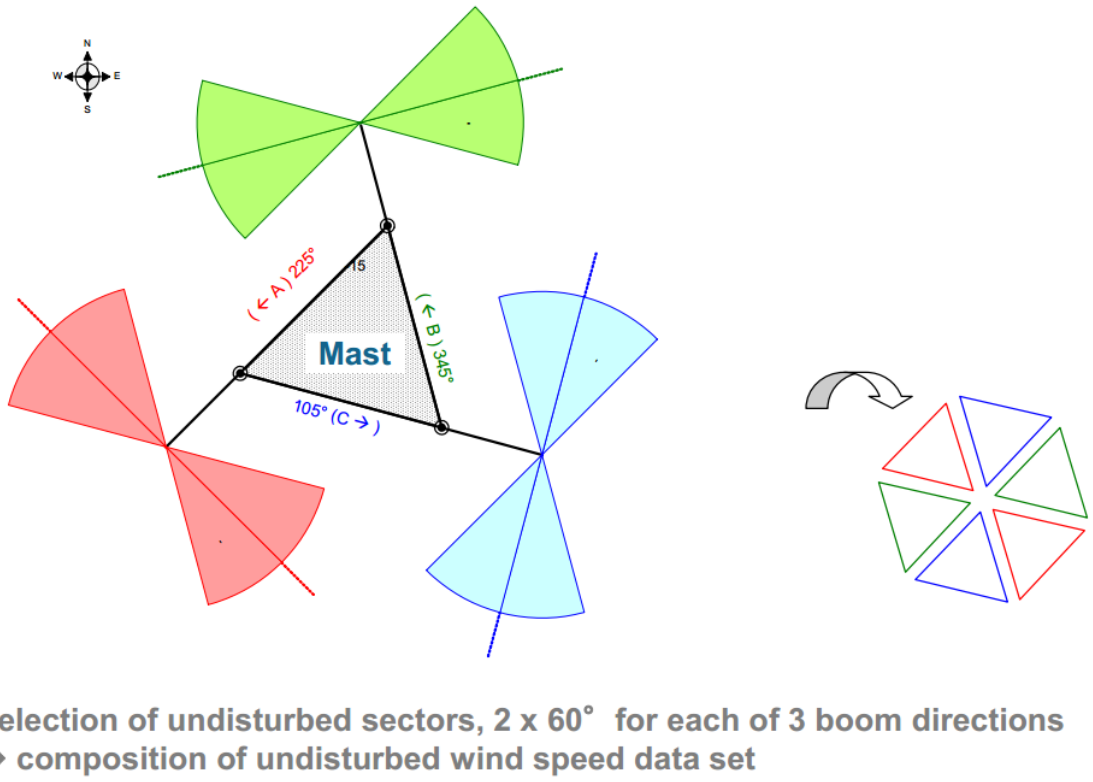

Figure 3.19: *Boom orientations at the F3 mast. Each anemometer is used for the flow that is least influenced by mast shadow and speed up effects which corresponds to 120 degree sectors each. This image is fully owned by Detlef Stein at DNV GL [35]*

3.4.3 One Dataset at Height Surrounded by Heights with Two Datasets

This one-sided correction is for a height with anemometers on just one side but on a mast that has adjacent heights with measurements from both sides.

Under these circumstances, a linear regression polyfit analysis is performed to use the relationship between this height and the one above or below it (mast corrected using the 1st method above: section 3.4.1) to correct for directions when the one-sided observation is shadowed. The steps completed are discussed in detail in Appendix C.

An example of the correlation plots from SF1 at 55m from before and after this one-sided correction are displayed in figure 3.20. The top two plots display the before and after speed correlations between the 55 meter and 45 meter wind speeds while similarly the bottom two are of the wind speed standard deviation. For both metrics the correlation increases as is evident by the more linear curves observed.

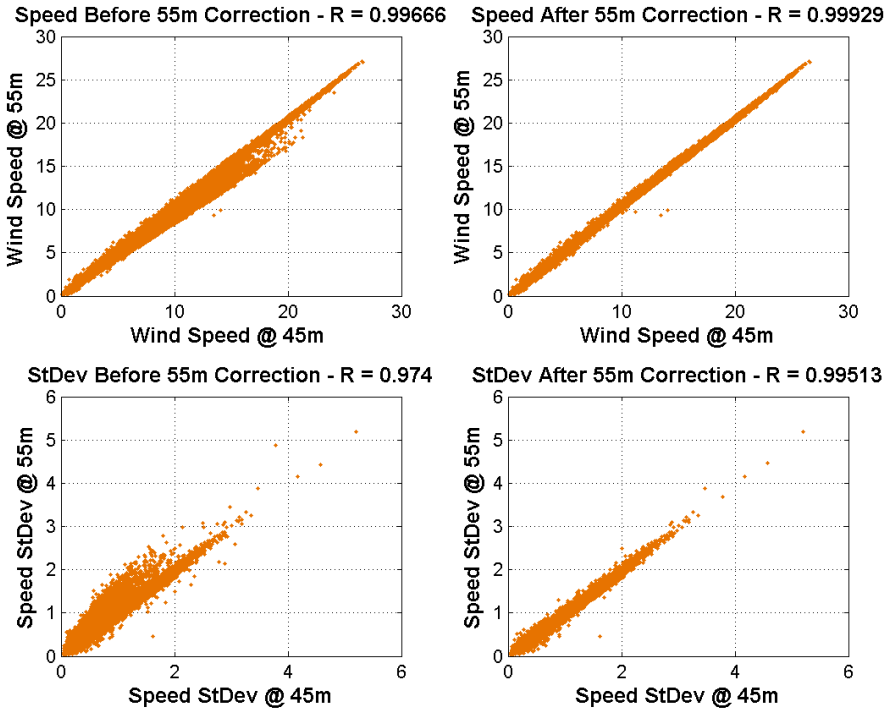

Figure 3.20: *Before and after the application of the one-sided filter at 55m on SF2*

3.4.4 One Dataset at All Heights on Mast

In this case, all of the available or analysis-worthy data are located on only one side of the mast. Therefore it is not possible to use the linear regression detailed in method 3 (section 3.4.3) and therefore no mast correction is possible per-say. Instead data must be filtered out for wind directions that cause the anemometer to be shadowed. For example in F1, data between 280 and 360 degrees area removed because the boom is oriented in the southeast direction.

3.5 Lightning Rod Correction

Correction of the top cup anemometers due to lightning rod shadow effects were necessary for F3, HU, SF1 and SF2, while F1 needed correction due to a lightning cage. The correction implemented is identical to method 3 (Section 3.5.3) detailed above. Figure 3.21 display the ratio between the 57m and 45m observations as a function of wind direction from before and after the implementation of the lightning correction. In the former, clear distruption as a result of the lightning rod is visible from 69 through 102 degrees. Figure 3.22 shows plots of correlations of the wind speed and wind speed standard deviation from before and after removal of the lightning rod-generated flow distortion. Correlations of wind speed increased from 0.99775 to 0.99896 while those of wind speed standard deviation increased from 0.97519 to 0.99381.

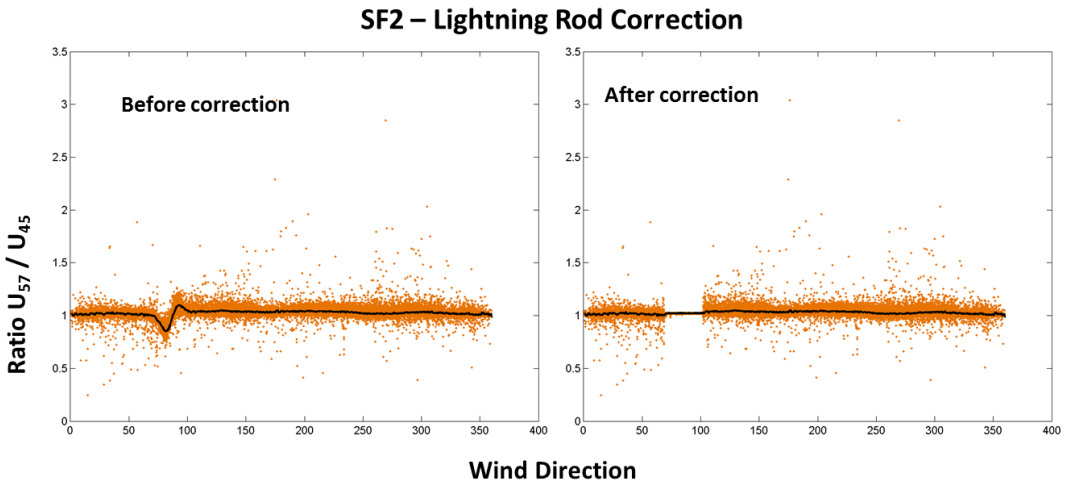

Figure 3.21: *Influence of the lightning rod at the top of the SF2 mast (57m), before and after correction using one-sided linear regression method*

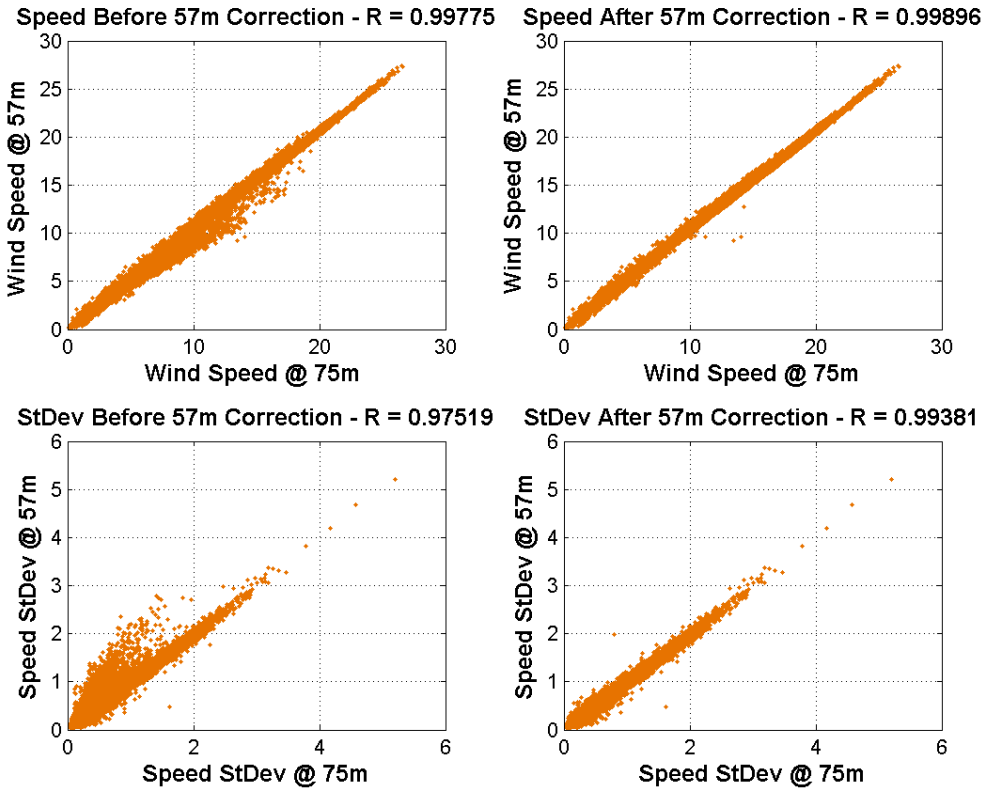

Figure 3.22: *Correlations before and after correction for lightning rod*

This chapter discussed the tedious but crucial task of preparing the data for analysis and the methods that were applied to quality control it. Being meticulous in this process assures us that only data of utmost quality was used for the analysis presented in the next chapter.

Chapter 4

Results and Discussion

While the characteristics of turbulence intensity as a function of wind speed have been examined in the past [11][28][33], it has never been done on such a large scale by examining and comparing this many masts. The vast amount of data available for analysis in this thesis provides a fantastic opportunity examine the various dependencies of TI and σ_U.

The results and discussion presented here probe into the intricacies behind the behavior of offshore turbulence intensity by examining the relationships between four turbulence metrics (σ_U,σ_{σ_U},TI,σ_{TI}) and three parameters, namely:

- Wind Speed (Chapter 4.1)
- Height (Chapter 4.2)
- Wind Direction & Fetch (Chapter 4.3)

All of the plots within each of these chapters compare the four turbulence metrics as a function of the parameters in the section title.

4.1 Dependency of Wind Speed ($\overline{U}$) on Turbulence Characteristics

4.1.1 σ_U vs $\overline{U}$

The first relationship under examination here is that of the wind speed standard deviation(σ_U) and average wind speed($\overline{U}$), as these are two parameters that derive turbulence intensity, the nucleus of this Masters thesis project.

The first set of plots (figure 4.1) provide an overview of the variation of σ_U when averaged in one meter-per-second bins for each mast at its nearest height of observation closest to 50 meters. 50 meters was selected solely for comparative reasons because each mast had an observation near this height. The plots also provide insight into the spread around this average by scatter plotting each individual data-point and depicting the 25th and 75th percentiles via the errorbars.

It is clear that the σ_U increases with increasing $\overline{U}$ as a result of larger variations possible as $\overline{U}$ increases. While this general trend is obvious through examination of all 9 plots, the magnitude and rate of the change does vary, some between the masts. The IEC 61400-3 standards [8] state that σ_U is a linear function of $\overline{U}$, but this is not observed at any of the masts under analysis here. A recent study by Wang et al [10] examining three masts, all on different continents, also report observing this discrepancy [10].

For example, at F1 in figure 4.1a, a clear change in the slope of the curve is seen just around 12 meters per second (see yellow dotted lines on plot). In offshore environments at low wind speeds, the turbulence is mostly thermally driven while at higher wind speeds the effects of the waves take over as the main turbulence generating source. When this transition to the wave or mechanically-driven turbulence occurs, the rate of change increases [10][14]. This change in slope incidentally also corresponds to the point in which TI begins to increase with wind speed as will be revealed in section 4.1.4.

While the change in slope is quite evident in F1 and M8, not all of the masts have such distinct transition points which could be the result of different stability and wave conditions present at the different masts. Additionally, the range of scatter between the masts varies and is the subject of analysis when analyzing the standard deviation of the wind speed standard deviation (σ_{σ_U}) presented in the next subsection (4.1.2).

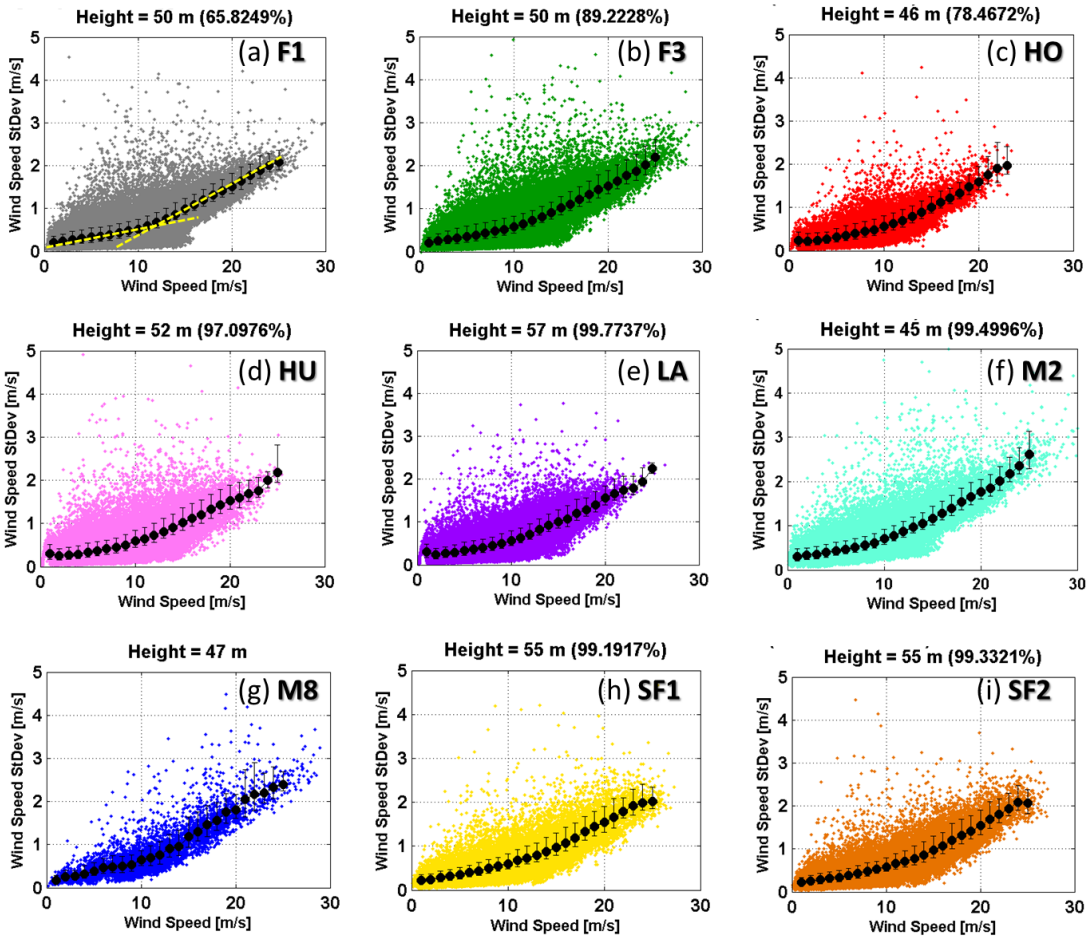

Figure 4.1: *Scatterplots of $\overline{U}$ versus σ_U for each mast at its closest observation to 50 meters. The black dots indicate the mean σ_U within each wind speed bin, and the errorbars are the 25th and 75th percentiles. Some masts have more distinct changes and transition points than others.*

In addition to variations of σ_U between the sites at 50m, there also exist differences in the vertical. Figure 4.2 provides a closer look at the differences in scatter and trends between the masts at different measurement heights. F1 and HO were selected because they exemplify a representative look of all of the masts. At HO, the change in σ_U with increasing $\overline{U}$ is more gradual than in F1 and the spread between the maximum and minimum values is reduced. Notice though that both have many extremely low σ_U values up until about 20 m/s at 100m (see purple dotted oval in figure). This can be caused by very stable conditions.

It is also important to point out that the speed bin in which this transition occurs depends on the height. By examining the dotted yellow lines on the F1 plots in figure 4.2 it is possible to see that the transition occurs at higher speeds at higher heights, as the influence of the ocean surface decreases on winds higher aloft . On F1 at 100m, the transition occurs at a wind speed of approximately 14 m/s while at 33m, this transition occurs at a much lower 8 m/s.

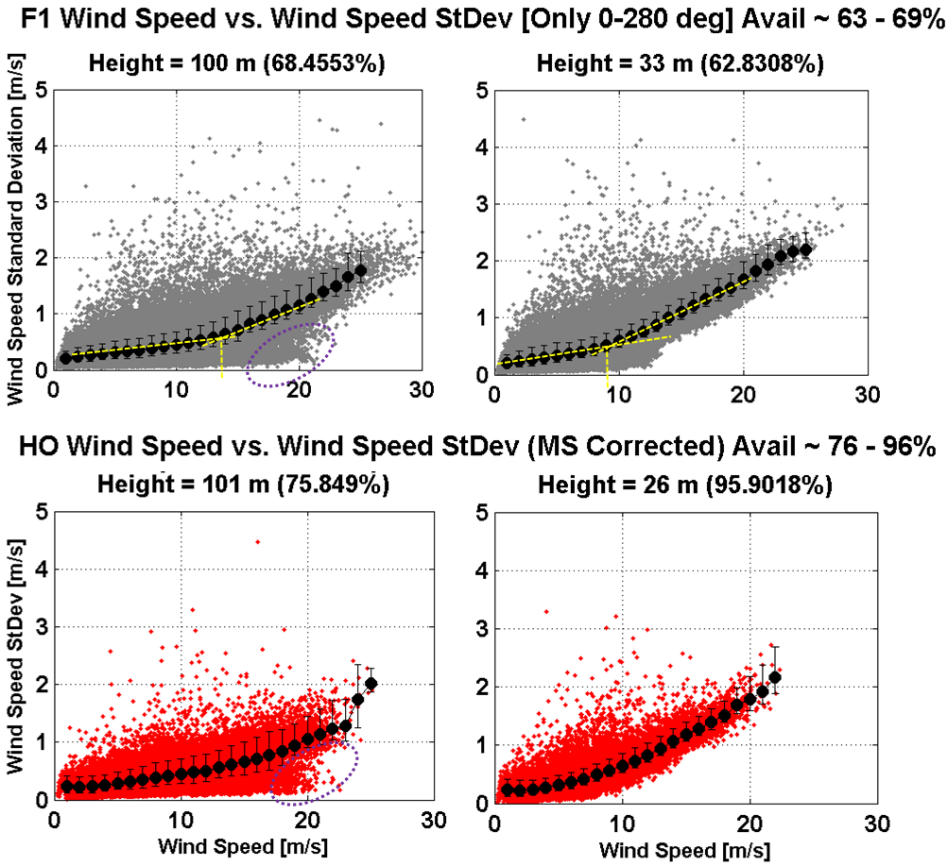

Figure 4.2: *σ_U vs $\overline{U}$ scatterplots at two different heights for F1 and HO. The transition point (slope change) at F1 is much more distinct than at HO.*

To probe further into the differences of σ_U vs U with height we turn to figure 4.3. The lowest heights (lighter colors) at both masts have nearly the same trends while at the top of the masts (darkest color), the σ_U is slightly lower at HO. While it seems like the spacing in the trends between heights is more varied at HO than at F1, it deceiving because the changes in height at F1 are at even increments of 10 meters while at HO the change is at some points 5m and at others 20m. Even still though, at HO, σ_U does change more rapidly with height. This is interesting to note given that both are categorized in the far offshore region. The plots presented above are also available for each mast and appear in Appendix E.

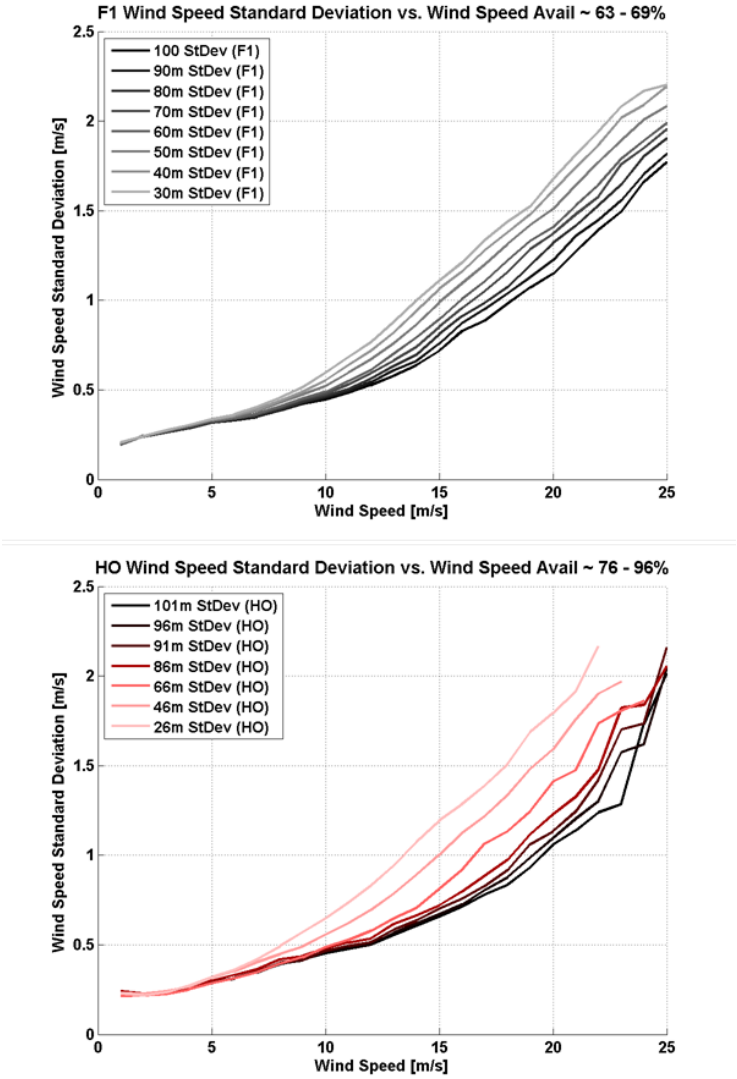

Figure 4.3: *Analyzing the change of σ_U with height at F1 and HO.*

For a more direct comparison of the σ_U vs. U relationship between the masts, select heights (30, 50, 70 and 90 meters) were chosen from which data from each mast that has an observation near that height are plotted (Figure 4.4).

The results were astounding for two reasons, the first being the striking similarity between the curves from all of the masts except for M2 and M8, and the second being the suspicious closeness of the trends between the M2 and M8 outliers.

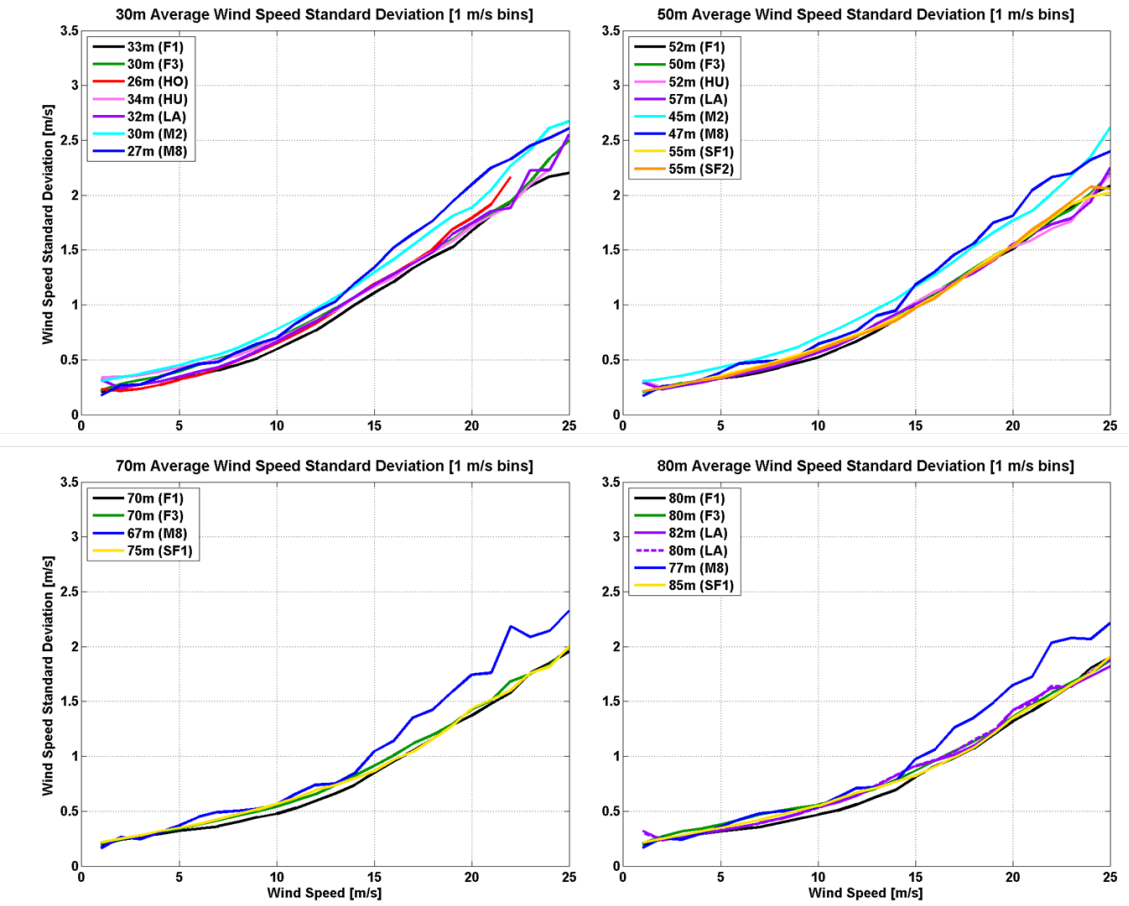

Figure 4.4: *Comparison of σ_U versus $\overline{U}$ at all of the masts at 30m, 50m, 70m and 80m. The striking similarity between the masts (except M2, M8) indicates that when averaging over all wind directions, this relationship is uniform over Northern Europe. Agreement between the masts is slightly less at lower z*

This staggering closeness of curves between the masts (except M2, M8) shows that the relationship of σ_U vs. U is not site dependent when averaging over wind directions within Northern Europe. These findings are most apparent at 50, 70 and 80 meters and less present at 30 meters, leading to the belief that local wave or stability conditions at lowest parts of the MABL cause these site specific deviations.

The second observation, about the discernible differences realized between M2 and M8 and the other masts proves to be quite interesting. By examining figure 4.5, it is realized that the relative differences between M2 and the other masts is larger at lower wind speeds while at M8 the opposite is true. The difference grows with increasing wind speed.

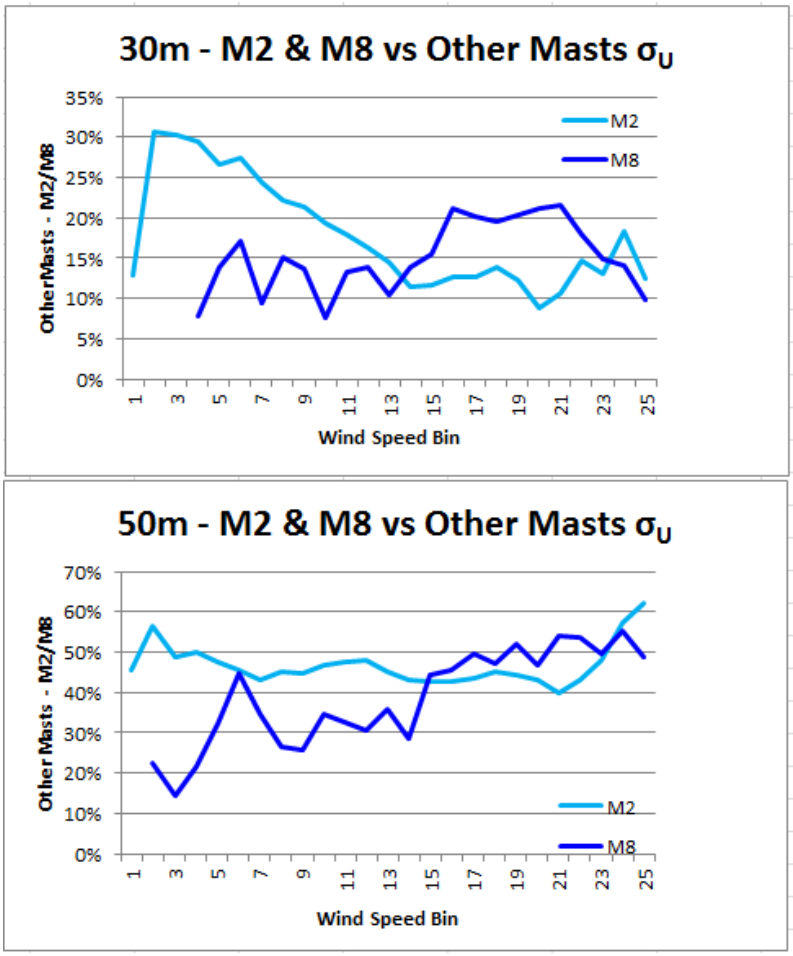

Figure 4.5: *Percentage differences between M2, M8 and and average of all of the other masts*

The larger deviations realized at high wind speeds at M8 is seemingly due to the fact that the sector under analysis is solely sea-fetched and thus strongly impacted by the increase in turbulence generated by the waves. All of the other sites have some fetchs' influenced by the coastal discontinuity and thus would have such sectors averaged in.

The source of the larger deviations at lower wind speeds for M2, especially at 30m is more difficult to pinpoint, but could be related to stability effects, which are not analyzed in this study.

4.1.2 σ_{σ_U} vs. $\overline{U}$

A further sub-classification is the examination of the inherent extreme tendencies of σ_U over time. This in some form can be examined by taking the standard deviation of the wind speed standard deviation (σ_{σ_U}) which is displayed in figure 4.6 for four of the masts. (Note: all of the y-axis scales are the same except for M8 which had a significantly larger magnitude).

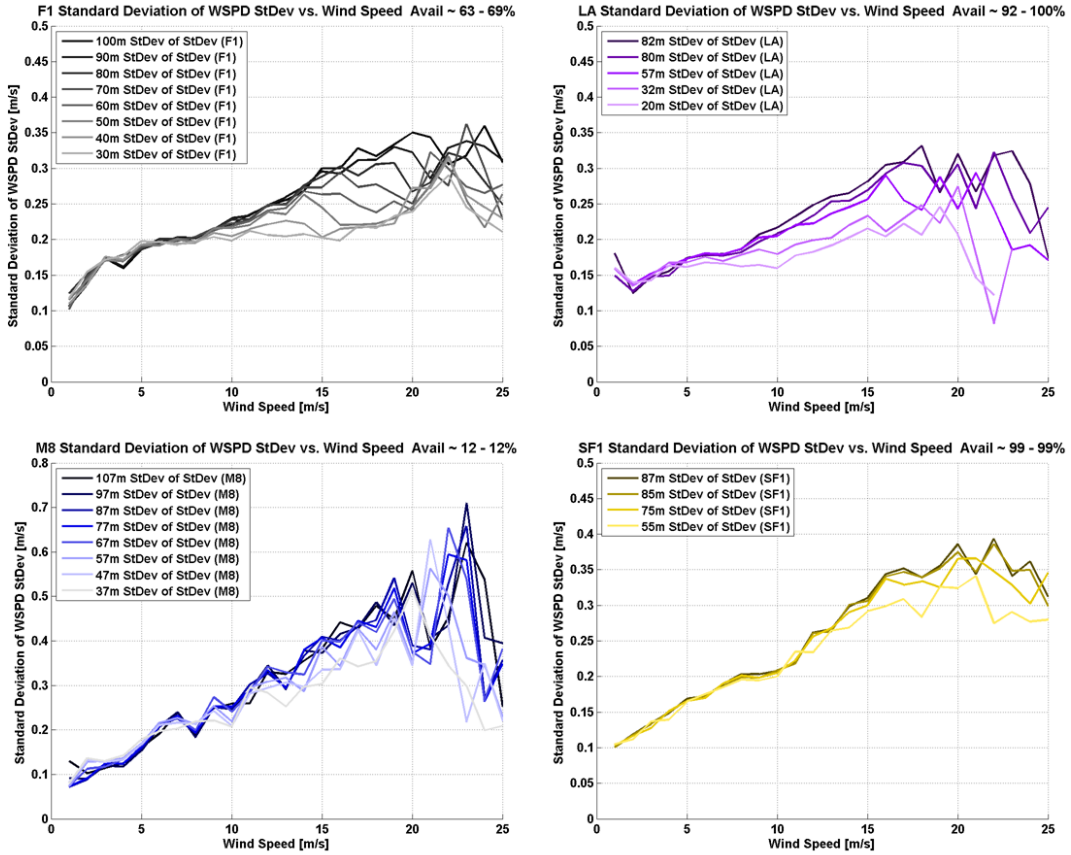

Figure 4.6: *σ_{σ_U} vs $\overline{U}$ for two of the four masts. Note that the y-axis scale is different for M8*

The two general findings from these plots are:

1. Variations of σ_{σ_U} grow with increasing wind speed
2. Variations of σ_{σ_U} amplify with increasing height

The explanation for the first derives from the increasing positive skewness or spread of σ_U at larger wind speeds. Refer back to Figure 4.1 where the 75th percentile (errorbars) are noticeably larger in magnitude than the 25th percentile and whose value increases with wind speed at a faster rate than that of the 25th percentile. This was also seen in [10].

It is interesting to notice that at very high wind speeds σ_{σ_U} starts to decrease some. To understand the physics, refer back to Figure 4.2 and examine the lowest scatter dot

noticeable within each general wind bin. These minimum values do not follow the average, but instead stay very close to zero, especially at higher z. This can be attributable to cases of very stable atmospheric conditions that can persist even with relatively large wind speeds. Such conditions occur in cases of warm air advection over very cold water surfaces. This possibility is not limitless as pointed out by Turk et al [11] who found that above about 20 m/s, the effect of increased sea surface roughness is large enough for the frictional stress to break up these very stable layers. Interestingly enough, the data presented here confirm this. At the 100m heights in figure 4.2, there are not many near-zero σ_U points above 20 m/s. As expected this threshold is much lower at lower heights.

The second finding that σ_{σ_U} increases when moving vertically is likely due to the varying heights that the turbulent eddys generated by the waves pervade and mix into. Notice that at low wind speeds, σ_{σ_U} is nearly identical at all heights while after the transition to mechanically driven turbulence, the spread of values between the heights grows. In other words, at lower heights, it is more likely that the waves have a more constant influence while at higher heights this effect is not as consistent.

Differences of σ_{σ_U} versus $\overline{U}$ at different masts are minimal at lower wind speeds but amplify in larger wind regimes, similar to the increased stratification of σ_{σ_U} seen between heights at individual masts seen above (figure 4.6).

Figure 4.7 displays a comparison of σ_{σ_U} vs. $\overline{U}$ at all of the masts with observations at 30, 50, 70 and 80m. A general trend does exist when comparing the masts, but there are no discernible patterns visible based on region.

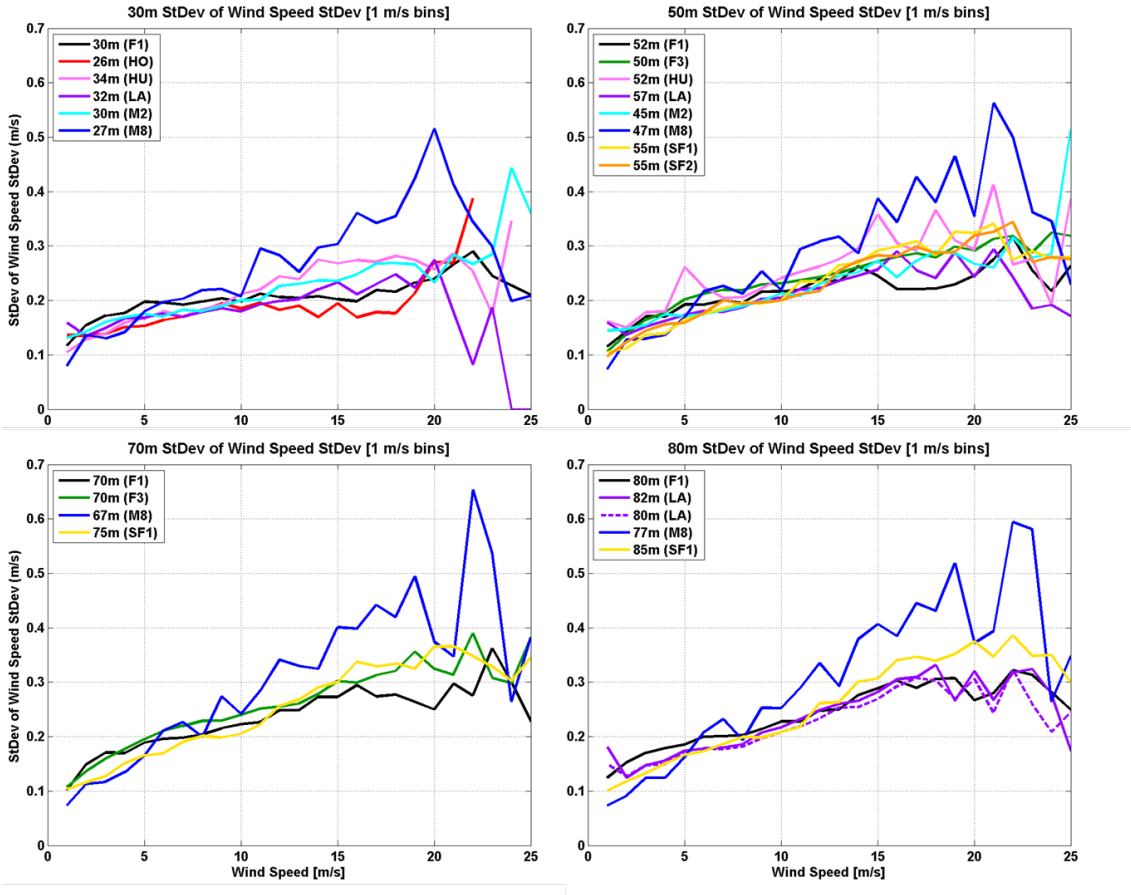

Figure 4.7: *Comparison of σ_{σ_U} versus $\overline{U}$ at all of the masts at 30m, 50, 70m and 80m.*

4.1.3 Comparison of Calculated σ_{σ_U} with IEC Standard

It was mentioned in the IEC 61400-3 standard that the definition of $\Delta\sigma = (1.84 \text{ m/s})I_{ref}$ and $\sigma_{\sigma_U} = (1.44 \text{ m/s})I_{ref}$ at 15 m/s where $\Delta\sigma$ is the difference between the 90th and 50th percentiles of σ_U [8][9]. The observed values of $\Delta\sigma$ at these nine masts are significantly higher than the standard (see table in figure 4.8), in resemblance with the findings in [10]. Figure 4.8 lists the range of $\Delta\sigma$ at all of the masts at all heights. When considering the heights of 50m at all masts except M2 and M8, $\Delta\sigma$ are between 3.65 and $5.30I_{ref}$.

Additionally, the standards also declare that both parameters are unchanging in height [8][9]. This is also not the case when looking at these observations as is indicated by the disproportional values of σ_σ between heights in figure 4.7. σ_{σ_U}'s relationship with height is discussed in further detail in section 4.2.2 and in figure 4.18.

	Z [m]	Δσ = (value)TI @ 15 m/s [m/s]
F1	100	6.51
	90	6.31
	80	6.12
	70	5.51
	60	4.72
	50	4.30
	40	3.40
	30	3.09
F3	106	6.05
	90	5.15
	70	4.73
	50	3.97
HO	101	7.79
	96	7.57
	91	7.03
	86	6.82
	66	5.81
	46	3.65
	26	2.63
HU	90	5.98
	88	6.26
	70	5.72
	52	4.89
	34	3.89

	Z [m]	Δσ = (value)TI @ 15 m/s [m/s]
M2	62	3.82
	45	3.39
	30	2.96
	15	2.22
M8	107	14.59
	97	13.26
	87	12.55
	77	9.84
	67	9.36
	47	8.51
	37	6.82
	27	6.42
LA	82	5.28
	80	4.88
	57	4.20
	32	3.36
	20	2.80
SF1	87	6.67
	85	6.69
	75	6.08
	55	4.95
SF2	57	5.30
	55	5.03
	45	4.47

Figure 4.8: *Values within $\Delta\sigma$ equation at each height on each mast.*

4.1.4 TI vs $\overline{U}$

Now that the description of the relationship between the two deriving variables of turbulence intensity is complete, examination of how the turbulence intensity varies with wind speed is presented.

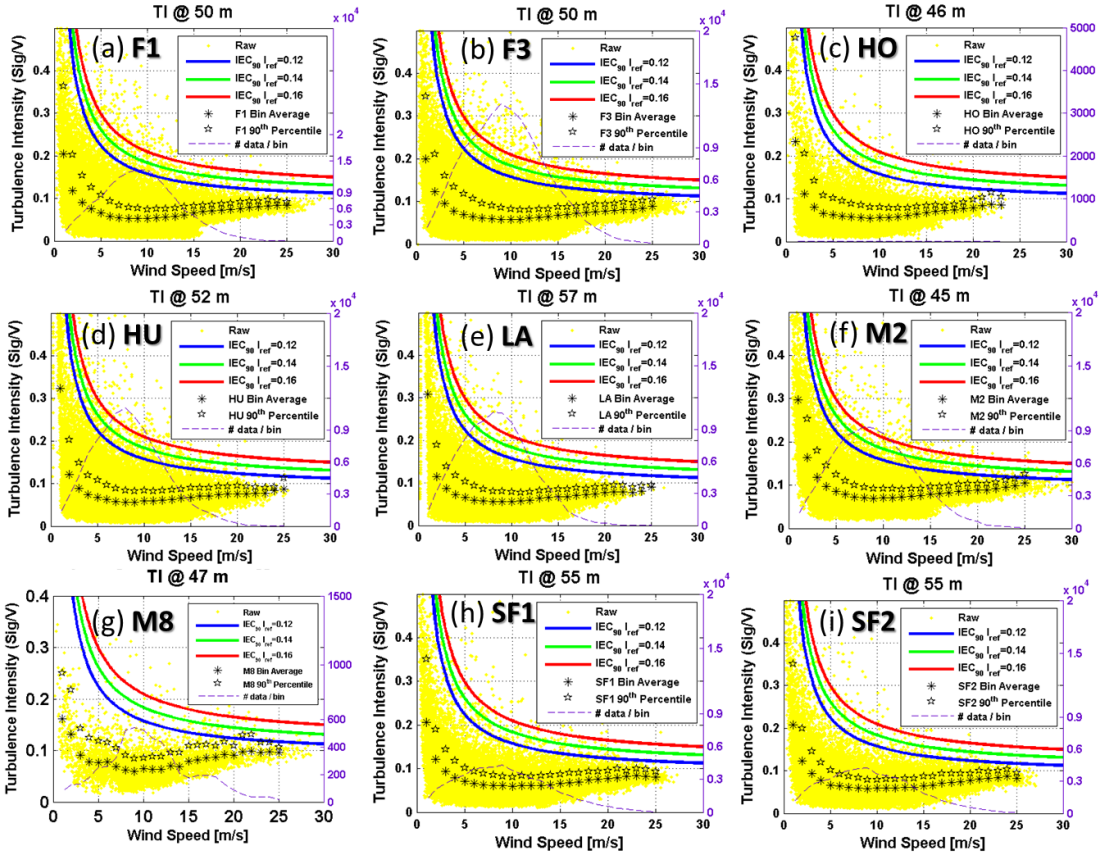

Figure 4.9: *Scatterplots of TI at all of the masts at their closest observational height to 50m*

Figure 4.9 is a panel of TI vs $\overline{U}$ plots for each of the masts at its closest observation to 50 meters, once again selected due to the availability of observations at this height at all of the masts. The raw data are represented by the yellow dots, while the averages (TI) within each 1 m/s bin and its' 90th percentile values (TI_{90}) are depicted by the asterisks and stars respectively. The three solid color curves signify the three different IEC 61400-3 90th percentile standards for onshore wind turbines (Chapter 2.8). And lastly, the dotted purple line (values on secondary y-axis) represents the number of data points that were averaged within each bin to get the average and 90th percentile values.

The general trend visible in the variation of TI_{90} with $\overline{U}$ at low speeds from the 9 different masts match closely with the 90th percentile IEC curves, albeit with much lower magnitudes. The curves reach a minimum at around 8 to 14 m/s (depending on height) and then increase in contrast to the IEC curves. This is expected because as discussed previously, the IEC 61400-3 standards are based on onshore wind turbines and thus do

not account for the expected increase of turbulence intensity at higher wind speeds due to the subsequent increase of the sea surface roughness from waves. This was also observed in other studies [10][11].

A tabular view of the key turbulence intensity values for each of panels above is listed in figure 4.10.

Turbulence Intensity Statistics @ Heights ~50m							
Location	Mast	z [m]	$\overline{U}$ [m/s]	$\overline{TI}$	TI_{min}	Speed Bin w/ TI_{min}	$\overline{\sigma_{TI}}$
Irish Sea - West Coast of UK	SF2	57	9.51	7.14%	5.83%	9	0.050
	SF1	55	9.29	7.29%	6.02%	10	0.047
	SF2	55	9.44	7.14%	5.85%	9	0.048
	SF2	45	9.24	7.41%	6.12%	9	0.048
East Coast UK	LA	57	8.37	6.80%	5.55%	8	0.057
	HU	52	8.42	6.93%	5.60%	8	0.060
North Sea West Coast DK	M8	47	10.79	7.44%	5.98%	9	0.034
	F3	50	9.65	6.74%	5.79%	10	0.037
	M2	45	9.18	8.34%	6.88%	9	0.052
North Sea (far offshore) >40 km	F1	50	9.31	6.32%	5.22%	10	0.038
	HO	46	8.79	6.46%	5.44%	9	0.044
	F3	50	9.65	6.74%	5.79%	10	0.037

Figure 4.10: *TI summary information for each mast at its nearest measurement to 50m. This information includes, from left to right: height, average wind speed, average TI, the minimum average TI, the wind speed bin in which this minimum occurs and lastly the average σ_{TI}*

It is interesting to note the similarity in the average turbulence intensities among sites within the four distinct regions that were crafted above. When considering all of the sites, the range of $\overline{TI}$ is only from 6.32% to 7.44% when excluding M2 (see figure 4.10). These values are a bit lower than the 8% observed by [28] at a height of 48m.

The next panel of plots (Figure 4.11) exhibits the change in TI_{90} versus $\overline{U}$ with height for four of the nine masts: F1, HO, M2, and M8. These four in particular were chosen to accentuate the differences between the uncharacteristic trends seen in M2 and M8, and the other seven masts as indicative in F1 and HO. The differences between the magnitude of the turbulence intensity between the top (F1,HO) and bottom (M2,M8) panels are rather significant and are discussed in the proceeding paragraphs.

In all, the turbulence intensity decreases with height as the distance from the water surface, the interface from which nearly all of the turbulence is generated, increases. The difference is accentuated with increasing wind speed as the mechanically-driven turbulence term dominates over the thermally-driven term.

Despite this, none of the masts have 90th percentiles that exceed even the lowest IEC standard apart from the exceptional and surprising case of M2. M8 also has values that exceed the Class C IEC standard, but this could once again be a result of the reduced 255-285 degree sector considered here.

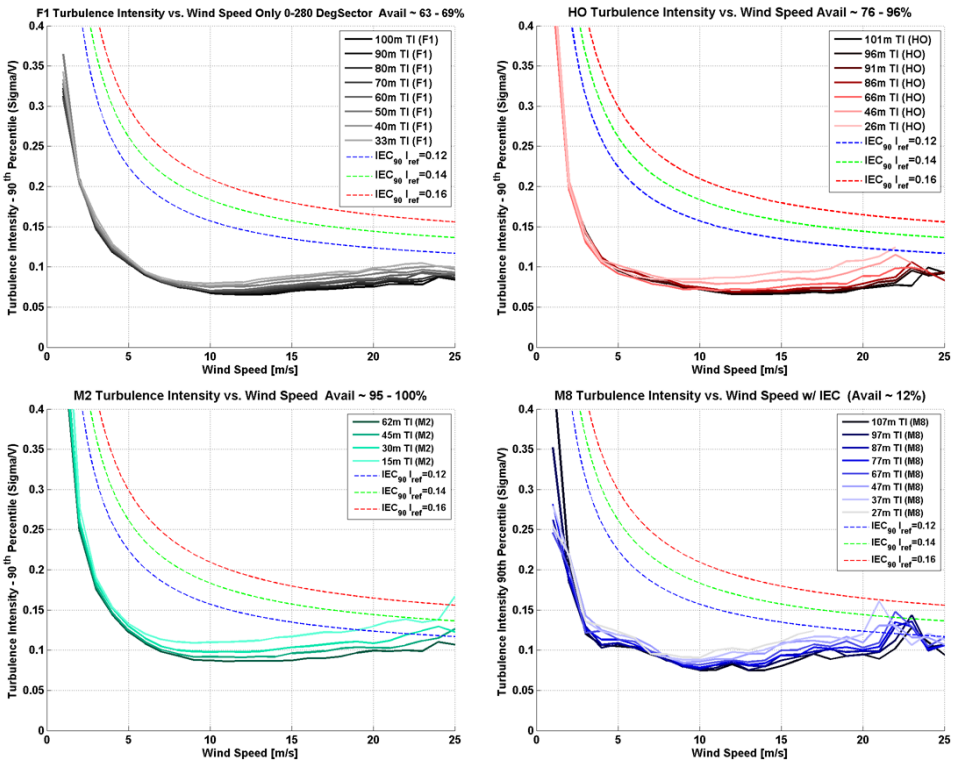

Figure 4.11: *Comparison of TI versus $\overline{U}$ for different heights at four of the masts.*

The wind speed in which the transition from thermal to mechanical turbulence occurs ranges between 8-14 m/s as discussed above and is highly dependent on height. The transition occurs at higher wind speeds at higher z. The respective one wind speed m/s bins in which the minimums in $\overline{TI}$ and TI_{90} are realized, and their respective values are detailed for the 50m heights in figure 4.10. For the other heights look to Appendix F where all of the turbulence statistics are listed. They reveal that the wind speed bin in which this transition occurs is also site dependent and could be related to each sites' stability and wave conditions (which dominates the flow regime). Additionally Appendix G displays the the $\overline{TI}$ vs $\overline{U}$ for the other 5 sites.

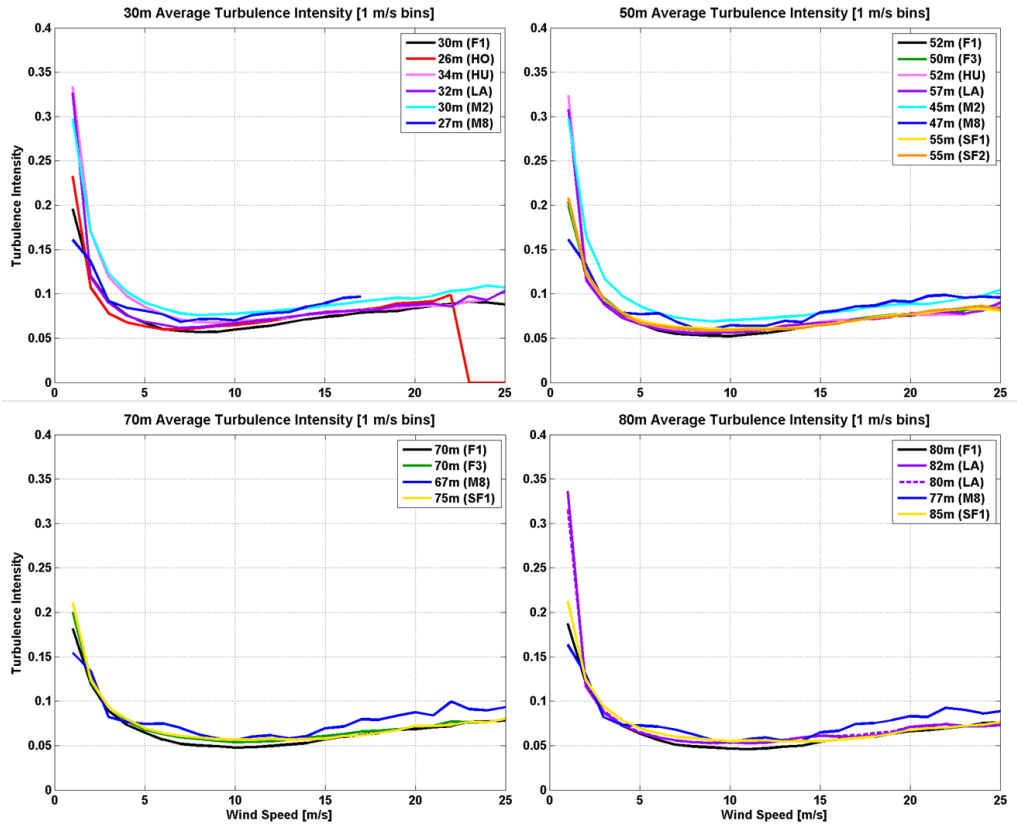

Figure 4.12: *Comparison of TI versus $\overline{U}$ for all masts at 30, 50, 70 and 80 meters*

Parallel to the similar plot of σ_U versus $\overline{U}$, TI versus $\overline{U}$ also is nearly independent of site on average for 50, 70 and 80 meters height (except M2,M8). This is especially true with wind speeds greater than about 14 m/s, where differences among the masts are are almost indistinguishable. For 30m, deviations do exist between the masts, especially at the lowest wind speeds.

Examination of the percentage change between M2, M8 and the average of the other masts (Figure 4.13) yielded very similar trends, and therefore explanations, to those seen with σ_U in figure 4.5.

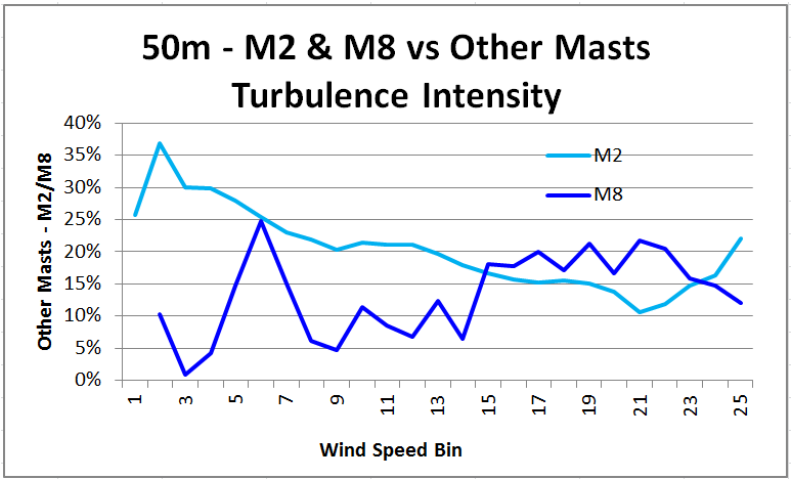

Figure 4.13: *Percent difference in turbulence intensity between M2, M8 and the average of the other masts at 50m*

4.1.5 σ_{TI} vs $\overline{U}$

The last two figures of this section (4.14 and 4.15) examine the relation between σ_{TI} and wind speed. Unlike TI, σ_{TI} continually decreases with increasing wind speed, which makes sense given the overwhelming dominance of mechanically driven turbulence with increasing $\overline{U}$, as discussed in the previous section. This can also be seen by the reduction of scatter in Figure 4.9 after 15 m/s where like discussed above, the friction stress breaks up any lingering stable layers.

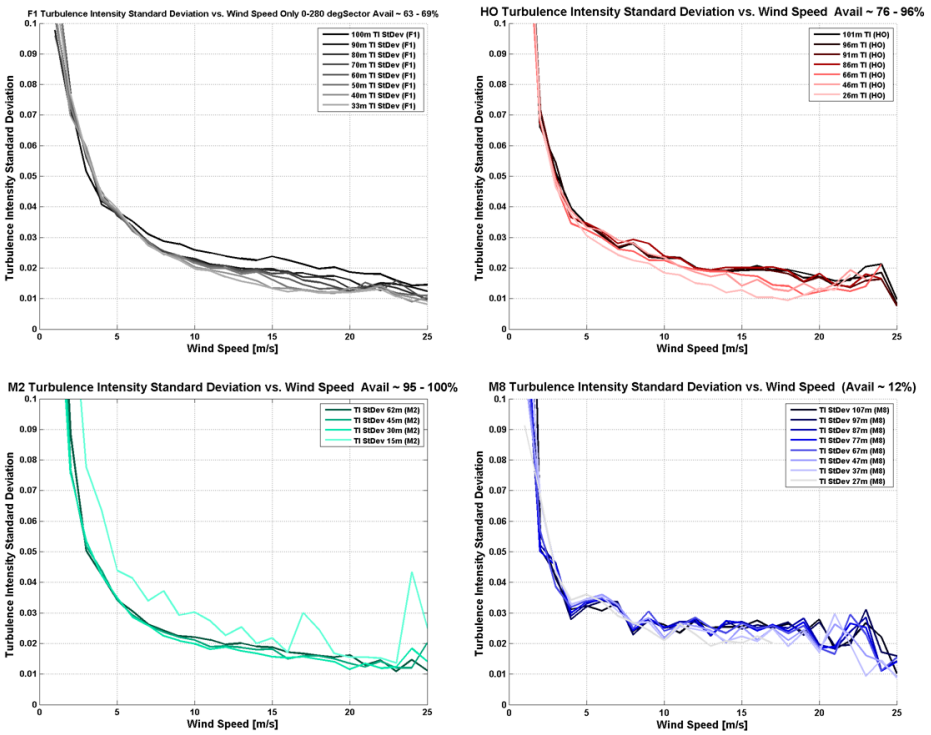

Figure 4.14: *σ_{TI} versus $\overline{U}$ for four of the masts*

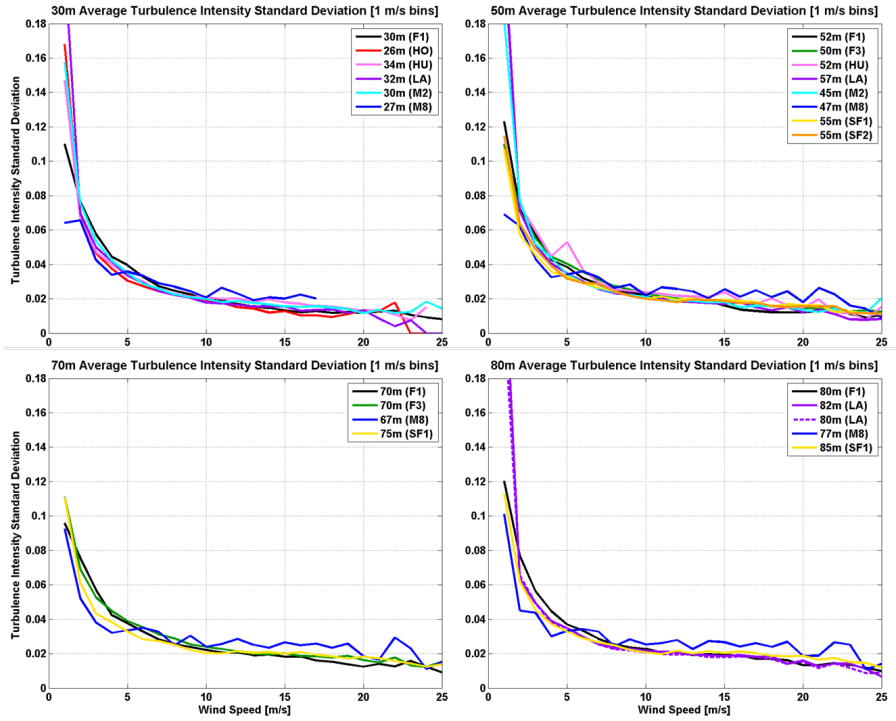

Figure 4.15: *Comparison of σ_{TI} versus $\overline{U}$ at all of the masts for 30, 50, 70, 80m*

4.2 Turbulence Parameters as a Function of Height (z)

Wind turbines have blade swept areas that traverse a large swath of heights, over which values of many parameters of interest to this study change. This section aims to examine how turbulence parameters vary with height and provide essential information that can be used by the wind energy industry when designing wind turbines to withstand these stresses.

4.2.1 σ_U vs z

Figure 4.16 illustrates the vertical profile of σ_U averaged across all wind speeds. The sites within the Irish Sea and East Coast UK regions have very similar profiles respectively. The sites further offshore in the North Sea and close to Denmark's Jutland peninsula differ more, such as HO, F1 and F3.

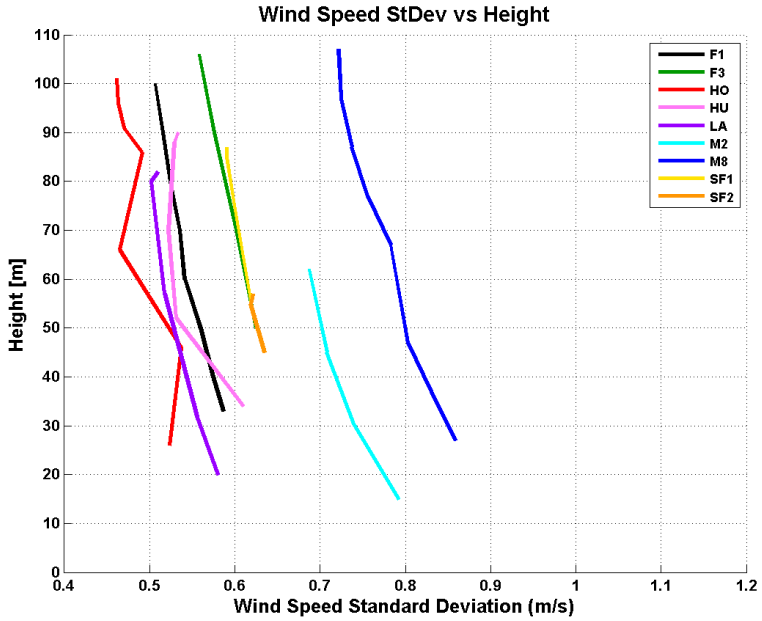

Figure 4.16: *Vertical profile of* σ_U

These differences at these far offshore sites are due to differences in average wind speeds between them as when looking at turbulence intensity, the profiles of these three far offshore sites are similar (see figure 4.12). It is noteworthy that σ_U is not independent with respect to height, when averaged across all $\overline{U}$.

Next, plots were generated for 2 m/s wide wind speed bins with bin centers from 2 to 16 m/s, in increments of 2 (the 6 m/s bin for example considers wind speeds of between 5.0 and 7.0 m/s). In figure 4.17 and all subsequent plots, only the 6 m/s and 16 m/s bins are displayed as they exemplify the characteristic differences between high and low wind speeds. When examining these plots it important to be conscientious of the turquoise and blue lines as they represent data from the uniquely-signaled M2 and M8 masts respectively.

Plotting this relationship in sorted groups of U revealed patterns that were untraceable when averaging across all U. In this figure, the change seen in σ_U between low and high wind speeds is apparent.

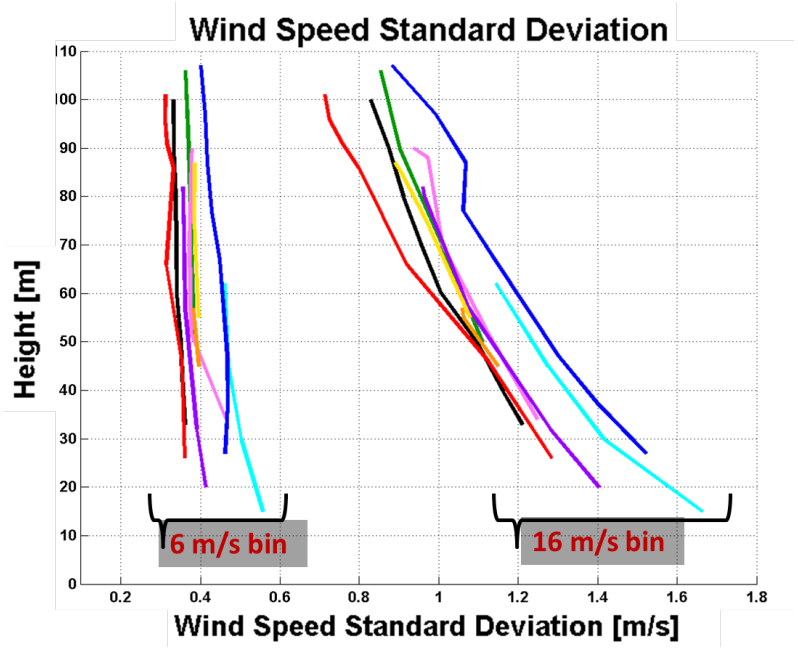

Figure 4.17: *Vertical profile of σ_U in slow and fast wind regimes*

At low wind speeds σ_U is nearly uniform and thus independent with height. This is attributable to the well-mixed thermally-driven turbulence that is dominant in these speed regimes. In contrast, at wind speeds of 15-17 m/s, the magnitude of σ_U increases at all heights but is significantly larger closer to the surface. This is a result of the mechanical wave-driven turbulence that is pervasive within high wind speed regimes and largest at the lowest heights. As the distance from the atmospheric-oceanic interface increases, the σ_U decreases as the flow therefore has less contact with the turbulent eddies generated there. Besides M2 and M8, the only other mast that separates from the pack is HO which has lower values within both wind speed bins, but especially at the highest heights at 16 m/s. This could be the consequence of dominating stability and wave effects at far offshore sites [33][34]

4.2.2 σ_{σ_U} vs z

A similar explanation of the trends seen can be applied to the σ_{σ_U} as portrayed in figure 4.18. At wind speeds of 5-7 m/s, the dominance of thermally-driven turbulence creates a convective mixed-layer where similar conditions are observed across all heights. For large wind speeds σ_{σ_U} increases with height as the pervasiveness of turbulence generated at the atmospheric-oceanic interface becomes more variable.

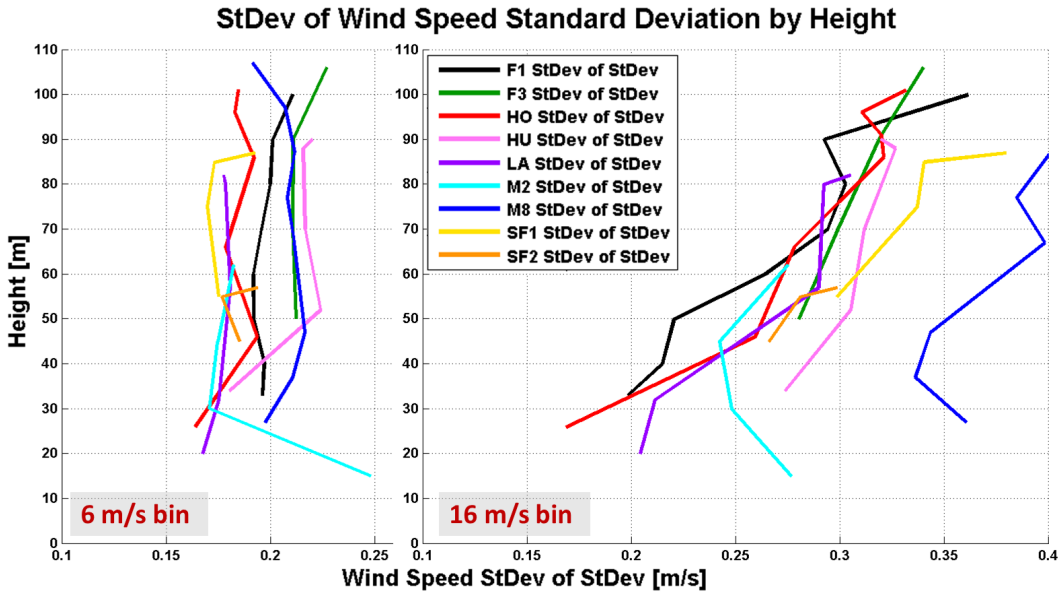

Figure 4.18: *Vertical profiles of* σ_{σ_U}

4.2.3 TI vs z

When examining profiles of $\overline{TI}$ between the sites (figure 4.19), it is revealed that there are strong similarities among masts within each of the four regions. Additionally, the TI profiles are mostly logarithmic with height as is ascertained by figure 4.20.

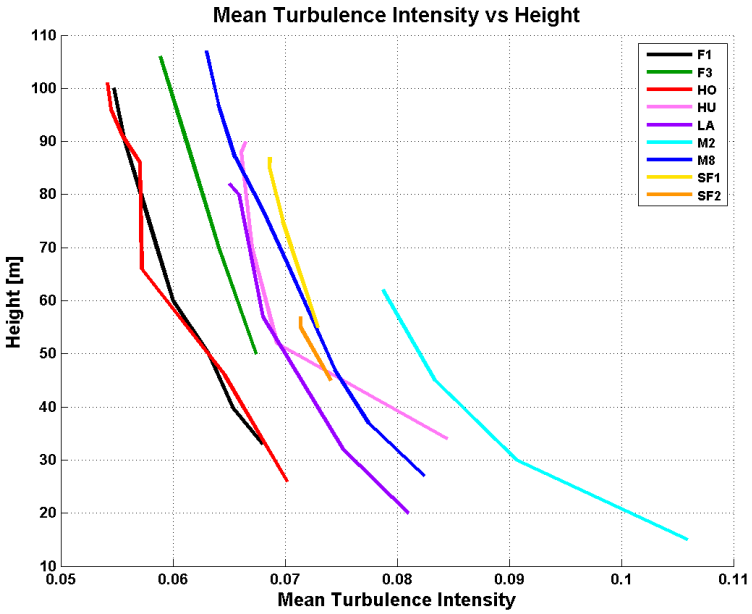

Figure 4.19: *Vertical profiles of TI*

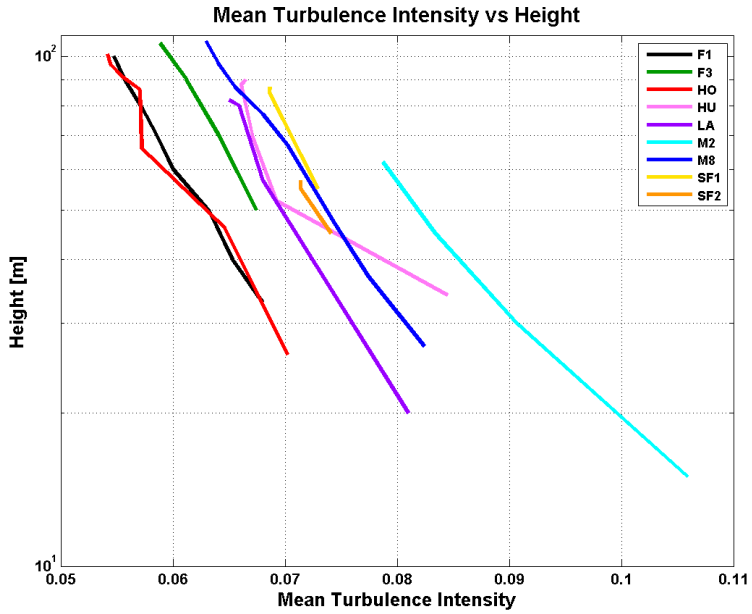

Figure 4.20: *Vertical profiles of TI in a semilog vertical axis*

The difference in TI versus z between low and high wind regimes is more subtle than that of σ_U, but exists nonetheless (figure 4.21).

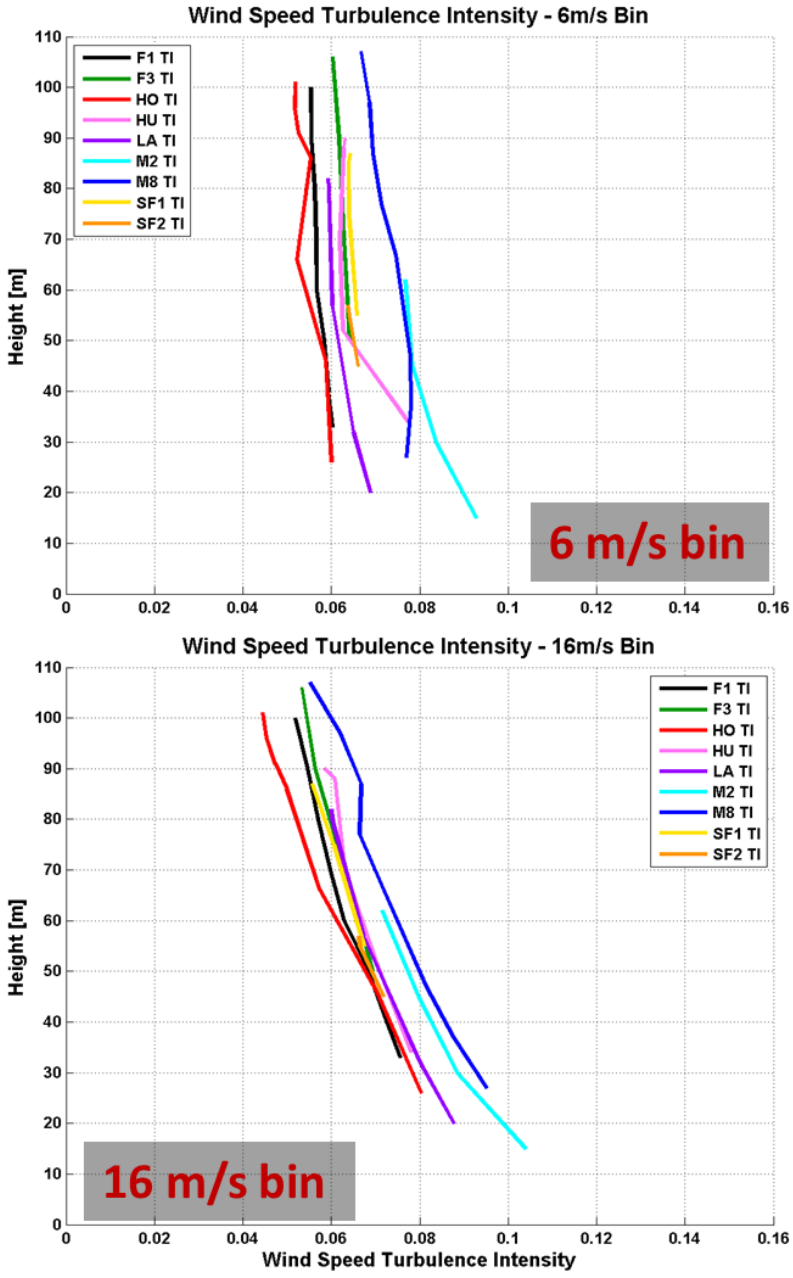

Figure 4.21: *Vertical profiles of TI in slow and fast wind regimes*

In the low wind speed regime turbulence intensities are rather uniform with height while in higher wind regimes they decrease more rapidly with height. These differences can be seen by re-examining figure 4.11 and looking at the vertical spacing between the lines at wind speeds between 5 and 7 m/s and then again between 15 and 17 m/s. The spacing is much larger at the higher wind speeds, which matches the ideas presented here. Aside

from M2 and M8, the HO mast does seem to have potentially significant differences in its turbulence intensity trend at higher heights and in the high wind regime. This is also portrayed with the even larger spread between the lowest and highest value of TI in figure 4.11. Once again this could be the result of the strong effects of stability and waves at far offshore sites.

The similarities of TI among sites within the same regions show even more similarities than when looking at σ_U. This is especially the case with the far offshore sites F1, F3 and HO.

4.2.4 σ_{TI} vs z

The variability of turbulence intensity (σ_{TI}) describes the spread of the various scatter-points around the TI mean. It is interesting and important to point out that for the most part that σ_{TI} does not have a significant dependence on height (figure 4.22) but has a much stronger dependence to wind speed (figure 4.23).

With these data it seems to be that there is a relationship between the profiles of σ_{TI} and fetch and distance to shore. The highest σ_{TI} occurs at HU and LA which are both less than 10 km from the East Coast of the UK where the predominant wind direction is from land-based sectors. The next highest are at SF1 and SF2 which are between 10 and 15km off the West Coast of the UK where the prevailing wind direction is from sea-sectors, though with limited fetch.

The lowest variation of σ_{TI} occurs at the far offshore masts which leads to the belief that on average that the coastal continuity exerts a greater influence on the variability of turbulence than at the far offshore sites. Among these though, HO does not match closely which could be due to it being the furthest from the nearest land at 110 km. Fetch dependencies are discussed in more detail the forthcoming directional dependency section (Chapter 4.3).

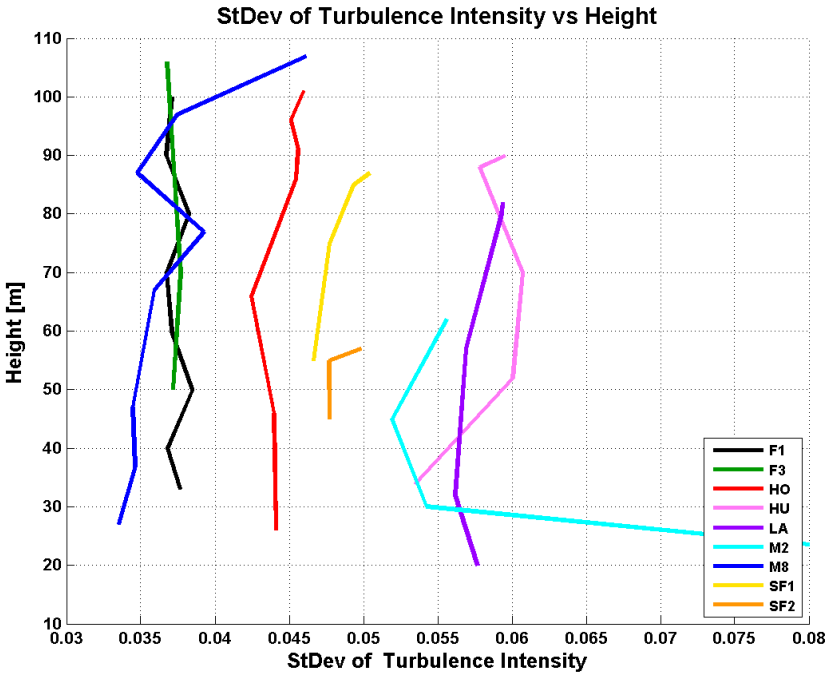

Figure 4.22: *Vertical profile of* σ_{TI}

When plotting σ_{TI} compartmentalized into different wind speed bins, the relationship between the masts becomes indistinguishable (Figure 4.23). It is observed though, as expected, that σ_{TI} decreases with increasing wind speed. This makes sense given that at higher wind speeds, it is harder for the thermal induced stability to hold out over the increasing mechanically generated turbulence [11]. This also once again detectable by revisiting figure 4.9 where it is seen that the minimum TI yellow scatter points begins to increase from around zero after about 15-20 m/s, depending on height [11].

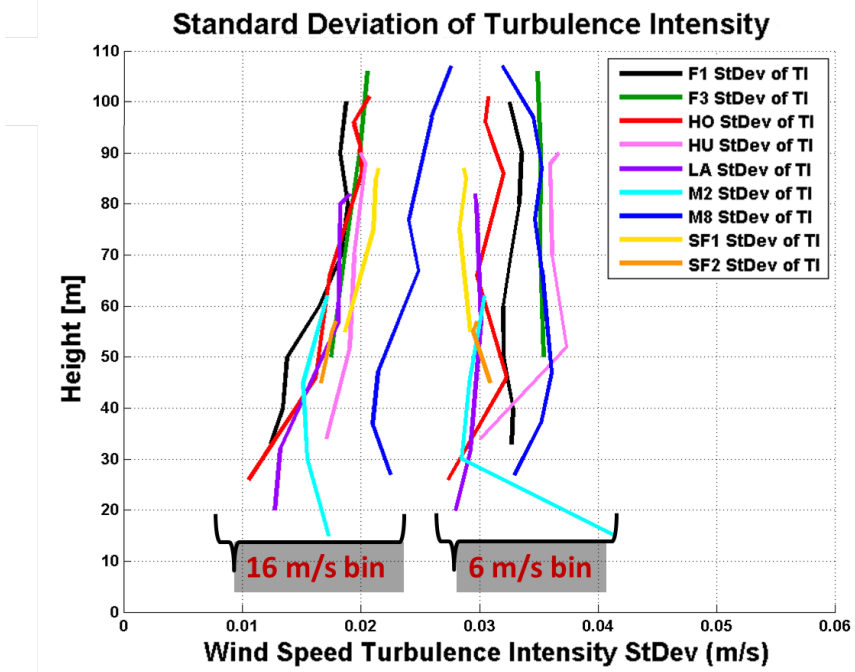

Figure 4.23: *Vertical profile of σ_{TI} in slow and fast wind regimes*

4.3 Directional Dependencies of Turbulence Characteristics

The purpose of creating these plots of σ_U and TI versus wind direction (θ) is to analyze any dependency of wind direction on turbulence intensity and therefore dependency on fetch. Only the TI plots are discussed here; the σ_U plots appear in Appendix H. The directional dependencies on TI were found here to be highly dependent on region, but rather similar within the regions. This is due to influences of the local meso-scale meteorological conditions and geographical details. To show the differences between regions and similarities within regions, plots of TI vs θ are generated for each mast.

The plots show the average turbulence intensity value per 3 degree wind direction sector for each height on the mast. Darker color indicate higher heights and lighter colors, lower. The secondary y-axis, values given by the dotted black line, dictates the number of data points that are used within each sector to calculate the respective TI values. This metric helps gauge the level of confidence of the findings. Lastly the colored bars at the bottom of each figure gives the fetch range to the nearest land mass. A detailed description of what fetch each of the colors corresponds to is detailed in figure 4.24.

Figure 4.24: *Legend for forthcoming plots displaying what fetch the various colors at the bottom of the plots correspond to.*

The blue based colors indicate fetch greater than 50 km, while the brown/orange colors note fetch of less than 50 km. The darkest brown dictates the range of the wind directions with the shortest fetch, a distance noted by the white numerical value.

Many similarities were found on the directional dependencies of TI between masts within the same regions. Therefore the following subsections (4.3.2 - 4.3.5) will be separated into the four regions. But before going into the regional analysis, a quick general proximity to land / fetch analysis is performed.

4.3.1 General Fetch Analysis

Before examining each site individually, a plot was made that compared the distance to the nearest land, or fetch, at each mast, to its' average turbulence intensity (taken from figure 4.10) at its near observation to 50m (figure 4.25).

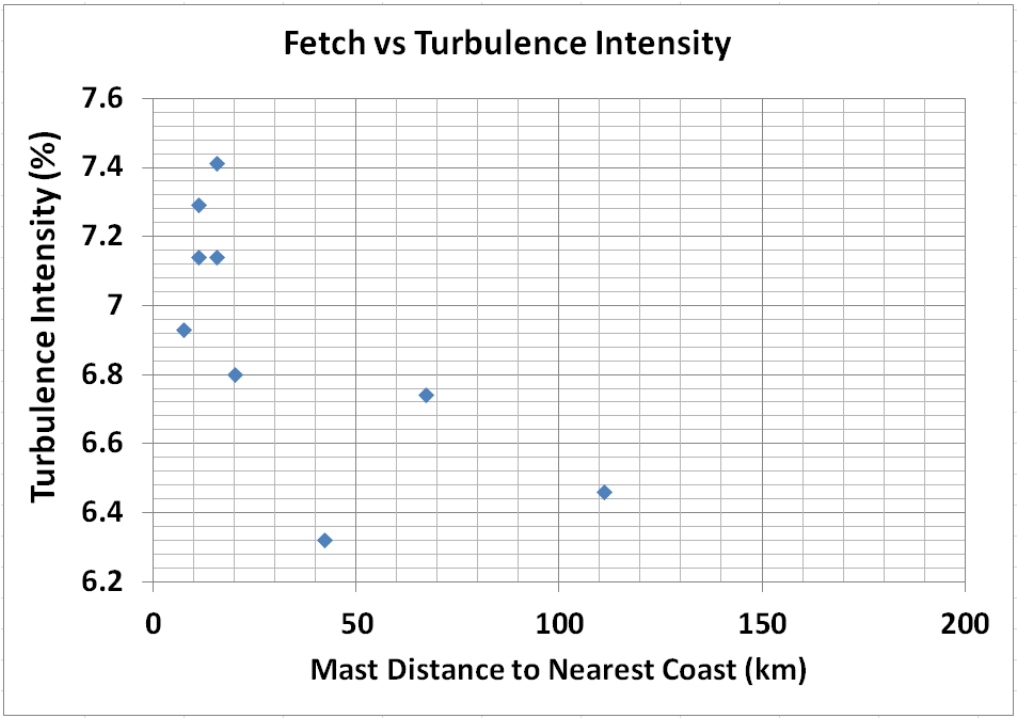

Figure 4.25: *Fetch versus average TI at each of the sites. Most of the decrease in TI with increasing fetch occurs in first 40-50km and thereafter it rises some.*

As discussed in chapter 2.7, it can be seen that most of the decrease in turbulence intensity as a result of coastal effects is realized within the first 15-40 km. Interestingly though, as was pointed out by [33], there is a certain distance from the coast beyond which turbulence intensity begins to increase again. The analysis within the next four sections agrees with this. Especially at sites that are further from the coast, or do not have sectors with fetch larger than about 200 km, the turbulence intensity is largest in the offshore sectors.

4.3.2 Far Offshore Region: F1, F3, HO

The first plot here shows the TI at F1 within 3-degree wide sectors of wind direction, encompassing all wind speed bins (Figure 4.26). It was surprising to find that there was slightly lower TI with sectors with flow from land. At first thought, given that turbulence intensity is generally higher over land, it would have been expected for these land sectors to have higher TI. Previous studies have noted that while the effects of the coastal discontinuity can be felt as far as 100-200 km out from the coast in very stable conditions, most of this influence is felt within about 15-20 km [28][31][32].

This plot also shows that large fetch within this region is associated with higher turbulence intensity, meaning that wave height plays a very important role in turbulence generation. For example, [33] found that in the short fetch sectors at F1, the wave height was much less than in the longer fetch sectors (nearly half).

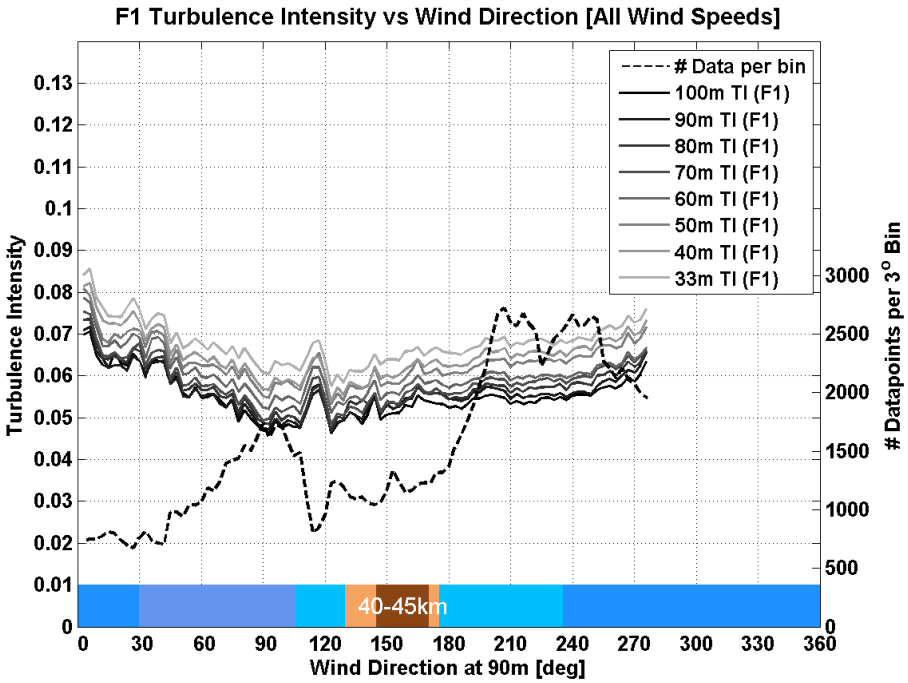

Figure 4.26: *TI versus θ at F1. TI is slightly lower in land sectors.*

Figure 4.27 assesses the same relationship at F1 but groups for different wind speed bins. The 5-7 m/s and 13-15 m/s bins are chosen to spotlight the disparities that are hidden when examining the plot that includes all wind speeds. As is clear, there is little variation of TI with height at low wind speeds, whereas at high speeds the change with height is indisputable, especially in the eastern wind sectors where the TI at 33m is more than twice the value of the top 100m observation. This also corresponds with the the eastern sector which is closest, at 40-45 km, to land.

Therefore, given that highly stable conditions often suppress turbulence, it is possible that this is one of the reasons for the dip in TI at F1 from the land sectors in high

wind regimes, especially at higher heights. Very shallow stable layers could be occurring, especially in instances of warm air advection in the spring, leading to an inversion layer and thus decoupling of the surface flow to the air higher aloft.

Lower wave heights as a result of very small fetch [33] in the eastern sectors could also be responsible for the lower turbulence intensity, though if this were the case it would be more likely for all heights to exhibit this dip (not the case in the bottom plot of Figure 4.27 where at 33m, the TI is nearly constant with wind direction).

An analysis further categorizing the data into seasons and stability classes should be performed in the future to confirm these two explanations. It is be expected that stable conditions would prevail in the spring, and unstable in the fall.

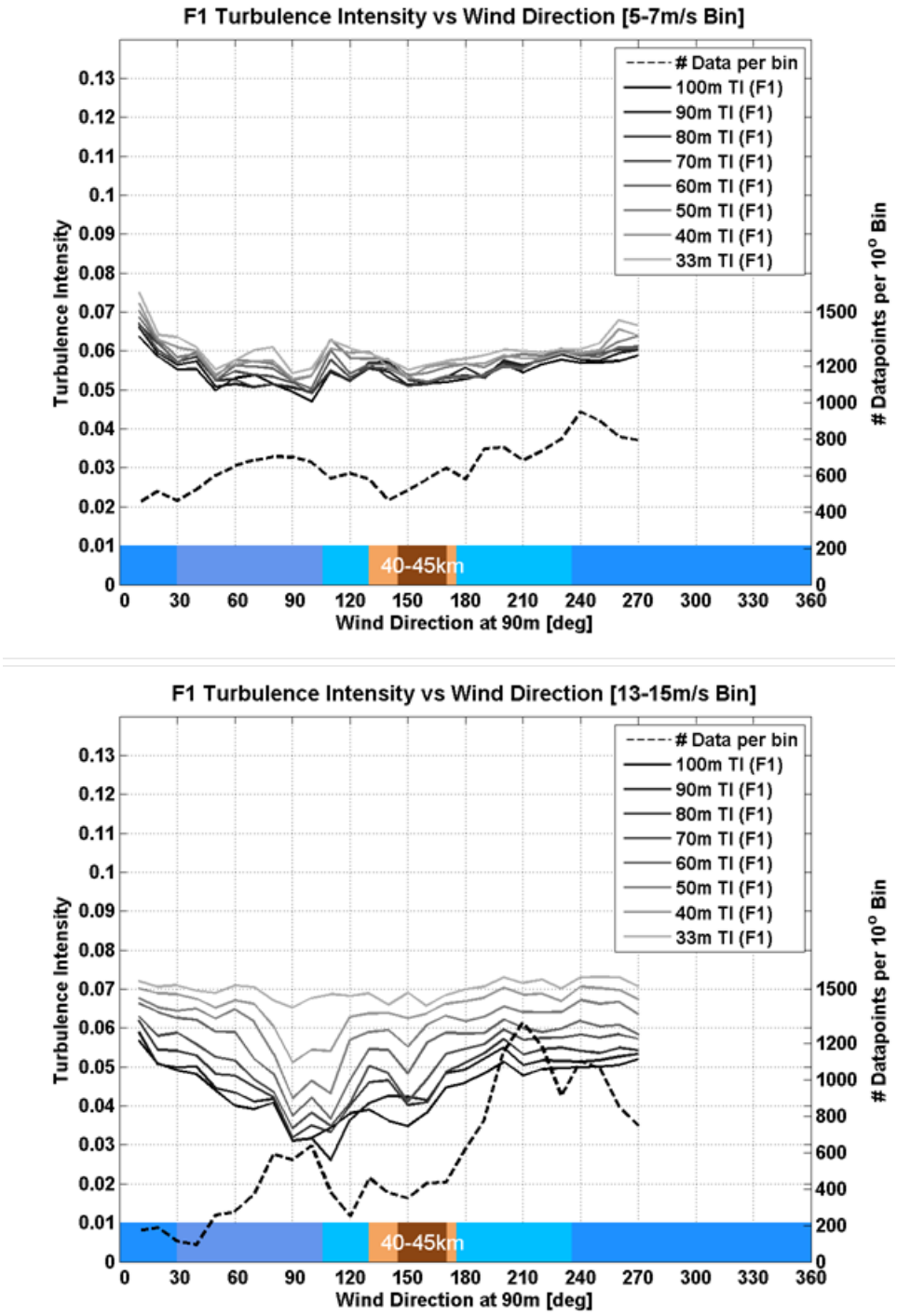

Figure 4.27: *TI versus θ at F1 for low and high wind speeds. TI varies more with wind direction in fast regimes and also at the highest heights.*

In contrast to F1, F3 does not have as stark a visible dependency of wind direction on TI (figure 4.28). There appear to be two relative peaks in the TI curves; one in the northeast sectors and the other in the northwest sectors. Even more interesting is the

dependence that these peaks have on wind speed. At low wind speeds the peak in the northeast sectors is dominant while at high wind speeds the opposite is true. Additionally, at intermediate speeds, the distribution of TI with wind direction is rather uniform with no distinct peaks. This also points to the differences between the sources of turbulence generation within different wind regimes. At lower wind speeds, stability affects dominate therefore making the peak in the closer-fetched northeast sector likely due to very unstable or very stable conditions. The very unstable conditions would likely arise from cold air advection over the warm water surface whereas highly stable conditions would develop from warm air advection. Normally stable conditions suppress turbulence but it is possible to have a low-level jet associated with the presence of an inversion. Conversely, within the high speed regimes, wave-driven turbulence dominates and provides reasoning for the northwest peak, where fetchs' are the largest.

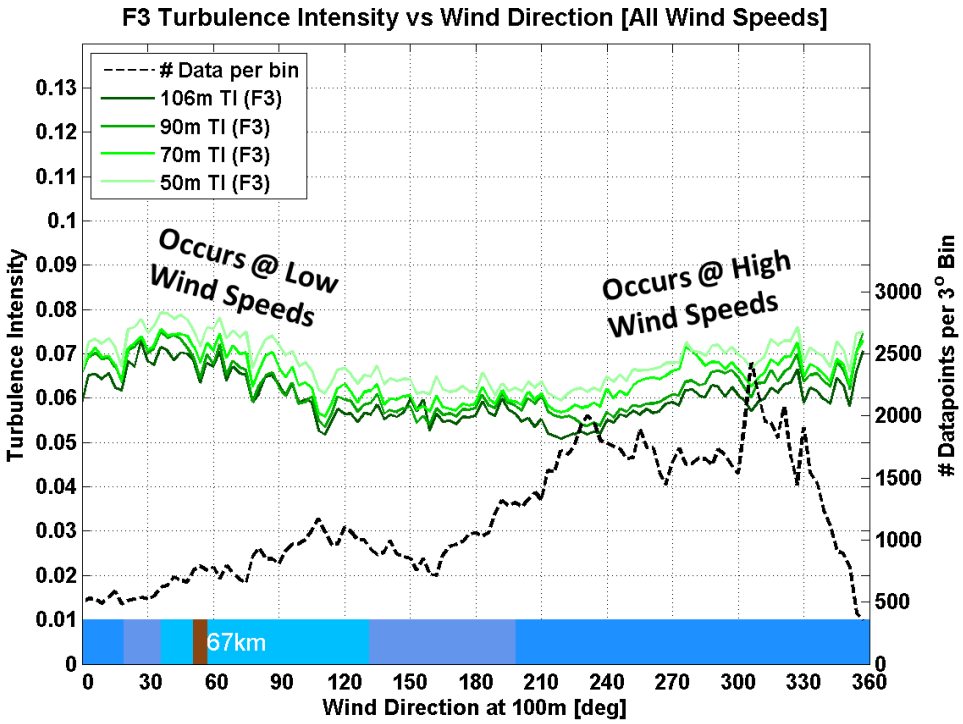

Figure 4.28: *TI versus θ at F3. There are two peaks one that occurs at low speeds and the other at high speeds, the first likely corresponding to stability effects from the coastal continuity and the later to wave-induced mechanically-generated turbulence*

HO, the site furthest from the nearest landmass, has similar signatures to F1 and F3 (figure 4.29). The largest turbulence intensity is observed when fetch is greater than 200 km and additionally is where the most bin-to-bin fluctuations in TI with wind direction are observed.

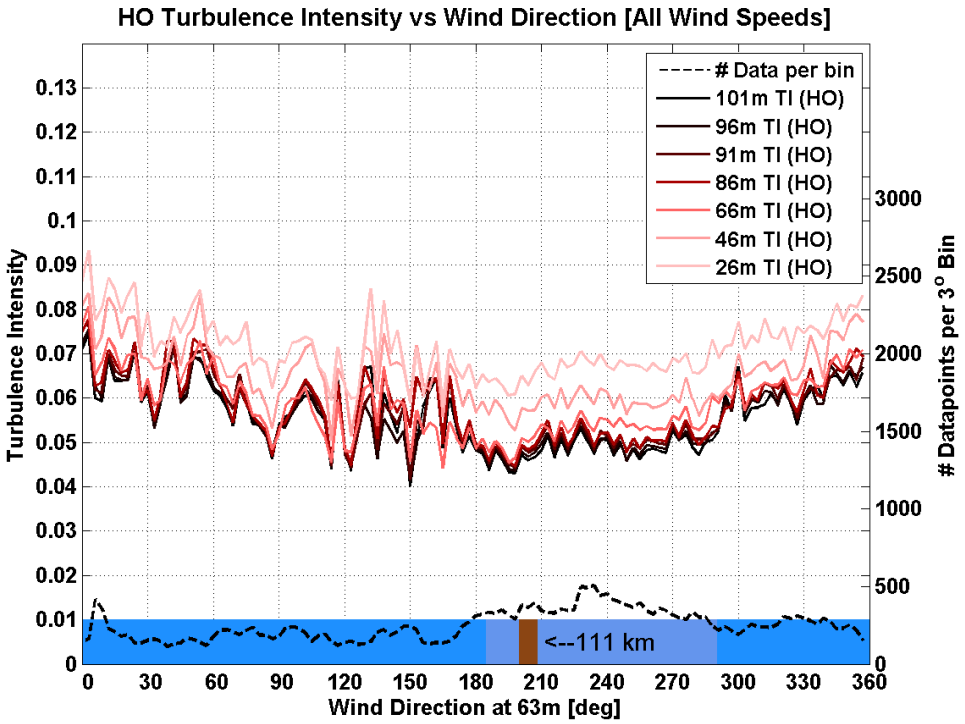

Figure 4.29: *TI versus θ at HO. Marginally lower TI in the sectors with the smallest fetch.*

To probe further into the dependence of TI on wind speed and wind direction together, polar plots were created that portray wind speed on the radial axis and wind direction in the azimuth. The filled-in colors represent TI. The general characteristics observed in section 4.1.4 with the TI vs $\overline{U}$ curve, are apparent with the minimum TI value occurring generally between 8-14 m/s, depending on height.

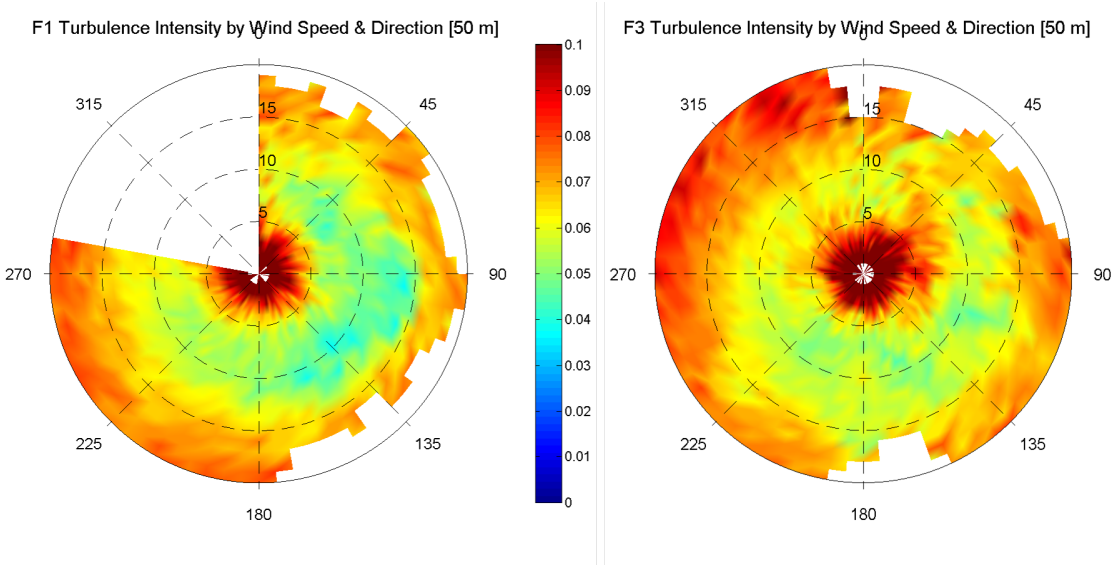

Figure 4.30: *Polar plots that show TI as a function of θ and $\overline{U}$ for F1 and F3. Along with HO in the next figure, they are very similar. It is easy to see the minimum of TI at wind speeds of between 8-14 m/s. TI is higher in the sectors with the largest fetch.*

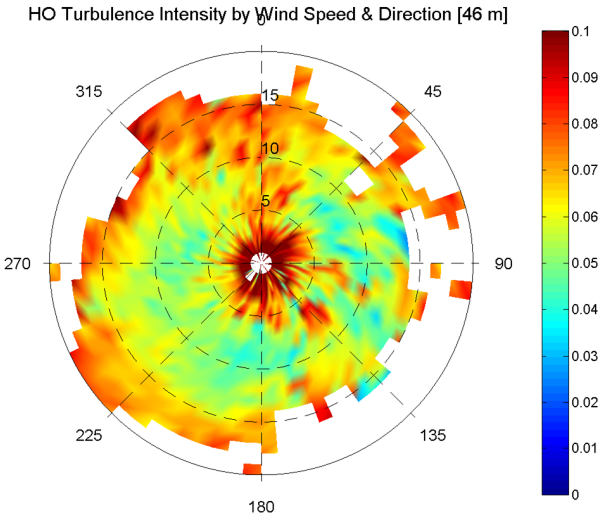

Figure 4.31: *Polar plot that shows TI as a function of θ and $\overline{U}$ for HO. TI is marginally higher in the sectors with the largest fetch.*

All three of these polar turbulence intensity plots (figures 4.30 & 4.31)point to the aforementioned finding that turbulence intensity at far offshore locations, especially in high wind regimes, is largest in the sectors with the largest fetch and vice versa.

Note that all of the polar plots in this and the coming subsections are for the heights nearest to 50m, to make direct comparison easier. The polar plots for all of the heights appear in Appendix I.

4.3.3 East Coast UK Region: HU, LA

The two sites in this region have the lowest average wind speeds among the nine masts but have average TI that are larger than the further offshore sites. This is intuitive given their close proximity to land.

Figures 4.33 and 4.34 show TI versus wind direction for the HU and LA masts respectively. Both are located within 20 kilometers of the shore. Examination of these TI-θ relationships proved very interesting, as there are both onshore and offshore sectors that yield the lowest TI values. Just like fetch over water is an important metric, onshore fetch seems to be important as well. Onshore fetch meaning how much distance is covered over land in a specific sector before reaching water again. On a larger geographical scale, this eludes to the effects of the general coastal orientation.

The turbulence intensity at these two sites are maximized within sectors that fall under any of these criteria:

- Where fetch is greater than 100 km
- Where the presence of sea/ocean is much more common than land when considering outward distances of around 500km. Refer to the yellow dotted line on the map in figure 4.32. In the land sector to the east of this line, this criteria is fulfilled.
- Where there are mountains ranges with elevations of greater than 2,000 feet or 600m within 150 km of the mast. The magenta circle on figure 4.32 represents this 150 km arc.

Coversely, the lowest TI occurs in sectors where none of the above conditions are met.

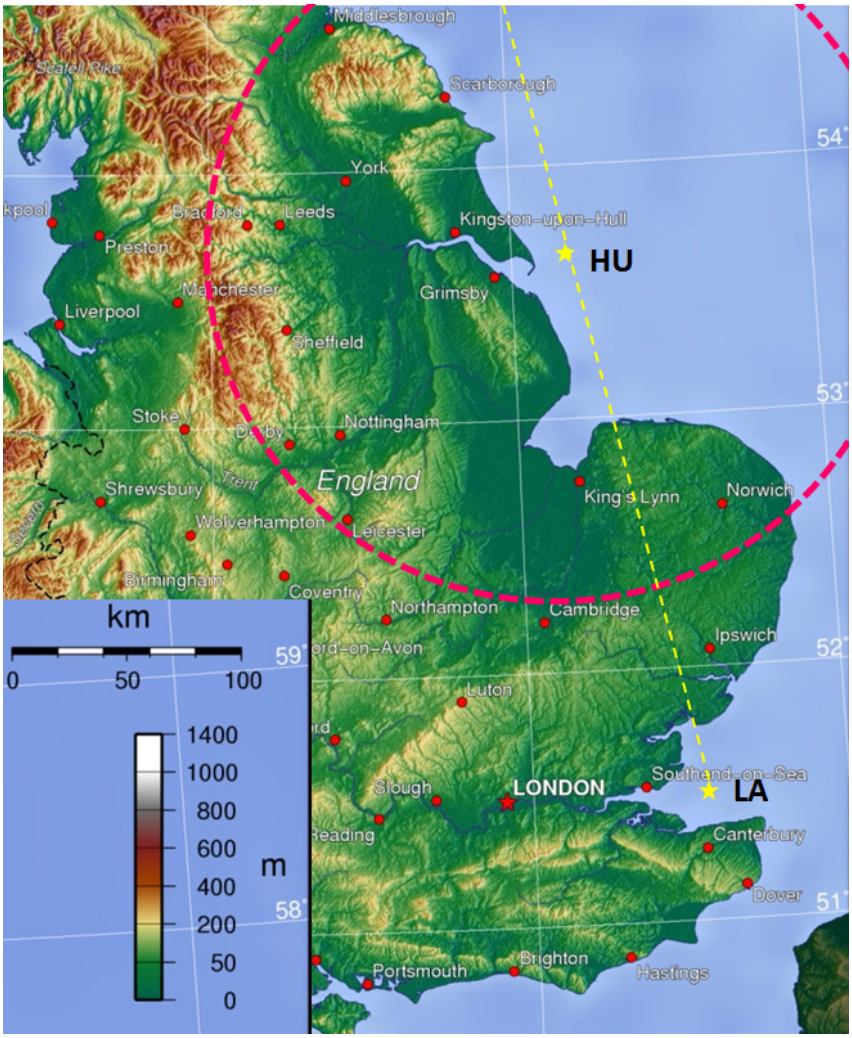

Figure 4.32: *Map of the two east coast of UK sites: LA and HU that show two of the three criteria that described sectors with the largest turbulence. The first (yellow line) is rrelated to the coastal orientation, where east of this general coastline largest TI are realized despite local proximity to the coast. The second (maroon circle) describes the increased TI when there are mountains higher than 600m within 150 km. The third criteria is when fetch is greater than 100 km and is not displayed on the map. (GNU free documentation)*

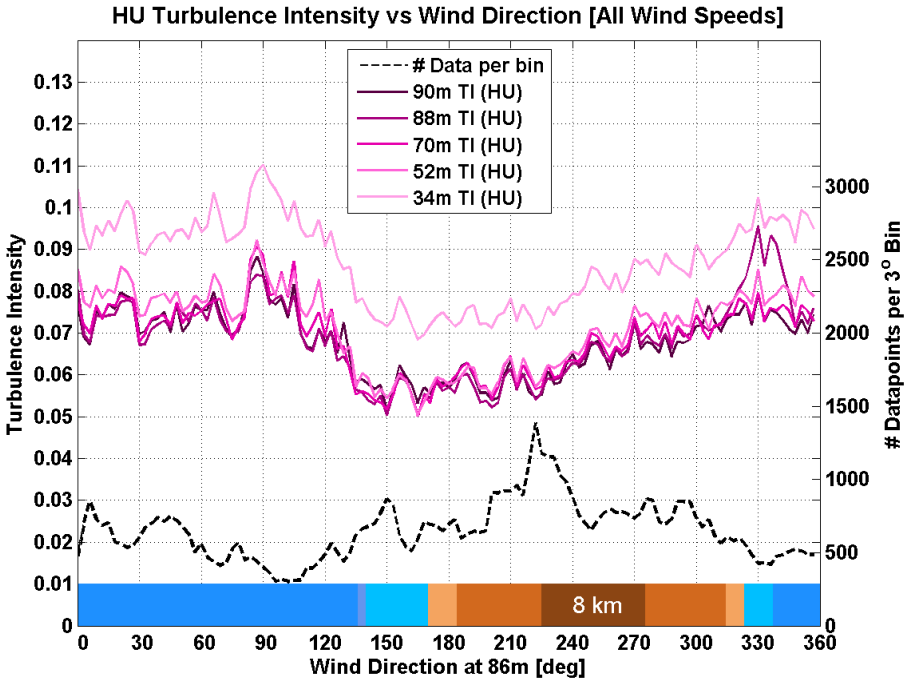

Figure 4.33: *TI versus θ at HU. TI is at its largest when fetch is greater than 100km or in the sectors with mountains taller than 600m within 150km.*

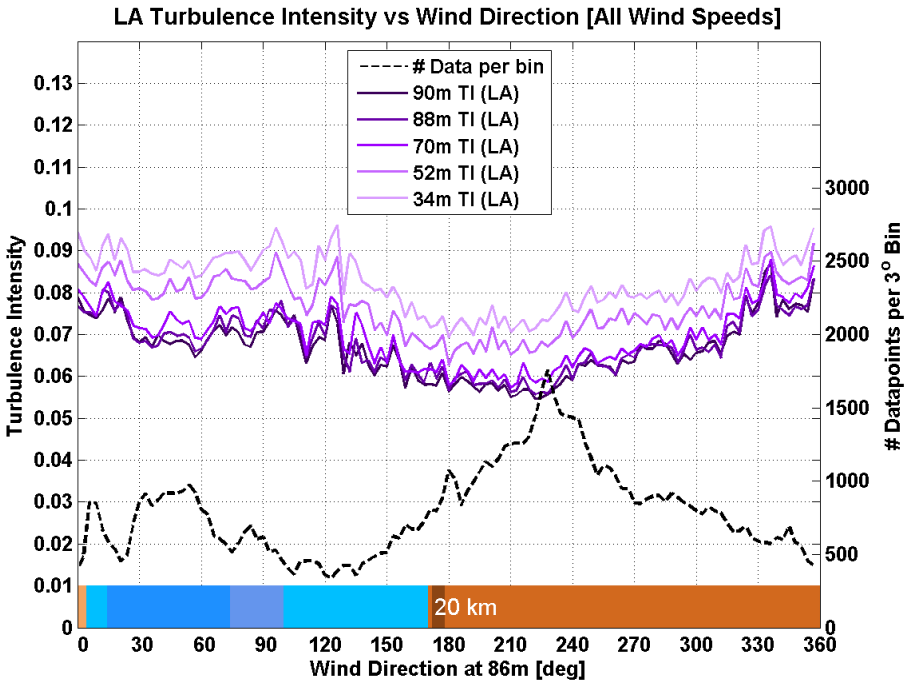

Figure 4.34: *TI versus θ at LA. TI is at its largest when fetch is greater than 100km or in the sectors which are east of the general UK east coast coastal orientation.*

While specific, these findings go in tandem with those from the far offshore region but also show that coastal orientation and type of orography inland play an critical role in dictating the characteristic turbulence climate. The polar plots for HU and LA are displayed below in figure 4.35.

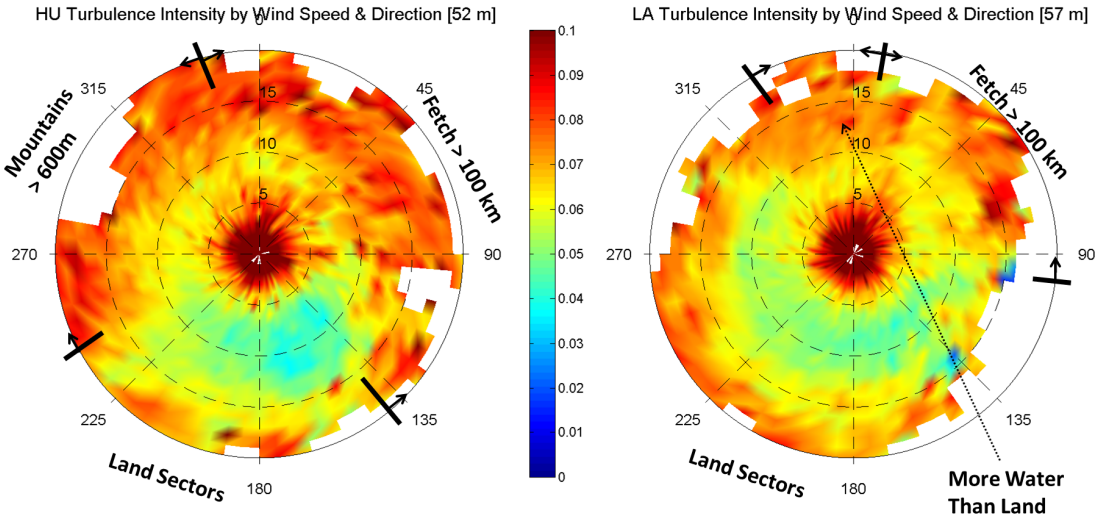

Figure 4.35: *Polar plots that show TI as a function of θ and $\overline{U}$ for HU and LA. TI is lowest in land sectors except for those with tall mountains in the proximity or those east of the general UK coastal orientation.*

4.3.4 Irish Sea - West Coast UK Region: SF1, SF2

Excluding M2 and M8, this region ties with the far offshore North Sea region for the largest average wind speeds. But to the contrary, it also has the highest average turbulence intensities. In comparison with HU and LA on the opposite side of the United Kingdom, SF1 and SF2 have higher average wind speeds and turbulence intensities.

Through examination of figures 4.36 and 4.37 it is clear that TI does vary with wind direction at SF1 and SF2 though no simple and strict dependency on fetch was realized. There are no sectors at either of these sites that had open fetches of greater than 200 km and less than 20 percent had fetches greater than 100 km, the threshold above which turbulence intensity reached its maximum value in the two previously analyzed regions. Therefore it can be concluded that the mechanisms causing these peaks are not expected to be as distinct within this region.

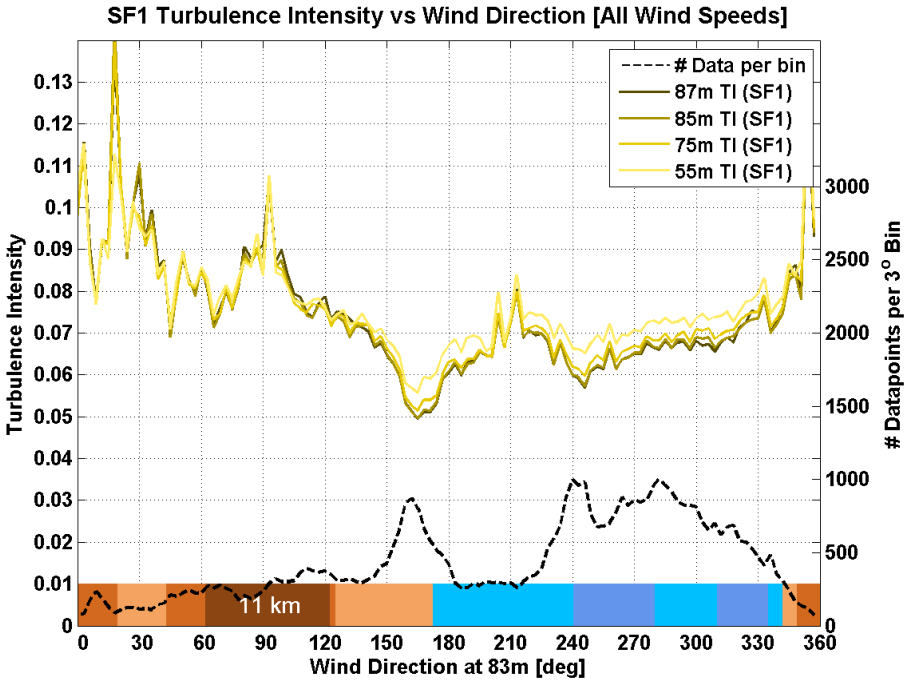

Figure 4.36: *TI versus θ at SF1. TI appears nominally larger over land sectors but these differences are harder to distinguish when examining the same figure in different wind speed bins.*

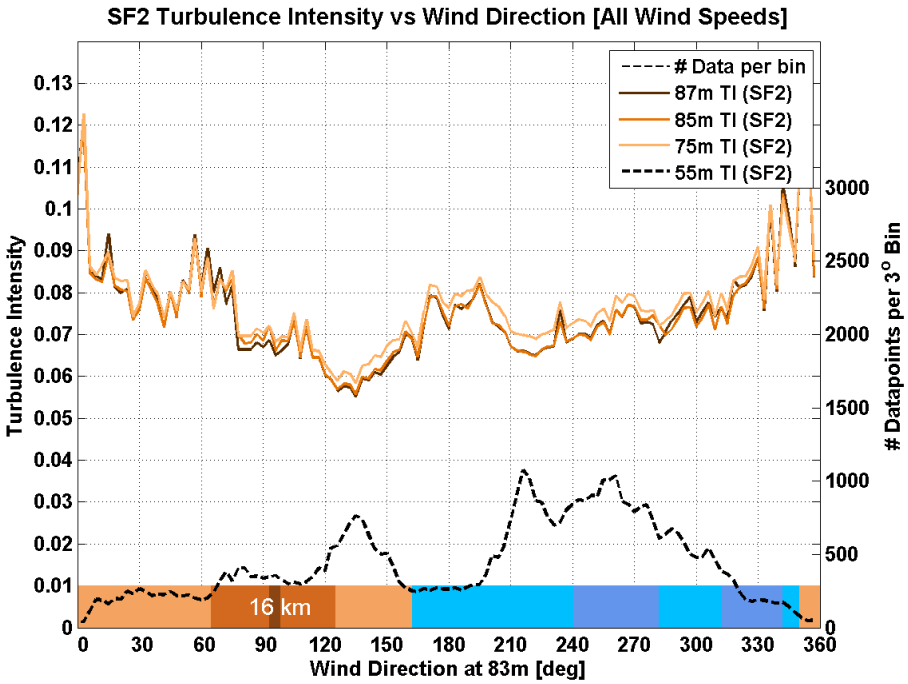

Figure 4.37: *TI versus θ at SF2. TI appears marginally larger over land sectors but these differences are less pronounced when examining the same figure in different wind speed bins.*

Neutral conditions do not occur incredibly often in the offshore environment leading to the belief that the MABL is often either stable or unstable, likely due to the seasonal air-sea temperature differences [18][19][36]. Studies that have specifically focused on SF1 and SF2 found a similar result, but one that is skewed more towards unstable conditions. Studies performed at these sites found that the conditions at these sites were unstable or very unstable approximately 75% of the time, especially the case at wind speeds up to 14 m/s [18][19]. These unstable conditions are understood by the higher average turbulence intensity in this region.

When comparing the polar plots (figure 4.38) there are two features that warrant attention. The first is the polka-dotted pattern of higher and lower turbulence intensities seen throughout and the second is the significant difference in values between the masts within the 45-135 degree and 5 to 15 m/s sectors (see bold section on right half). Despite being a mere 6.5 km from each other they display strong differences in TI, especially within this sector. This would not be expected given the predominance of unstable conditions and therefore strong atmospheric overturning and mixing. To gain a more concrete understanding, other factors must be examined such as stability and time of year, metrics that were not assessed in this thesis.

It is interesting to note though, at wind speeds greater than 15 m/s, when near-neutral conditions are more common, the TI between the two masts are very similar, especially in the western sectors where the largest fetch is realized (see bold section on left half) [18][19]. To fully understand the dominance of fetch and stability on TI at these sites, the analysis mentioned above should be done in the future.

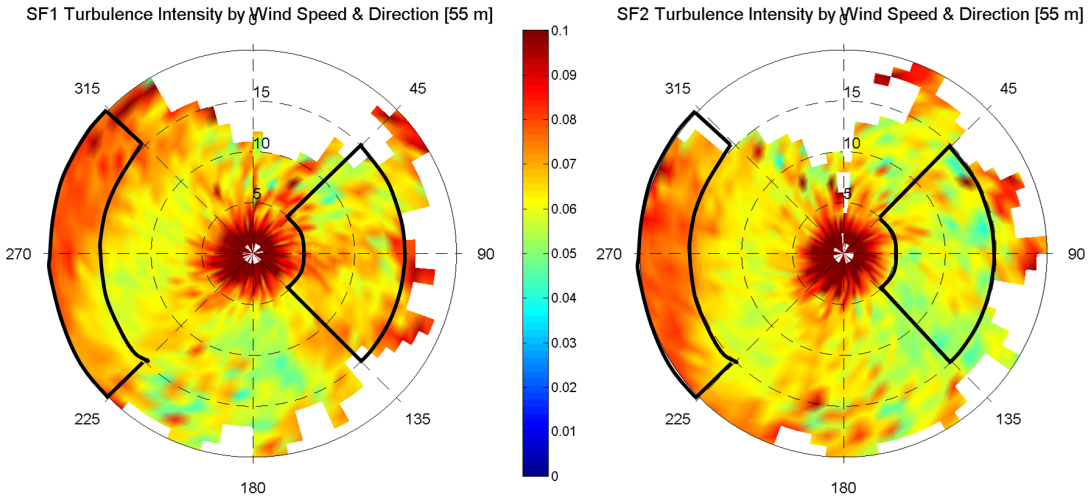

Figure 4.38: *Polar plots that show TI as a function of θ and $\overline{U}$ for SF1 and SF2. The two masts are in agreement at high wind speeds in the sector with the largest fetch (bold sector in west). Despite the masts' 6.5km proximity to each other, there is strong disagreement in the shortest fetch sectors (bold sector in east)*

4.3.5 West Coast Denmark: M2, M8, F3

This last region includes the remaining masts M2 and M8 which are located 18 and 36 km west offshore from the Jutland peninsula of Denmark respectively. Despite F3 being twice a far offshore as M2 and therefore considered to be in the far offshore category, it is re-examined here for comparative purposes given the large differences seen between M2, M8, and F3 despite their close proximity to each other (all within 55 kilometers).

The summary table of the turbulence and wind characteristics at these sites is given at the bottom of figure 4.10 and shows the significant differences between the masts. For M8, as discussed earlier, it is suspected that these discrepancies are the result of the significant wind direction filter that was applied in order to only consider the non-waked (from the Horns Rev II Wind Farm) flow. Consequently, this free stream flow (255-285 degrees) has a fetch of much greater than 100 km and thus given the previous analysis, can be expected to have the largest turbulence intensities and also the largest average wind speed (as is observed). The restrictive sector filter hinders development of a directional comparison between M8 and M2. As a result, M8 will not be discussed further in this section.

Instead, focus will be centered on the unexpected differences between M2 and F3. The explanation for the uncharacteristic difference between the two are unlikely the result of complex atmospheric dynamics present in this region. Both sites have very similar fetch values, and are far enough from the coast to avoid the strongest effects of the coastal discontinuity, as discussed in chapter 2.7.

Therefore, I postulate two potential explanations for the deviations between M2 and F3. The first is related to the North Atlantic Oscillation(NAO), an atmospheric teleconnection that dictates the majority of the interannual variability in synoptic weather conditions in North America and Europe. The data from M2 were taken between 1999 and 2001, years with strongly positive NAO, while F3 data were collected between 2010 and 2013, years with a slightly negative average of NAO.

The second hypothesis is based on the slim chance that fundamental problems are present with the dataset; for example, if the scaling from frequency output values from the data-logger were wrongly scaled. This explanation could be plausible given the strong relative similarity in directional dependency on TI seen between the M2 and F3 polar plots (Figure 4.39). Much like with the far offshore region, the turbulence intensity seems to be the largest in sectors with fetch of greater than 100 km. The signatures are relatively similar but differ in magnitude.

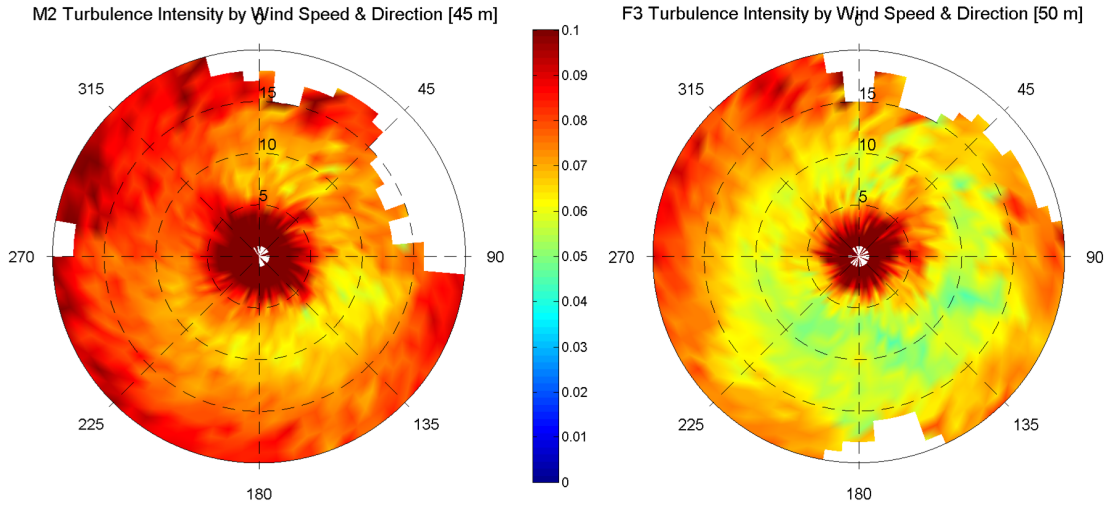

Figure 4.39: *Polar plots that show TI as a function of θ and $\overline{U}$ for M2 and F3. Both have similar sectors with the largest and smallest TI, although the magnitude at M2 is 20-30% larger.*

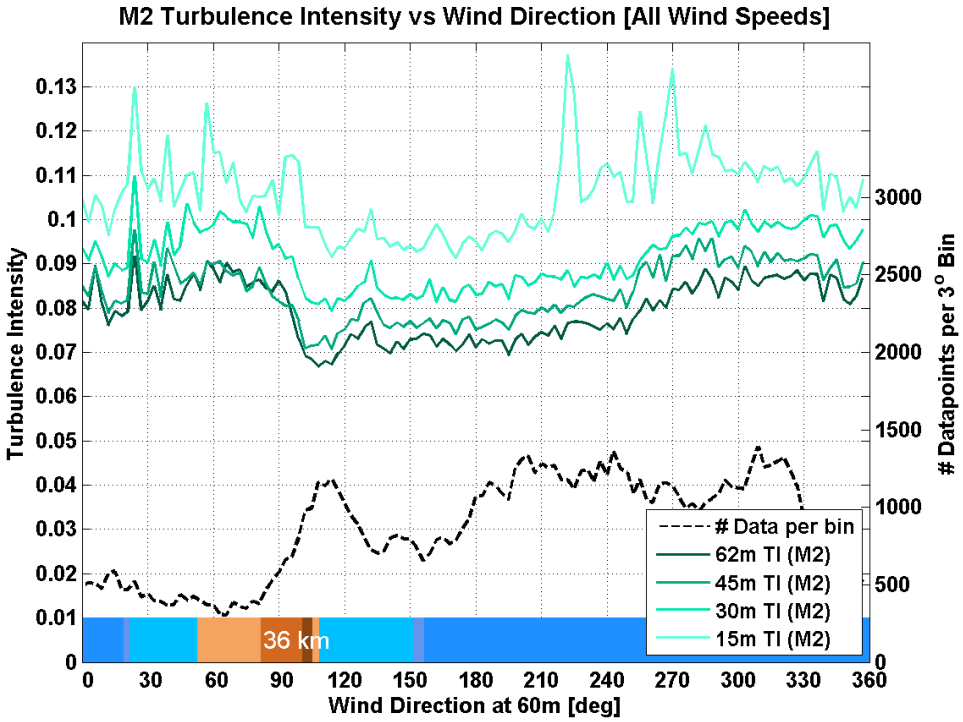

Figure 4.40: *TI versus θ at M2.*

Given time restraints, the comparative analysis between M2 and F3 has been left as future work. Instead, a supplementary report will be created to discuss the following plots. Figure 4.41 displays a table of key statistical information for both masts and the

difference between them. Figures 4.42 and 4.43 display the probability density function and cumulative distributive function for both masts, respectively.

		F3	M2	Δ% F3 → M2
General	z [m]	50	45	-5m
	$\bar{U}$ [m/s]	**9.65**	**9.18**	**-4.9%**
	$\bar{TI}_{90}$	9.97%	11.51%	15.5%
	$\bar{TI}$	**6.74%**	**8.34%**	**23.7%**
	$\bar{\sigma}_{TI}$	0.037	0.052	39.7%
	σ [m/s]	0.708	0.625	-11.7%
	σ_{σ} [m/s]	0.393	0.386	-1.8%
StDev	σ_{1pcn} [m/s]	0.10	0.17	73.0%
	σ_{10pcn} [m/s]	0.22	0.31	40.0%
	σ_{median} [m/s]	0.55	0.62	13.3%
	$\bar{\sigma}$ [m/s]	**0.63**	**0.71**	**13.3%**
	σ_{90pcn} [m/s]	1.12	1.20	7.2%
	σ_{99pct} [m/s]	1.89	2.01	6.4%
	σ_{max} [m/s]	5.60	4.98	-11.0%

		F3	M2	Δ% F3 → M2
Speed	z [m]	50	45	-5m
	U_{min} [m/s]	0.22	0.12	-45.5%
	U_{10pcn} [m/s]	4.17	3.90	-6.5%
	$\bar{U}$ [m/s]	**9.65**	**9.18**	**-4.9%**
	U_{90pcn} [m/s]	15.44	14.82	-4.0%
	U_{99pct} [m/s]	20.90	20.23	-3.2%
	U_{max} [m/s]	**29.52**	**43.10**	**46.0%**
Turb	TI_{1pcn} [m/s]	1.8%	3.2%	82.3%
	TI_{10pcn} [m/s]	3.6%	5.1%	43.2%
	TI_{median} [m/s]	**6.1%**	**7.5%**	**21.7%**
	$\bar{TI}$ [m/s]	**6.7%**	**8.3%**	**23.7%**
	TI_{90pcn} [m/s]	10.0%	11.5%	15.4%
	TI_{99pct} [m/s]	21.5%	26.6%	23.8%
	TI_{max} [m/s]	85.7%	177.0%	106.5%

Figure 4.41

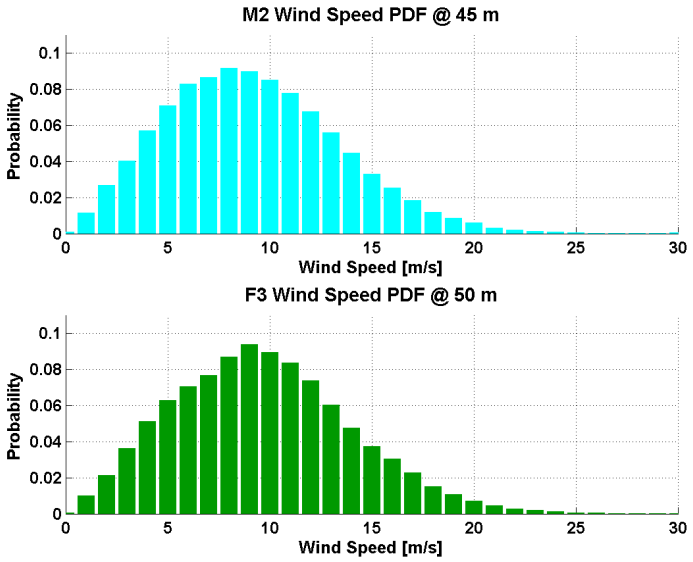

Figure 4.42

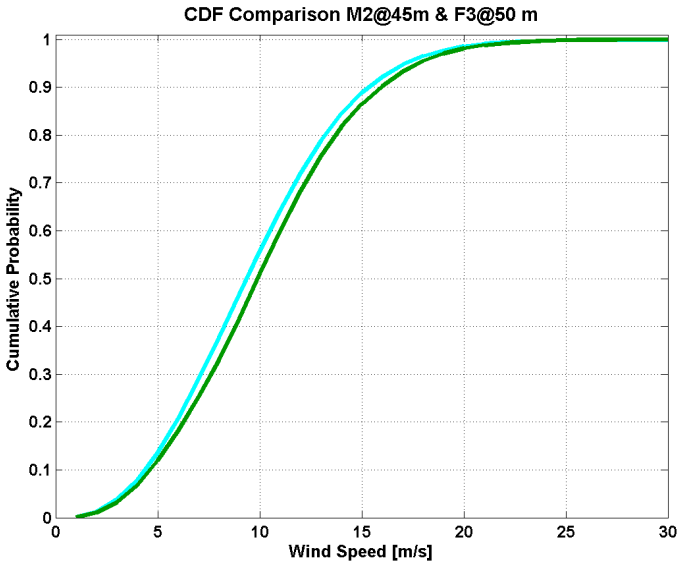
CDF Comparison M2@45m & F3@50 m
Cumulative Probability
Wind Speed [m/s]
0
0.1
0.2
0.3
0.4
0.5
0.6
0.7
0.8
0.9
1
0
5
10
15
20
25
30

Figure 4.43

Chapter 5

Conclusion

The research undertaken in this thesis has helped begin to unravel the complex and intricate dependencies of offshore ambient turbulence intensity. Never before has data from this many meteorological masts been examined simultaneously. This large-scale effort is fostering understanding of the differences and similarities seen between the four set regions and is laying the groundwork for a future, more in-depth study of the general turbulence characteristics in Northern Europe.

Studies such as these are of great value to the wind energy industry for two reasons. The first is that they assist in optimizing wind turbine design through understanding of the turbulence-induced fatigue loads. Secondly, as ambient turbulence intensity is a keystone input into wake modeling, it is of critical importance to accurately represent this parameter.

Given that TI is derived from σ_U, both were analyzed for dependencies on wind speed ($\overline{U}$), height (z), wind direction (θ) and fetch, in chapters 4.1,4.2 and 4.3 respectively. Their variations, σ_{TI} and σ_{σ_U}, were also investigated. Standard values for each of these four turbulence parameters are set by the IEC for both onshore [9] and offshore [8] environments, and are compared with values realized here from these data. The average turbulence intensity at 50m ranged from 6.32% to 7.44%.

The wind speed standard deviation (σ_U) increases with increasing wind speed, as expected, but does not increase linearly, as assumed in the IEC standards. In reality, it increases at lower rate before reaching a transition point where thermal to mechanically-induced turbulence occurs, at which point the slope of σ_U versus $\overline{U}$ increases. This transition point corresponds to the minimum in TI on the TI versus $\overline{U}$ plots and is the place where the actual curves (TI_{90}) begin to strongly deviate from the IEC 90th percentile curves (TI_{IEC}) which monotonically decrease with increasing wind speed.

This minimum in TI is height dependent and ranges from about 8-14 m/s. This intuitively makes sense given the fact that higher aloft, larger $\overline{U}$ and therefore larger waves must be achieved before the wave effects impact these heights. Therefore the lower end of this 8-14 m/s range is more prominent as the transition point at low heights and vice versa.

When looking the plots that compare σ_U and TI versus $\overline{U}$ for all of the masts at various heights, it can be seen, remarkably so, that seven of the masts show nearly ubiquitous agreement. This implies that when averaging over all θ and despite any geographical or climatic differences, these relationships are universal throughout Northern Europe.

This of course is not the case with M2 and M8. The reasons for M8's deviations are attributed to the small, long-fetched and prevailing wind sector considered for analysis. M2's deviations are subject of intense dialogue and could be the result of either measurement errors or due to large scale climate variability, which in this case would be the North Atlantic oscillation (NAO). Given the proximity of F3 to these two masts, and its similarity to the other 6 masts, it is reasonable to conclude that extremely site-specific local conditions are likely not the root cause of their outlier status.

With respect to the deviations of σ_U and TI, σ_{σ_U} is shown to increase with increasing $\overline{U}$ while σ_{TI} decreases with increasing $\overline{U}$. This is expected because in faster wind regimes, wave-induced turbulence dominates which leads to more turbulent fluctuations (σ_{σ_U}). At the same time its' consistent presence lowers σ_{TI}.

Chapter 4.2 examined the dependency of σ_U and TI on height and found that vastly different trends are revealed when plotting these relationships in different wind speed bins rather than averaging over all speeds. At low wind speeds σ_U did not change with height, while at high wind speeds a strong, nearly linear, decrease with height is realized. This is attributable to the difference in physics between the well-mixed nature of thermally-driven turbulence at low speeds and the air-sea interface where the mechanically-driven turbulence is generated at high wind speeds. A similar observation is applicable to the TI vs z plot.

The last dependency discussed is that of wind direction and fetch (chapter 4.3). This particular analysis was the most eye-opening in that it answered some questions, while also sparking ideas of future work that should be undertaken to further the understanding of the TI - θ relationship.

Fetch was found to be a vital proxy for predicting the turbulence intensity in different sectors. On a general level, it was found that TI decreased with increasing fetch or distance from shore up until about 40-50 kilometers, which makes sense given the lower roughness realized offshore. Beyond these distances though, a very interesting trend was observed. Turbulence intensity values actually increased slightly with increasing fetch, especially after about 100 kilometers. This is likely due to the effects of the well-developed waves and swell that dominate when wind flow is unobstructed over hundreds of kilometers.

It is for this reason that TI predominantly reached its highest value in offshore sectors at these 9 sites with fetch of greater than 100-200 kilometers. The similarities of this relationship were remarkable and strongly detectable in three of the four regions, the exception being the Irish Sea region, where fetch is limited in all sectors.

In the case of the sites off the eastern coast of the United Kingdom, there were two additional situations in which TI was maximized. The first was in sectors where sea is much more common than land when considering outward distances of about 500 kilometers, corresponding to the predominant coastal orientation. The second was due to complex terrain. Peaks in TI were observed in sectors with mountains of greater than 600m in elevation within 150 kilometers of the mast.

As expected given the reasoning above, F1 and HO in the far offshore group, had maximum TI realized in sectors with the largest fetch. F3, also within this region, observed this effect but also had a spike in TI visible in sectors with much smaller fetch. When examining these relationships in different wind speed bins it was ascertained that this land-sector peak occurred solely at low wind speeds which points to effects of stability that dominate in this wind regime. Interestingly enough, the peak in the large-fetched sector only occurred in fast regimes. This concurs with the results of [33] that stated that both fetch and stability dominate offshore environment.

This dual-dependency is further visible in the plots of SF1 and SF2 in the Irish Sea region. Given the scant prevalence of sectors with fetch greater than 100 kilometers, it is no surprise that there is reduced visibility of this dependence. Instead, the large variability seen between the sites and within the data at each site, is likely the result of the overwhelming occurrence of non-neutral atmospheric stability as observed by [18][19].

To further understand and explain the relationships observed in this thesis, there are many areas in which future work could be directed. Given the large effect that stability has on the offshore wind and turbulence climate, it is suggested that an analysis that groups the data by stability class or season be performed. For masts with high quality wave measurements, an assessment of the Charnock relationship could be performed as well as an analysis of the relationship between wind speed, fetch and wave height. Once complete, a more concrete understanding of the ambient offshore turbulence intensity in Northern Europe would be solidified, paving the way for development of more mechanically and financially efficient wind farms.

References

[1] US Energy Information Administration, *International Energy Outlook 2013*, US EIA, "http://www.eia.gov/forecasts/ieo/world.cfm", accessed 7/18/2014

[2] European Wind Energy Association, *The European offshore wind industry - key trends and statistics 2013*, EWEA, "http://www.ewea.org/fileadmin/files/library/publications/statistics/European_offshore_statistics_2013.pdf", accessed 7/12/2014

[3] United States Department of Energy, *20% Wind Energy by 2030*, NREL 2008, "http://www.nrel.gov/docs/fy08osti/41869.pdf", accessed 7/20/2014

[4] Manwell et al., *Review of design conditions applicable to offshore wind energy systems in the United States*, Renewable and Sustainable Energies, 2007.

[5] R. Downey, *Uncertainty in wind turbine life equivalent load due to variation of site conditions*, Masters Thesis, DTU, 2006.

[6] Hansen and Larsen, *Characterising Turbulence Intensity for Fatigue Load Analysis of Wind Turbines*, Wind Engineering, 2005.

[7] UN Environmental Programme, *Cities and Coastal Areas*, United Nations Environment Programme , "http://www.unep.org/urban_environment/issues/coastal_zones.asp", accessed 7/12/2014

[8] *IEC 61400-3 Part 3: Design requirements for offshore wind turbines*, International Electrotechnical Commission, 2005.

[9] *IEC 61400-1 Ed. 3: Wind turbines - Part 1: Design Requirements*, International Electrotechnical Commission, 2005.

[10] H. Wang, R. J. Barthelmie et al., *A new turbulence model for offshore wind turbine standards*, Wind Energy, 2013.

[11] Turk and Emeis, *The dependence of offshore turbulence intensity on wind speed*, Journal of Wind Engineering and Industrial Aerodynamics, 2010.

[12] T. Ishihara et al., *A Study of the Normal Turbulence Model in IEC 61400-1*, Wind Engineering, 2012.

[13] R. Stull, *An Introduction to Boundary Layer Meteorology*, Springer, 1988.

[14] S. Emeis, *Wind Energy Meteorology: Atmospheric Physics for Wind Power Generation*, Springer, 2013.

[15] Edson and Fairall, *Similarity Relationships in the Marine Atmospheric Surface Layer for Terms in the TKE and Scalar Variance Budgets*, Journal of Atmospheric Sciences, 1998.

[16] Lange et al, *THE INFLUENCE OF THERMAL EFFECTS ON THE WIND SPEED PROFILE OF THE COASTAL MARINE BOUNDARY LAYER*, Boundary Layer Meteorology, 2003.

[17] Sathe and Bierbooms, *Influence of different wind profiles due to varying atmospheric stability on the fatigue life of wind turbines*, The Science of Making Torque from Wind, 2007.

[18] Argyle and Watson, *A Study of the Surface Layer Atmospheric Stability at Two UK Offshore Sites*, Loughborough University, 2012.

[19] McMahon and Watson, *A Comparison of the Correlation between Onshore and Offshore Wind Speed Data*, Loughborough University.

[20] *Wind Resource Assessment Handbook*, The New York State Energy Research and Development Authority, 2010.

[21] Barthelmie et al., *The influence of humidity fluxes on offshore wind speed profiles*, Annales Geophysicae, 2010.

[22] van Wijk et al., *Evaluation of stability corrections in wind speed profiles over the North Sea*, Journal of Wind Engineering and Industrial Aerodynamics, 1990.

[23] R. J. Barthelmie, *The effects of atmospheric stability on coastal wind climates*, Meteorological Applications, 1999.

[24] Lange and Hojstrup, *THE INFLUENCE OF WAVES ON THE OFFSHORE WIND RESOURCE*.

[25] G. T. Csanady, *Air-Sea Interaction: Laws and Mechanisms*, Cambridge University Press, 2001.

[26] Charnock, *Wind stress on a water surface*, Quarterly Journal of the Royal Meteorological Society, 1955.

[27] SethuRaman and Raynor, *Surface drag coefficient dependence on the aerodynamic roughness of the sea*, Journal of Geophysical Research, 1975.

[28] R. J. Barthelmie et al., *Offshore Wind Resources at Danish Measurement Sites*, European Wind Energy Conference, 1999.

[29] Nino and Eecen, *ECN-DOWEC: Turbulence and Wind Shear - A Literature Study and Measurements*, DOWEC Conference.

[30] J. R. Garratt, *The stably stratified internal boundary layer for steady and diurnally varying offshore flow*, Boundary Layer Meteorology, 1987.

[31] Kallstrand et al., *Mesoscale wind field modifications over the Baltic Sea*, Boundary Layer Meteorology, 2000.

[32] Frank et al., *Simulated wind power off-shore using different parameterisations for the sea surface roughness*, Wind Energy 3, 2000.

[33] Westerhellweg et al., *Direction Dependency of Offshore Turbulence Intensity in the German Bight*, DEWI GmbH, DEWEK Conference, 2010.

[34] Lange et al., *Importance of thermal effects and sea surface roughness for offshore wind resource assessment*, Journal of Wind Engineering, 2004.

[35] D. Stein, *GL GH - Offshore Wind Measurements* Presentation Gdansk 12/12/2012 "http://www.ptmew.pl/media/pdf/akademiaOFFSHORE_12_12_12/Detlef_Stein_Prowadzenie_kampanii_pomiarowych_na_morzu.pdf", accessed 3/20/2014

[36] A. Sathe et al., *Influence of atmospheric stability on wind turbine loads*, Wind Energy, 2012.

Appendix A

Mast Instrumentation

Mast	Para-meter	Height [AMSL]	Orien-tation	Sensor Type	Sensor Model
F1	WSPD	103.2?	Top	Cup	Vector A100 - LM - WR - PC3
		101.7?	Top	Cup	Vector A100 - LM - WR - PC3
		90.2	SE	Cup	Vector A100 - LM - WR - PC3
		80.2	SE	Cup	Vector A100 - LM - WR - PC3
		70.2	SE	Cup	Vector A100 - LM - WR - PC3
		60.2	SE	Cup	Vector A100 - LM - WR - PC3
		50.2	SE	Cup	Vector A100 - LM - WR - PC3
		40.2	SE	Cup	Vector A100 - LM - WR - PC3
		33.2	SE	Cup	Vector A100 - LM - WR - PC3
		80.2	NW	Sonic	Windmaster USA
		60.2	NW	Sonic	Windmaster USA
		40.2	NW	Sonic	Windmaster USA
	WDIR	90.2	NW	Vane	Thies Wind Vane Classic
		80.2	NW	Sonic	Windmaster USA
		70.2	NW	Vane	Thies Wind Vane Classic
		60.2	NW	Sonic	Windmaster USA
		50.2	NW	Vane	Thies Wind Vane Classic
		40.2	NW	Sonic	Windmaster USA
		30.2	NW	Vane	Thies Wind Vane Classic
F3	WSPD	106	345 deg	cup	
		100	345 deg	cup	
		90	345 deg	cup	
		90	225 deg	cup	
		90	105 deg	cup	
		80	345 deg	cup	
		70	345 deg	cup	
		70	225 deg	cup	
		70	105 deg	cup	
		60	345 deg	cup	
		50	345 deg	cup	
		50	225 deg	cup	
		50	105 deg	cup	
		40	345 deg	cup	
		30	345 deg	cup	
	WDIR	100	225 deg	vane or sonic	
		60	225 deg	sonic	

HO	WSPD	101	NW (315)	Cup	Vector Instruments A100LM
		101	SE (135)	Cup	Risø P2546A
		96	NW (315)	Cup	Risø P2546A
		96	SE (135)	Cup	Vector Instruments A100LM
		91	NW (315)	Cup	Vector Instruments A100LM
		91	SE (135)	Cup	Risø P2546A
		86	NW (315)	Cup	Risø P2546A
		86	SE (135)	Cup	Vector Instruments A100LM
		66	NW (315)	Cup	Vector Instruments A100LM
		66	SE (135)	Cup	Risø P2546A
		46	NW (315)	Cup	Risø P2546A
		46	SE (135)	Cup	Vector Instruments A100LM
		26	NW (315)	Cup	Vector Instruments A100LM
		26	SE (135)	Cup	Risø P2546A
		~~83~~	~~SE (135)~~	~~Sonic~~	~~WindMaster 32Hz~~
		~~43~~	~~SE (135)~~	~~Sonic~~	~~WindMaster 32Hz~~
	WDIR	94	NW (315)	Vane?	Thies 4.3150.00.212
		83	NW (315)	Vane?	Thies 4.3150.00.212
		63	NW (315)	Vane?	Vector Instruments W200P
		43	NW (315)	Vane?	Vector Instruments W200P
HU	WSPD	90.15	Top	Cup	Risø P2546A
		87.65	W (270)	Cup	Risø P2546A
		87.65	NW (330)	Cup	Risø P2546A
		87.65	SE (150)	Cup	Risø P2546A
		69.65	W (270)	Cup	Risø P2546A
		69.65	SE (150)	Cup	Risø P2546A
		51.65	W (270)	Cup	Risø P2546A
		51.65	SE (150)	Cup	Risø P2546A
		33.65	W (270)	Cup	Risø P2546A
		33.65	SE (150)	Cup	Risø P2546A
	WDIR	85.65	NW (330) vs W	Vane	Vector Instruments W200P
		67.65	NW (330) vs W	Vane	Vector Instruments W200P
LA	WSPD	82.3	T	Cup	Risø P2546A
		79.8	SE	Cup	Risø P2546A
		57.2	NW	Cup	Risø P2546A
		57.2	SE	Cup	Risø P2546A
		32.2	NW	Cup	Risø P2546A
		32.2	SE	Cup	Risø P2546A
		20.2	NW	Cup	Risø P2546A
		20.2	SE	Cup	Risø P2546A
	WDIR	78.3	NW	Vane	Vector W200P
		29.3	NW	Vane	Vector W200P

M2	WSPD	62	T	Cup	EDSC cup anemometer
		45	NE	Cup	EDSC cup anemometer
		45	SW	Cup	EDSC cup anemometer
		30	NE	Cup	EDSC cup anemometer
		30	SW	Cup	EDSC cup anemometer
		15	NE	Cup	EDSC cup anemometer
		15	SW	Cup	EDSC cup anemometer
	WDIR	60	NE	Vane	ED Wind Direction sensor cos/sin 4 KHz
		43	NE	Vane	
		28	SW	Vane	
M8	WSPD	107	Top	Cup	EDSC cup anemometer
		97	NW	Cup	EDSC cup anemometer
		87	NW	Cup	EDSC cup anemometer
		87	SE	Cup	EDSC cup anemometer
		77	NW	Cup	EDSC cup anemometer
		67	NW	Cup	EDSC cup anemometer
		67	SE	Cup	EDSC cup anemometer
		57	NW	Cup	EDSC cup anemometer
		47	NW	Cup	EDSC cup anemometer
		47	SE	Cup	EDSC cup anemometer
		37	NW	Cup	EDSC cup anemometer
		27	NW	Cup	EDSC cup anemometer
		27	SE	Cup	EDSC cup anemometer
	WDIR	105	NW	Vane	ED Wind Direction sensor cos/sin 4 KHz
		65	SE	Vane	
		35	NW	Vane	
SF1	WSPD	87.3	Top	Cup	Vector A100L2
		85.3	SE	Cup	Vector A100L2
		75.3	NW	Cup	Vector A100L2
		75.3	SE	Cup	Vector A100L2
		55.3	NW	Cup	Vector A100L2
		55.3	SE	Cup	Vector A100L2
	WDIR	83.3	NW	Vane	Vector W200P
		83.3	SE	Vane	Vector W200P
SF2	WSPD	57.3	Top	Cup	Vector A100L2
		55.3	SE	Cup	Vector A100L2
		45.3	NW	Cup	Vector A100L2
		45.3	SE	Cup	Vector A100L2
	WDIR	53.3	NW	Vane	Vector W200P
		53.3	SE	Vane	Vector W200P

Appendix B

Additional Mast Shadow Plots

One one mast shadow plot is displays per mast so not all of the heights will be represented.

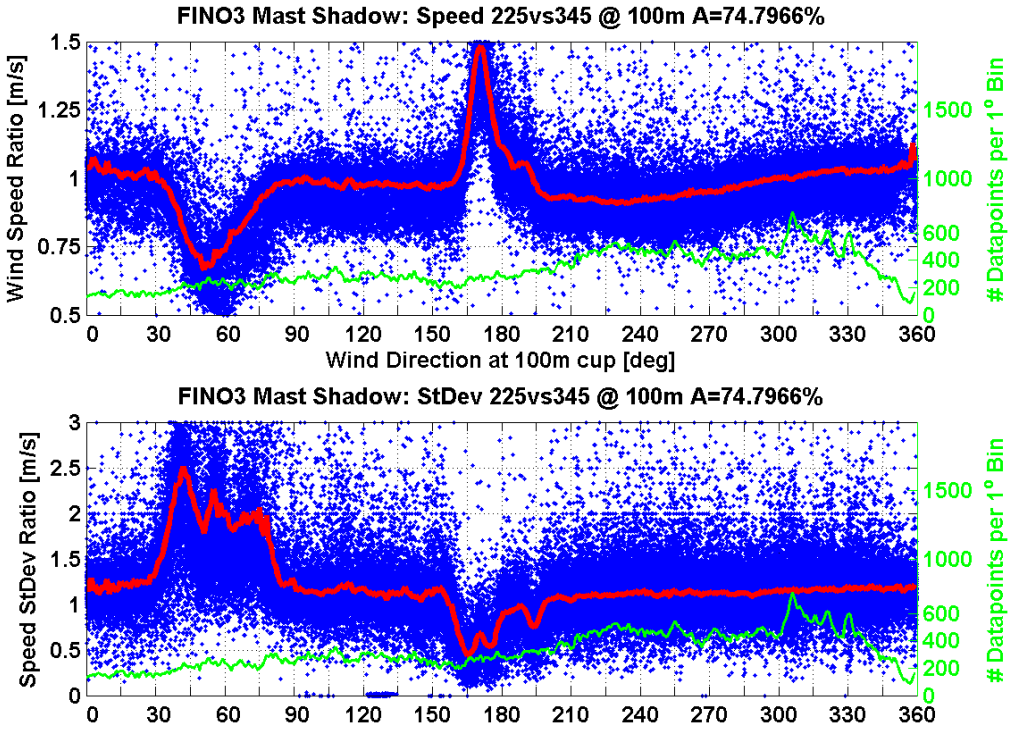

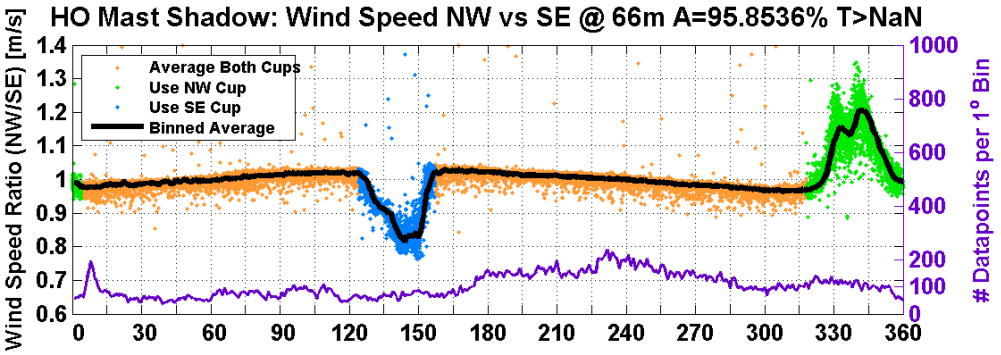
HO Mast Shadow: Wind Speed NW vs SE @ 66m A=95.8536% T>NaN
Wind Speed Ratio (NW/SE) [m/s]
Datapoints per 1° Bin
Average Both Cups
Use NW Cup
Use SE Cup
Binned Average

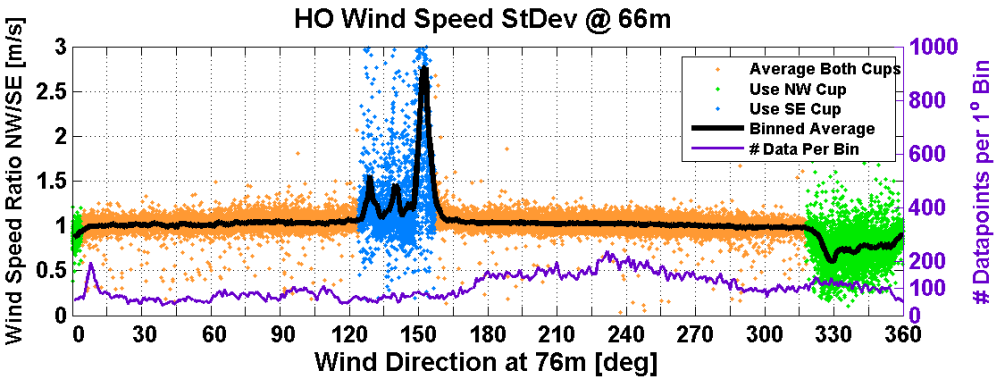
HO Wind Speed StDev @ 66m
Wind Speed Ratio NW/SE [m/s]
Datapoints per 1° Bin
Average Both Cups
Use NW Cup
Use SE Cup
Binned Average
Data Per Bin
Wind Direction at 76m [deg]

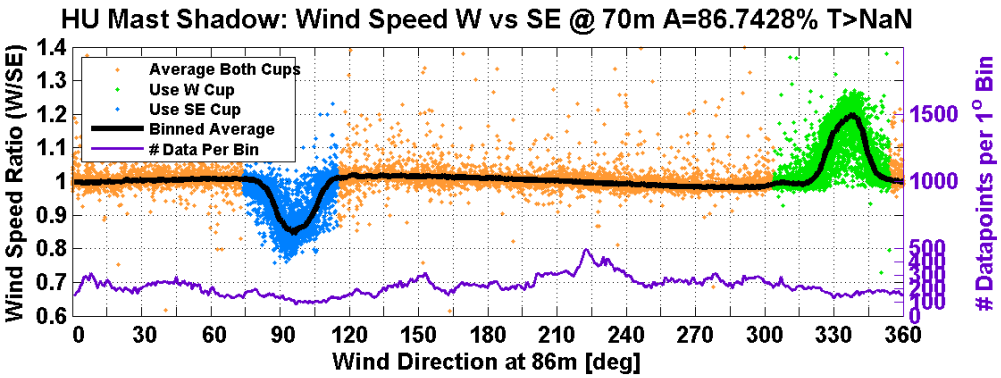
HU Mast Shadow: Wind Speed W vs SE @ 70m A=86.7428% T>NaN
Wind Speed Ratio (W/SE)
Datapoints per 1° Bin
Average Both Cups
Use W Cup
Use SE Cup
Binned Average
Data Per Bin
Wind Direction at 86m [deg]

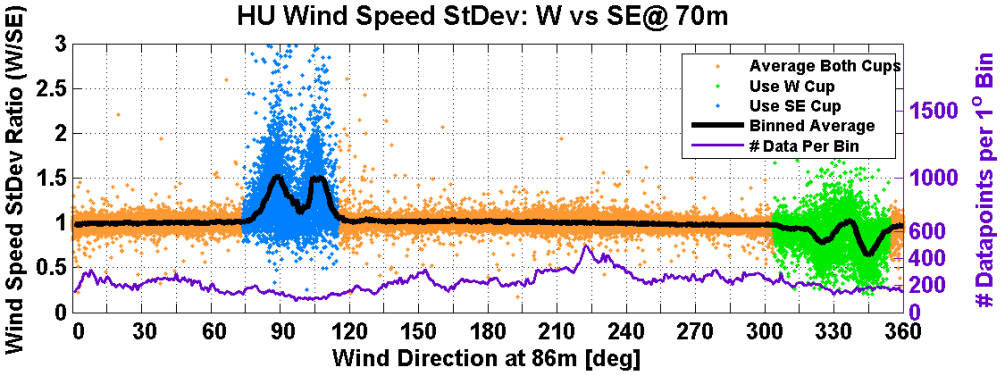
HU Wind Speed StDev: W vs SE@ 70m
Wind Speed StDev Ratio (W/SE)
Datapoints per 1° Bin
Average Both Cups
Use W Cup
Use SE Cup
Binned Average
Data Per Bin
Wind Direction at 86m [deg]

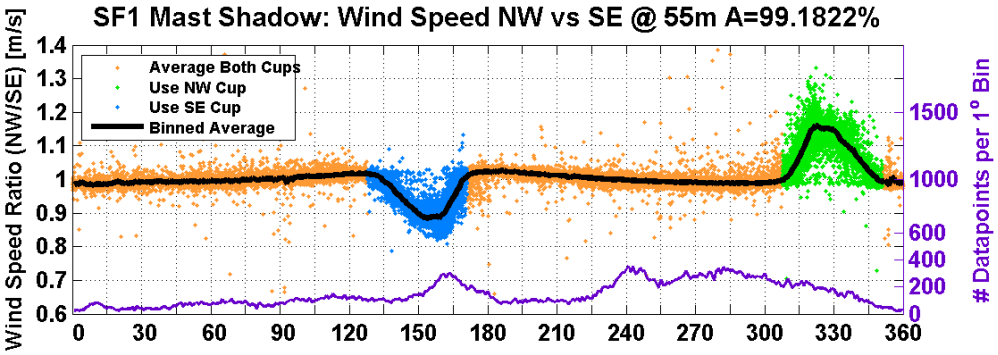
SF1 Mast Shadow: Wind Speed NW vs SE @ 55m A=99.1822%
Wind Speed Ratio (NW/SE) [m/s]
Datapoints per 1° Bin
Average Both Cups
Use NW Cup
Use SE Cup
Binned Average

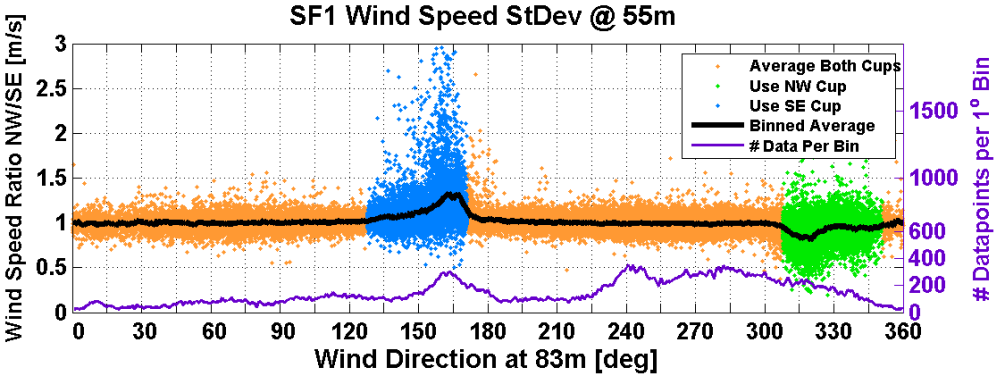
SF1 Wind Speed StDev @ 55m
Wind Speed Ratio NW/SE [m/s]
Datapoints per 1° Bin
Average Both Cups
Use NW Cup
Use SE Cup
Binned Average
Data Per Bin
Wind Direction at 83m [deg]

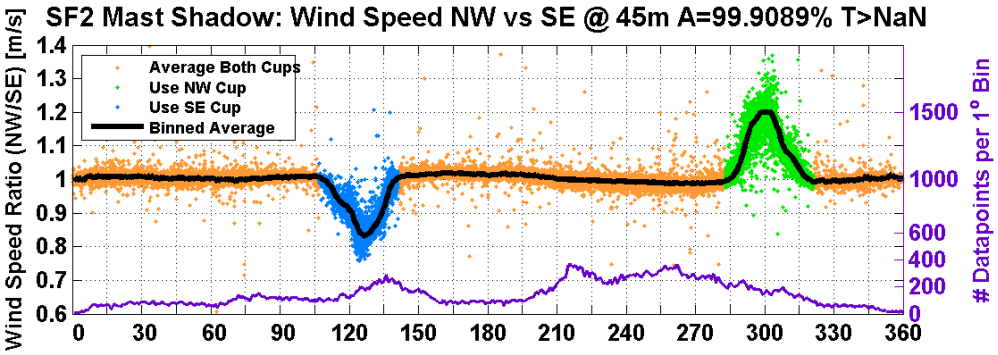
SF2 Mast Shadow: Wind Speed NW vs SE @ 45m A=99.9089% T>NaN
Wind Speed Ratio (NW/SE) [m/s]
Datapoints per 1° Bin
Average Both Cups
Use NW Cup
Use SE Cup
Binned Average

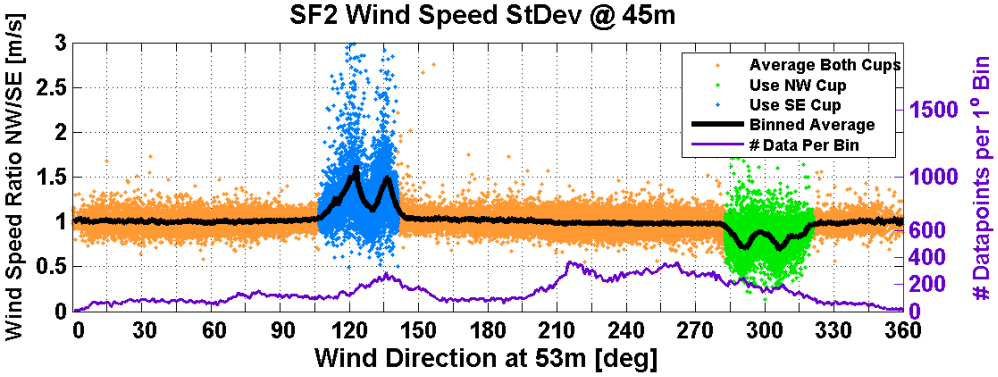
SF2 Wind Speed StDev @ 45m
Wind Speed Ratio NW/SE [m/s]
Datapoints per 1° Bin
Average Both Cups
Use NW Cup
Use SE Cup
Binned Average
Data Per Bin
Wind Direction at 53m [deg]

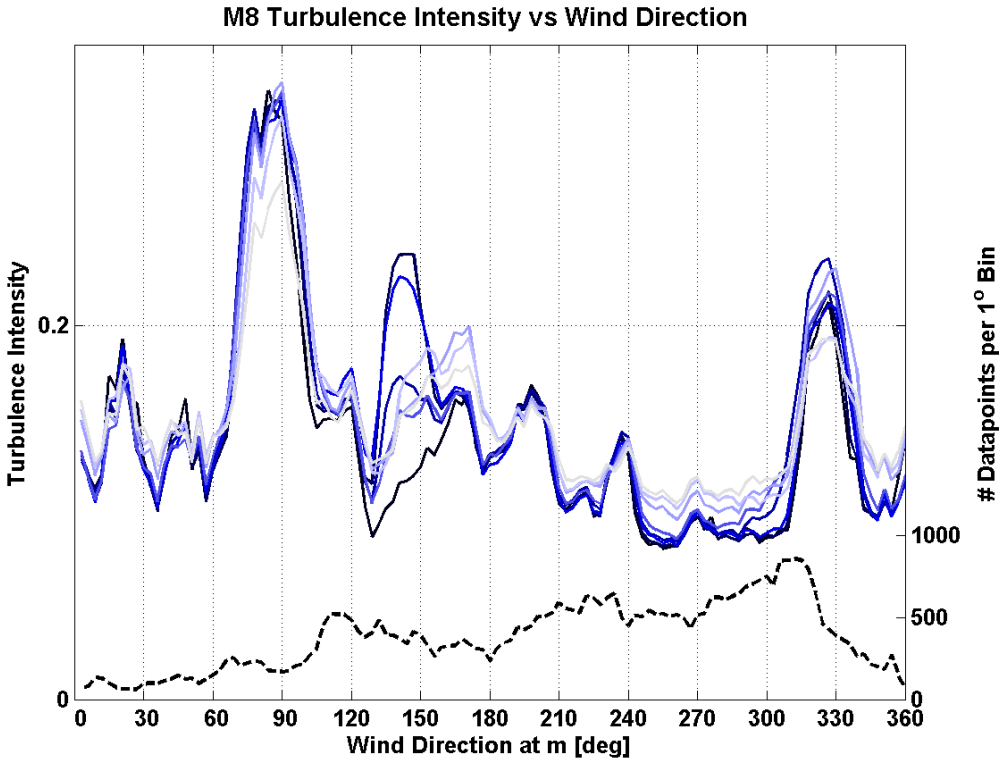
M8 Turbulence Intensity vs Wind Direction
Turbulence Intensity
0.2
0
0
30
60
90
120
150
180
210
240
270
300
330
360
Wind Direction at m [deg]
Datapoints per 1° Bin
1000
500
0

Appendix C

Coding Processes: MATLAB

After gaining familiarity with the data, a general filter code was created. This code is generic and applies all of the filters specified and discussed above for each height at each mast. As expected there are some slight differences in the filtering criteria depending on the mast shadow corrections needed for each dataset. Other than these slight differences, all filtering criteria applied are the same for each dataset. Using a generic code like this helps ensure that an analysis of the highest quality is created.

Once these mast shadow corrections are implemented, the main plot-producing file is developed and implemented ($XX\_Scatterplots\_WithMastCorrection$), where the XX are filled in with the mast name. This file runs all of the filters and corrections as functions.

The next paragraphs detail the steps undertaken in this code as well as the plots that are generated using this code. The code is generic among all of the masts though there are considerable differences in prose from differences in data notation between the masts.

First the data are imported and renamed generically to WSPD (wind speed), WDIR (wind direction) and TEMP (temperature) respectively (so code is most generic). The data is then clipped to a temporal period that is as close as possible to an integer number of years as is bounded by the start and end dates. The reasoning behind selecting data for analysis in yearly increments is to reduce the presence of any potential seasonal biases. For example (perhaps include). Additionally, data from FINO1 and M2 were filtered for specific dates due to the construction and then operation of wind farms close in proximity to these masts (Alpha Ventus and Horns Rev II respectively).

Next the boundary conditions for the filter were prescribed. Besides the special cases of FINO1 and M8, these conditions are the same for all masts:

- $V_{min} = 0.1\ \frac{m}{s}$
- $V_{max} = 100\ \frac{m}{s}$
- $\Theta_{min} = 0^o$ (255^o for M2)

- $\Theta_{max} = 360^o$ [285^o for M8; 280^o for F1]
- $\sigma_V = 3$
- $\sigma_\Theta = 40$
- Tfiltvalue = NaN (NaN because in the end no temp filter used)

These boundary conditions provided the inputs into the main filter (XX_Filter_date), whose output were then used as input into the mast shadow correction code ($XX\_MastShadowCorr$) where the XX refers to the Mast Name (Put this in somewhere). The output from these two functions includes the corrected wind speed, wind speed standard deviation and wind direction data in addition to two text files titled XX_FILT and XX_TOT_FILT. The first contains the counts of data removed for each filtering criterion, and the second counts the total number of data filtered and thus the data availability (for each height on the mast). Additionally, if one-sided mast correction is utilized (Type 3 reference to previous section) then a $SUMMARY$ text file is output that holds the values of pre- and post-filtering correlations between the data.

Now that a filtered, mast-corrected and thus a robust dataset is created it is possible to move into the analysis. The first calculation made is an average of the wind speed standard deviation values by bins of wind speed (1 m/s increments centered around integers). These binned averages in addition to the 90th, 75th, 25th, 10th percentiles and number of data within the bin are calculated and then saved to a file that is then used when comparing and plotting the data from all of the masts. These values are also used for some of the plots created by this main code.

Two last calculations are made before the final scatterplots listed below can be created. The first is to calculate the values of the IEC reference curves for both standard deviation and turbulence intensity. The second is to calculate the turbulence intensity which is accomplished by simply dividing the wind speed standard deviation by the wind speed. With this complete the plots can be made.

Appendix E

Additional σ_U vs $\overline{U}$ Plots - Individual Masts

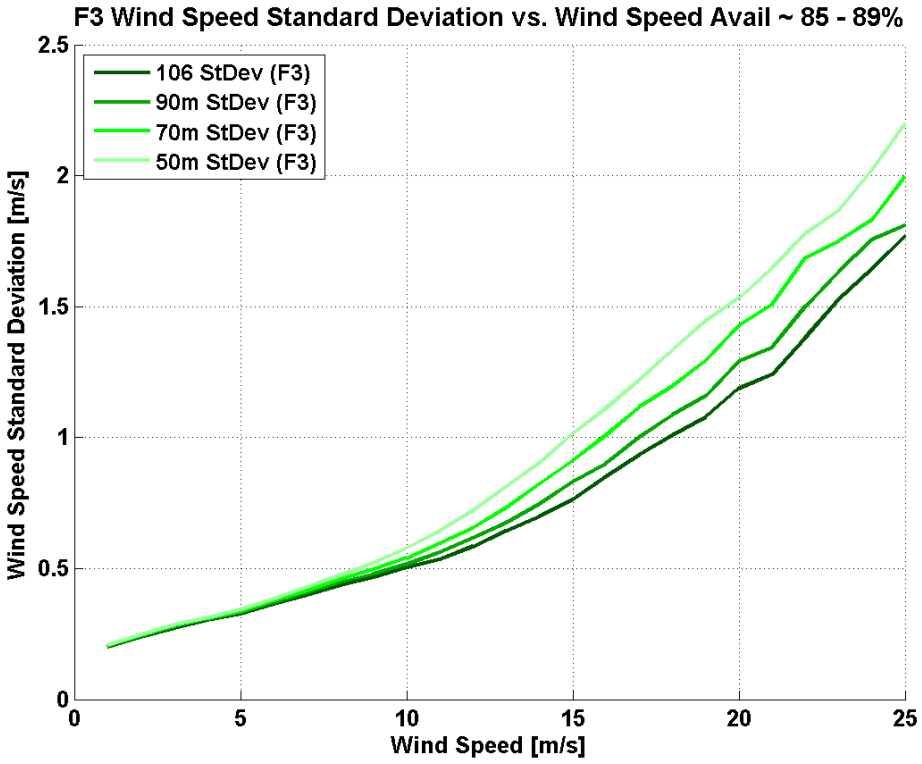

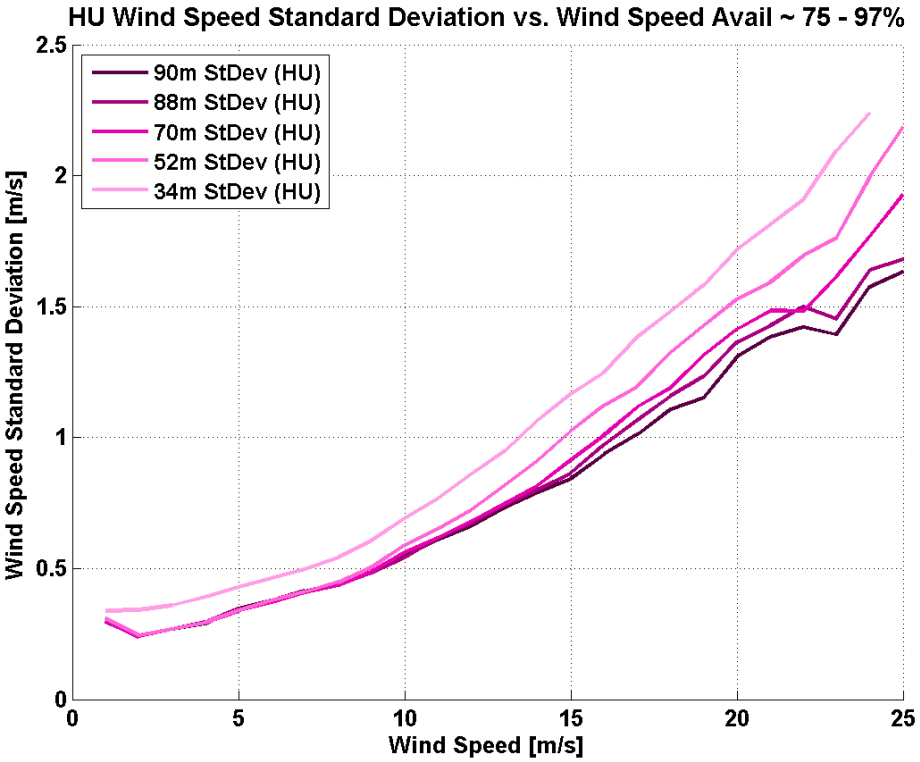
HU Wind Speed Standard Deviation vs. Wind Speed Avail ~ 75 - 97%
90m StDev (HU)
88m StDev (HU)
70m StDev (HU)
52m StDev (HU)
34m StDev (HU)
Wind Speed Standard Deviation [m/s]
Wind Speed [m/s]
0
0.5
1
1.5
2
2.5
0
5
10
15
20
25

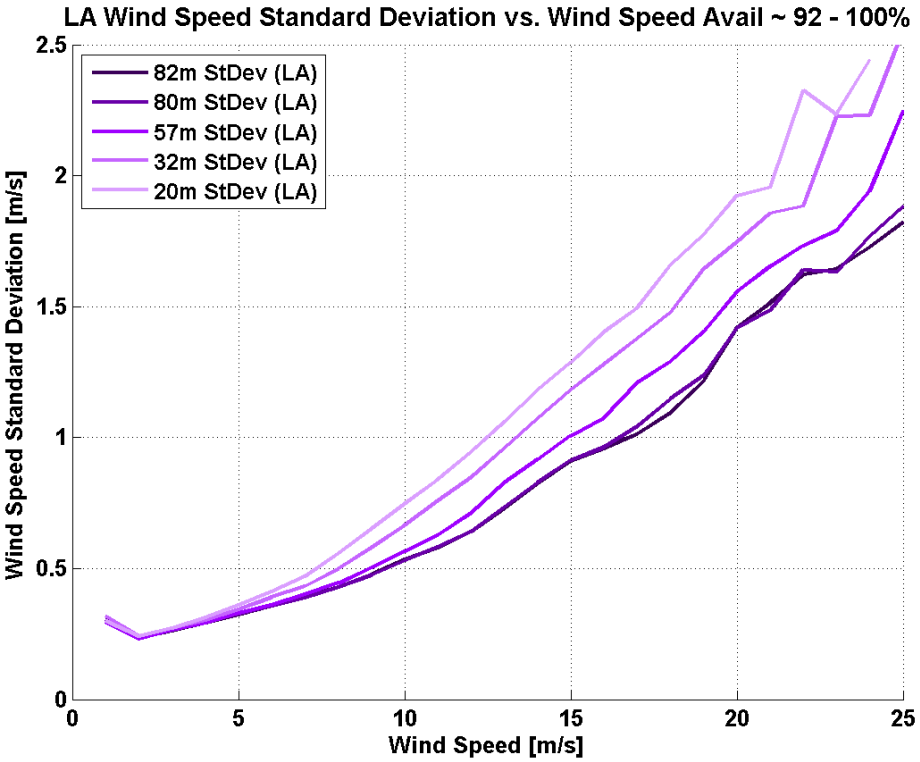
LA Wind Speed Standard Deviation vs. Wind Speed Avail ~ 92 - 100%
82m StDev (LA)
80m StDev (LA)
57m StDev (LA)
32m StDev (LA)
20m StDev (LA)
Wind Speed Standard Deviation [m/s]
Wind Speed [m/s]
0
0.5
1
1.5
2
2.5
0
5
10
15
20
25

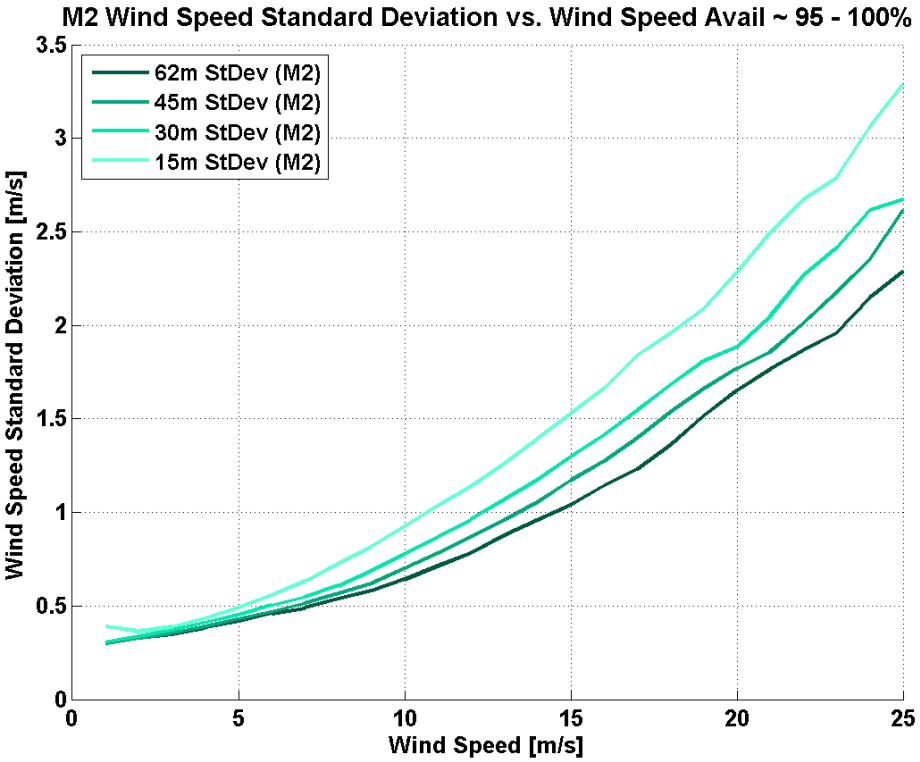
M2 Wind Speed Standard Deviation vs. Wind Speed Avail ~ 95 - 100%
62m StDev (M2)
45m StDev (M2)
30m StDev (M2)
15m StDev (M2)
Wind Speed Standard Deviation [m/s]
Wind Speed [m/s]
0
0.5
1
1.5
2
2.5
3
3.5
0
5
10
15
20
25

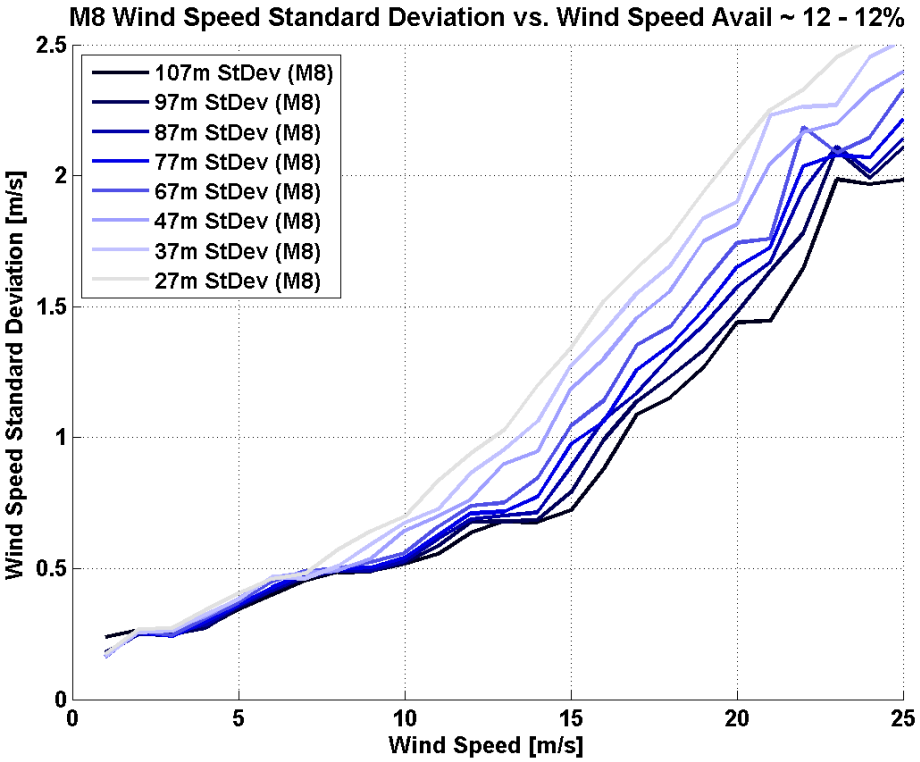
M8 Wind Speed Standard Deviation vs. Wind Speed Avail ~ 12 - 12%
107m StDev (M8)
97m StDev (M8)
87m StDev (M8)
77m StDev (M8)
67m StDev (M8)
47m StDev (M8)
37m StDev (M8)
27m StDev (M8)
Wind Speed Standard Deviation [m/s]
Wind Speed [m/s]
0
0.5
1
1.5
2
2.5
0
5
10
15
20
25

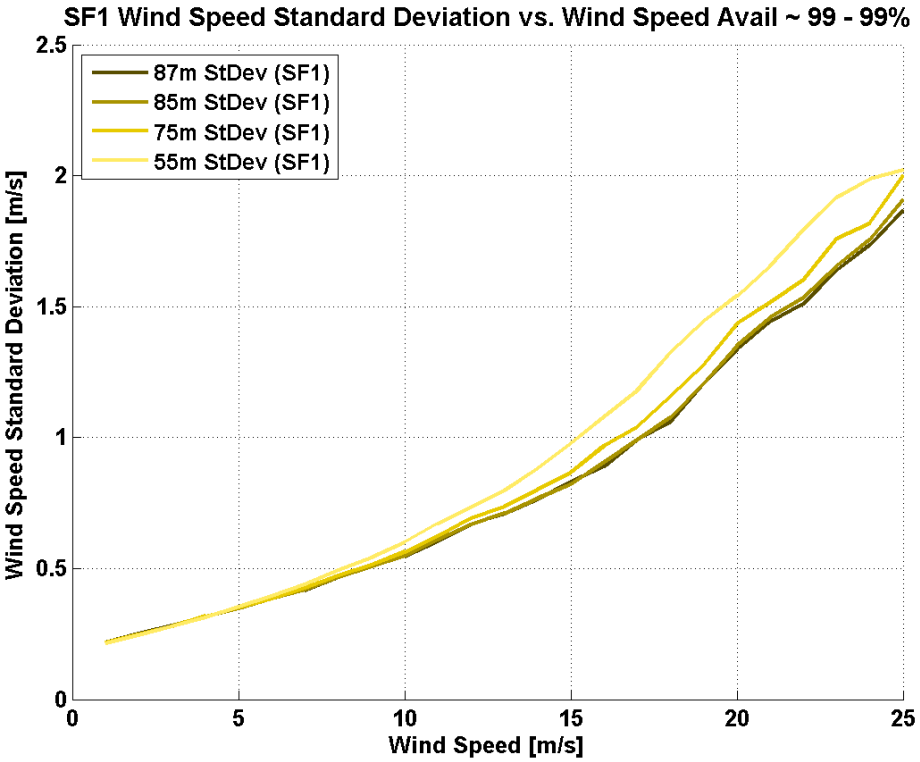
SF1 Wind Speed Standard Deviation vs. Wind Speed Avail ~ 99 - 99%
87m StDev (SF1)
85m StDev (SF1)
75m StDev (SF1)
55m StDev (SF1)
Wind Speed Standard Deviation [m/s]
Wind Speed [m/s]
0
0.5
1
1.5
2
2.5
0
5
10
15
20
25

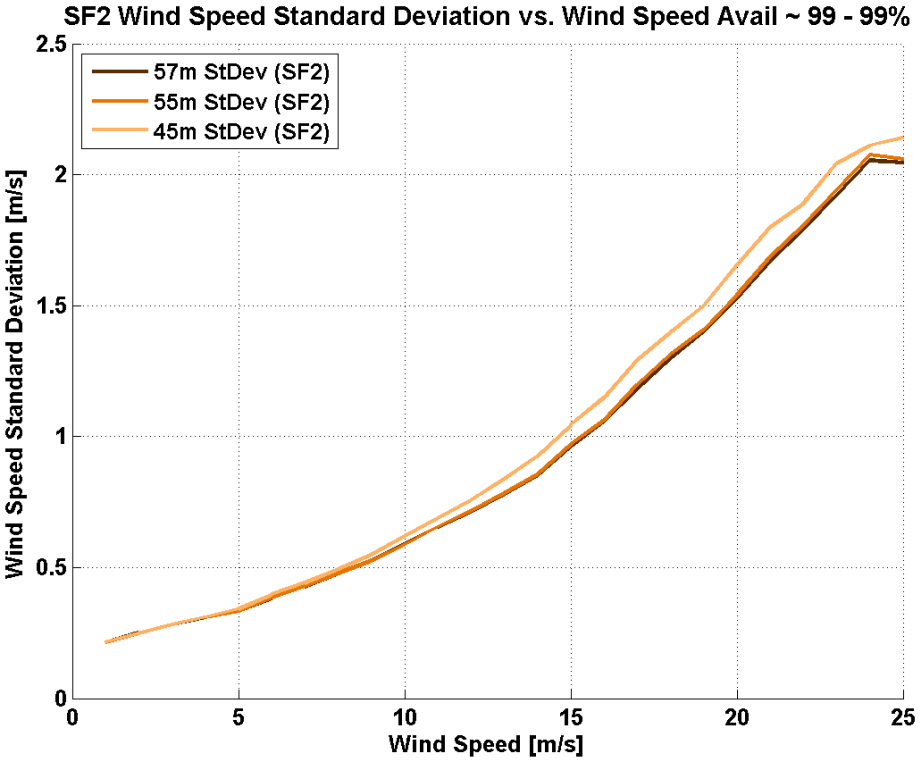
SF2 Wind Speed Standard Deviation vs. Wind Speed Avail ~ 99 - 99%
57m StDev (SF2)
55m StDev (SF2)
45m StDev (SF2)
Wind Speed Standard Deviation [m/s]
Wind Speed [m/s]
0
0.5
1
1.5
2
2.5
0
5
10
15
20
25

Appendix H

Plots of σ_U vs θ

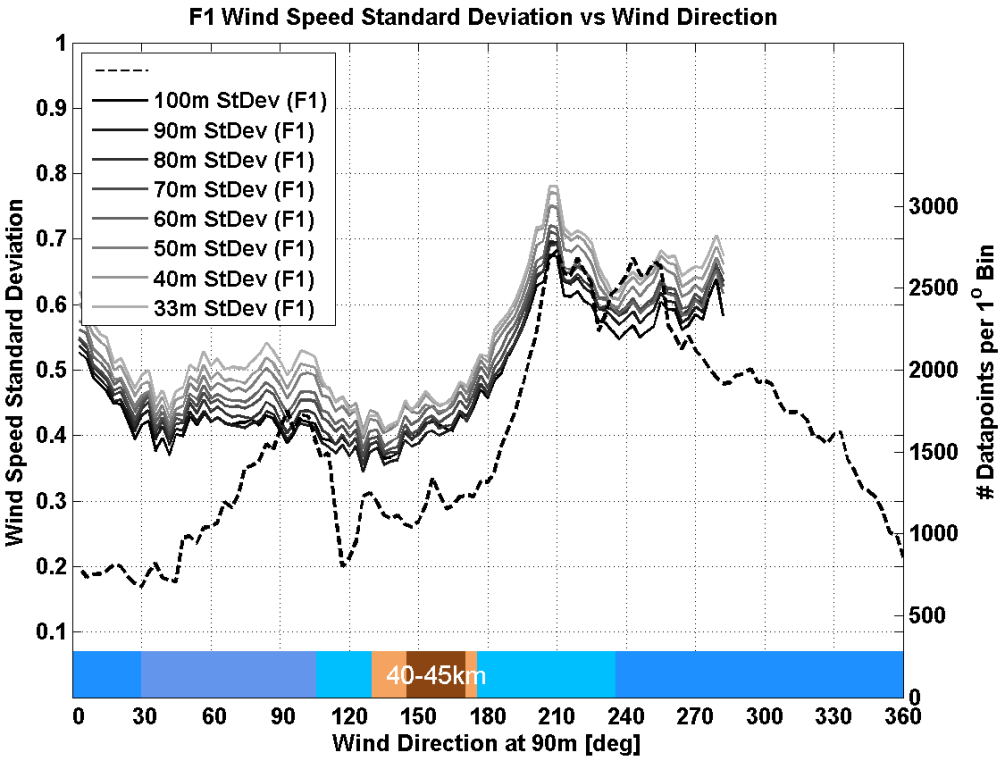

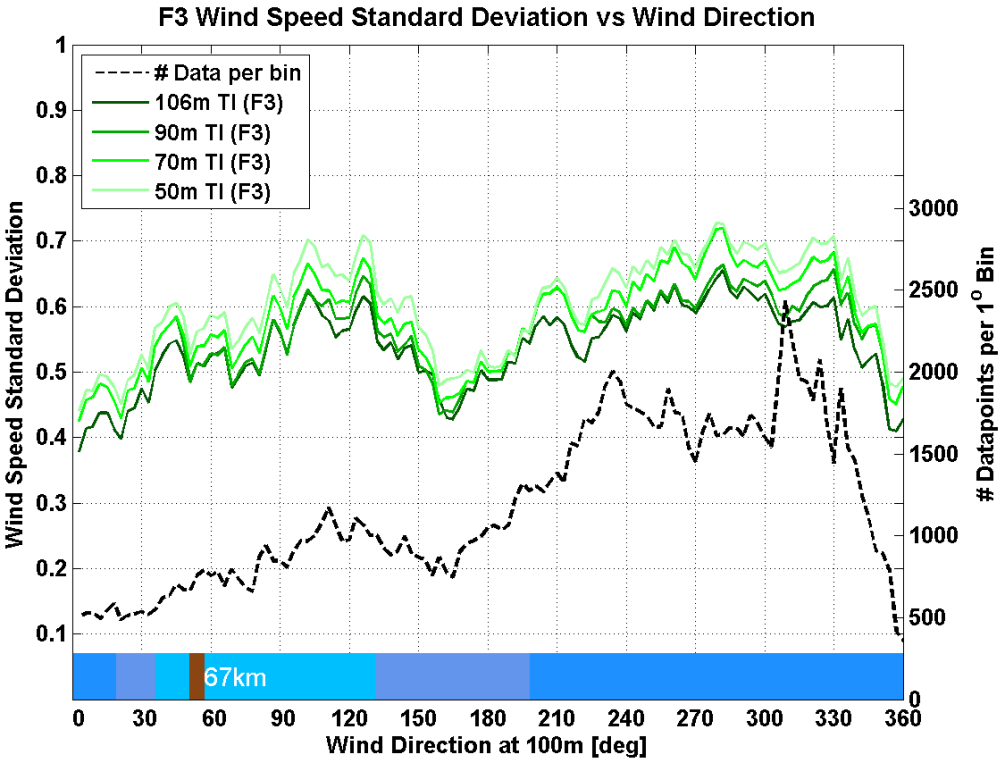
F3 Wind Speed Standard Deviation vs Wind Direction
Data per bin
106m TI (F3)
90m TI (F3)
70m TI (F3)
50m TI (F3)
Wind Speed Standard Deviation
Datapoints per 1° Bin
67km
Wind Direction at 100m [deg]

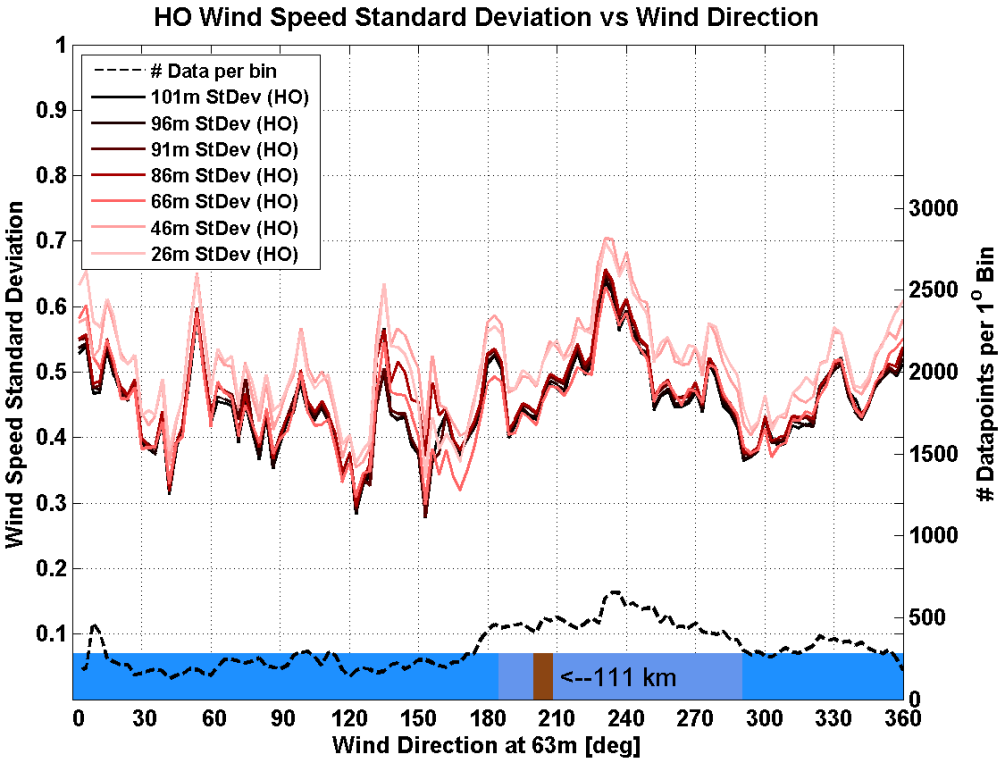
HO Wind Speed Standard Deviation vs Wind Direction
Data per bin
101m StDev (HO)
96m StDev (HO)
91m StDev (HO)
86m StDev (HO)
66m StDev (HO)
46m StDev (HO)
26m StDev (HO)
Wind Speed Standard Deviation
Datapoints per 1° Bin
<--111 km
Wind Direction at 63m [deg]

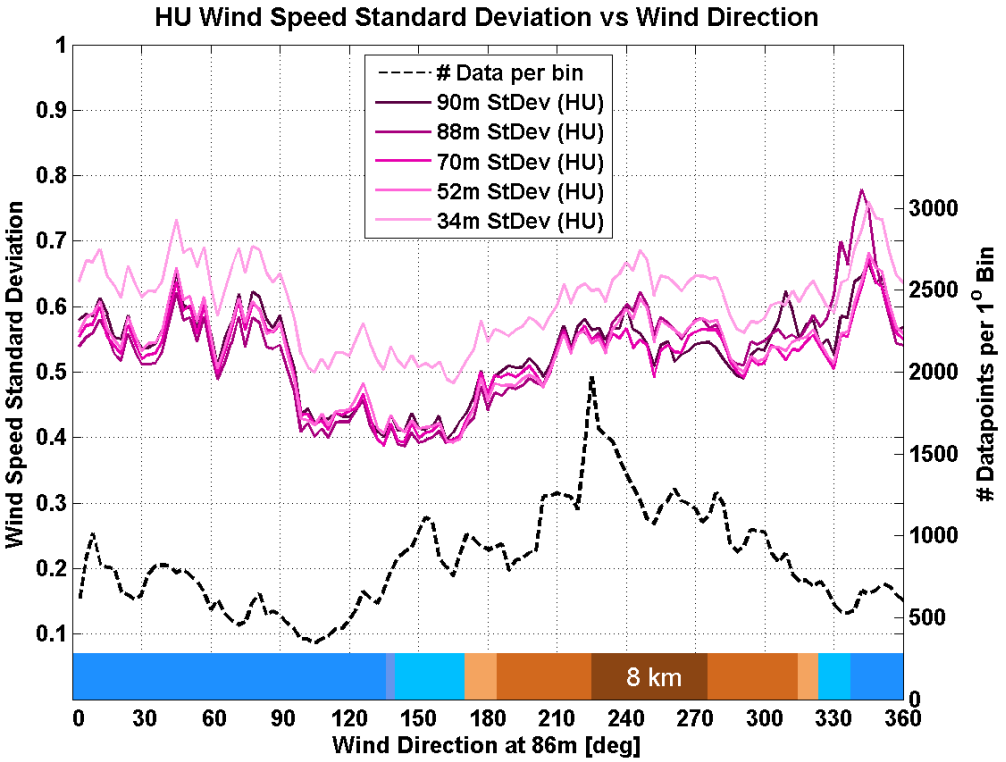
HU Wind Speed Standard Deviation vs Wind Direction
Data per bin
90m StDev (HU)
88m StDev (HU)
70m StDev (HU)
52m StDev (HU)
34m StDev (HU)
Wind Speed Standard Deviation
Datapoints per 1° Bin
8 km
Wind Direction at 86m [deg]

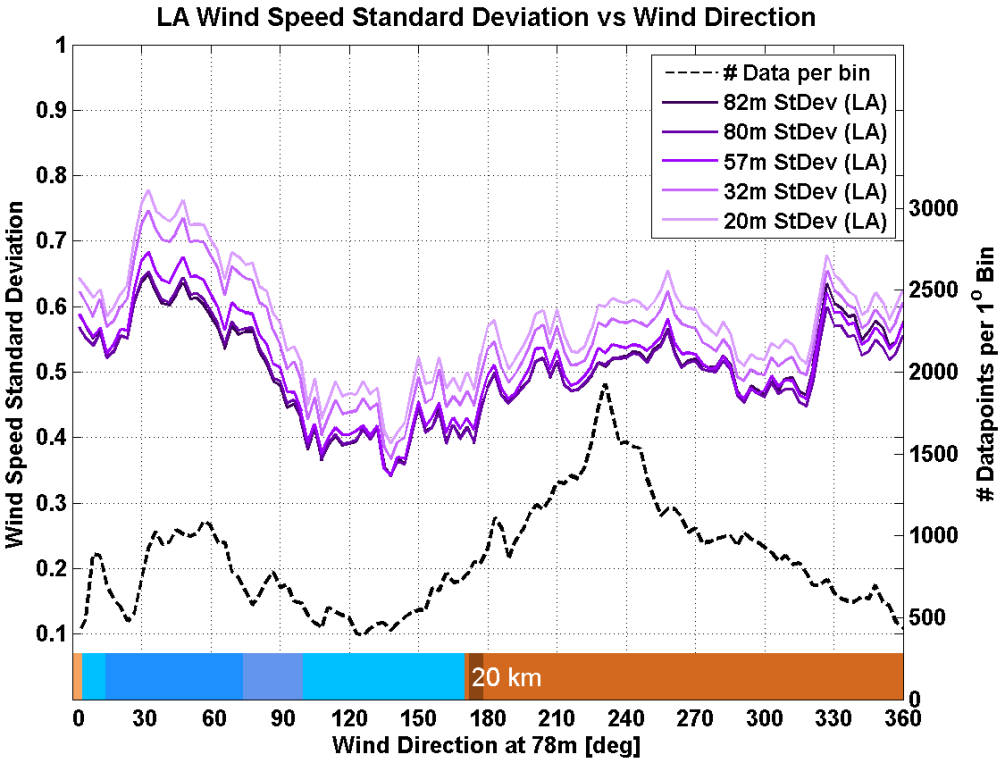
LA Wind Speed Standard Deviation vs Wind Direction
Data per bin
82m StDev (LA)
80m StDev (LA)
57m StDev (LA)
32m StDev (LA)
20m StDev (LA)
Wind Speed Standard Deviation
Datapoints per 1° Bin
20 km
Wind Direction at 78m [deg]

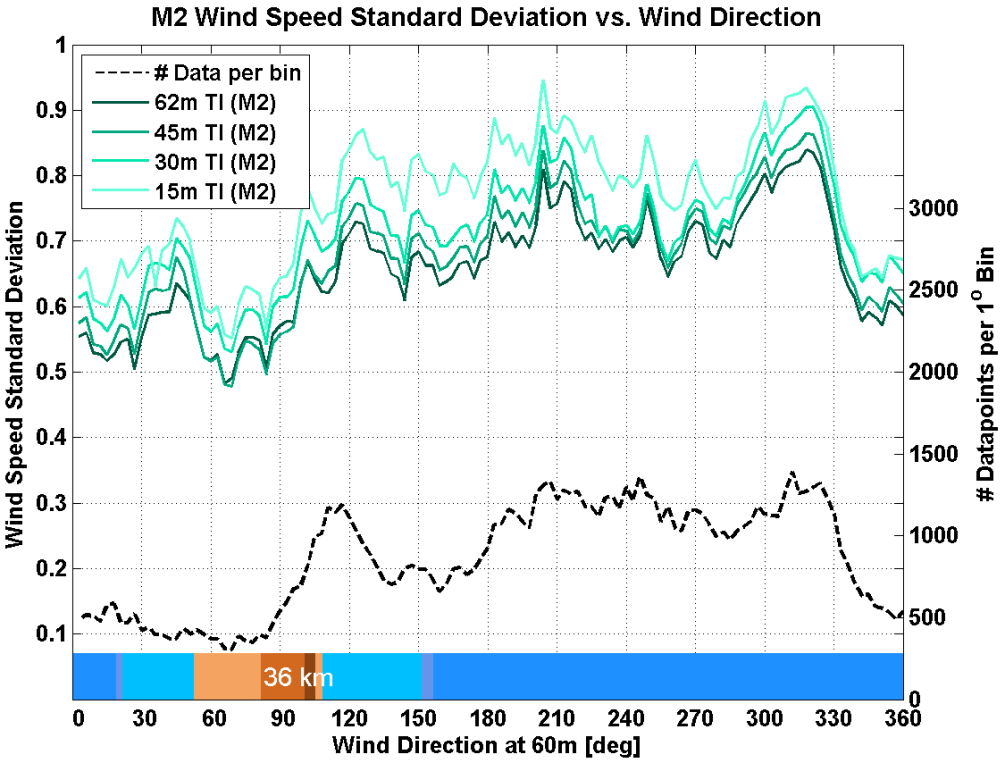
M2 Wind Speed Standard Deviation vs. Wind Direction
Data per bin
62m TI (M2)
45m TI (M2)
30m TI (M2)
15m TI (M2)
Wind Speed Standard Deviation
Datapoints per 1° Bin
36 km
Wind Direction at 60m [deg]

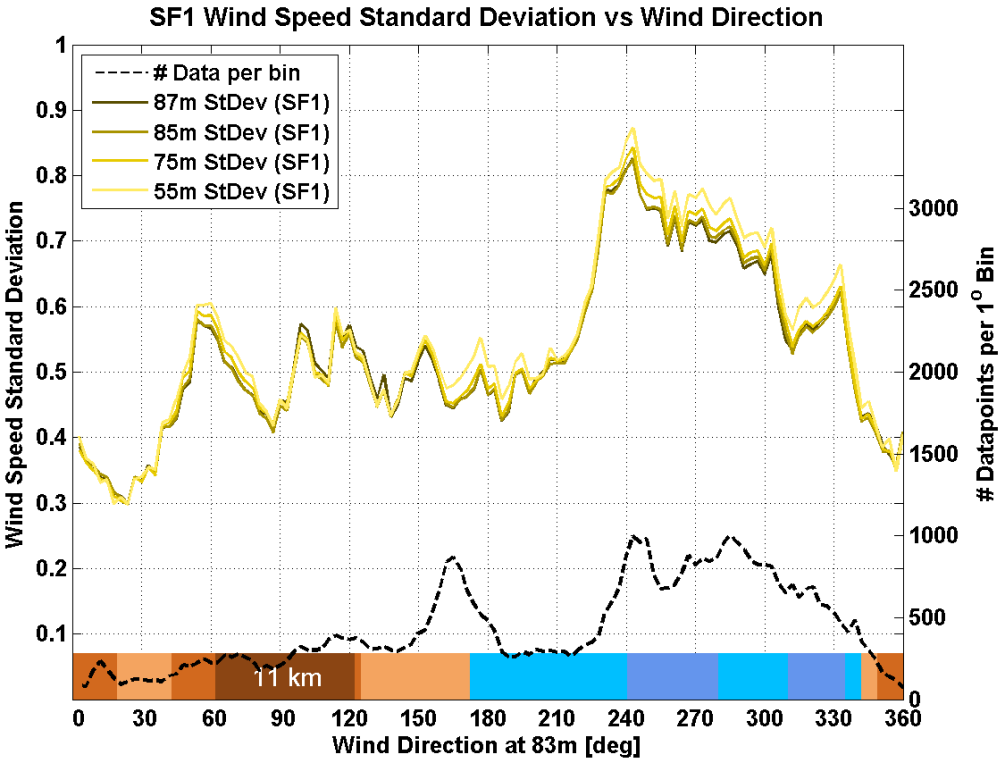
SF1 Wind Speed Standard Deviation vs Wind Direction
Data per bin
87m StDev (SF1)
85m StDev (SF1)
75m StDev (SF1)
55m StDev (SF1)
Wind Speed Standard Deviation
Datapoints per 1° Bin
11 km
Wind Direction at 83m [deg]

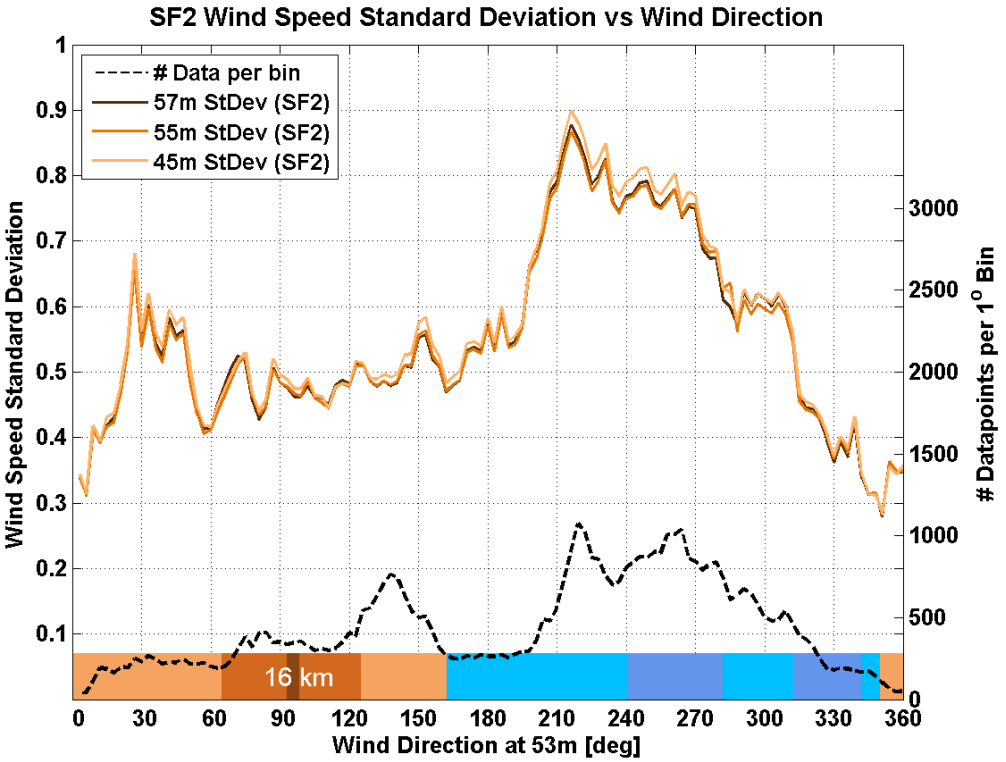
SF2 Wind Speed Standard Deviation vs Wind Direction
Data per bin
57m StDev (SF2)
55m StDev (SF2)
45m StDev (SF2)
Wind Speed Standard Deviation
Datapoints per 1° Bin
16 km
Wind Direction at 53m [deg]
0
30
60
90
120
150
180
210
240
270
300
330
360
0.1
0.2
0.3
0.4
0.5
0.6
0.7
0.8
0.9
1
500
1000
1500
2000
2500
3000

Appendix I

Polar Plots of Turbulence Intensity

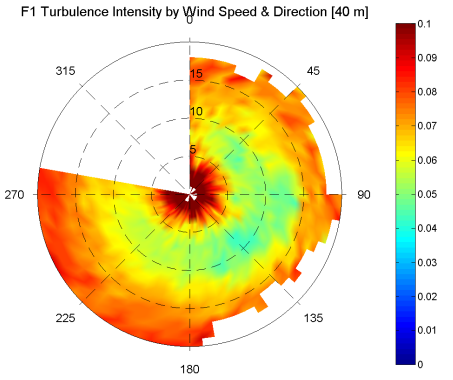

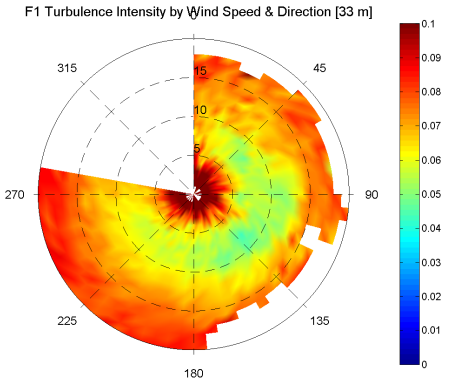

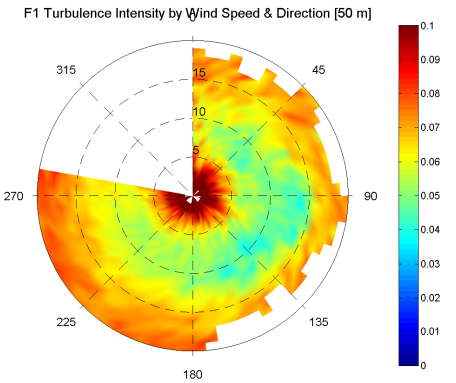

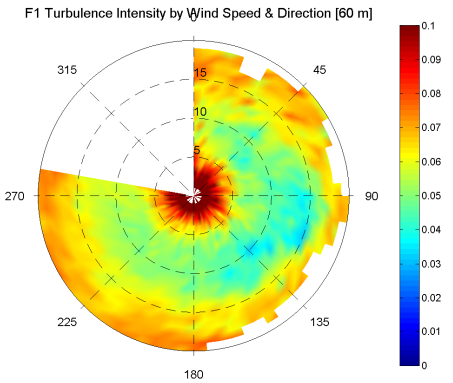

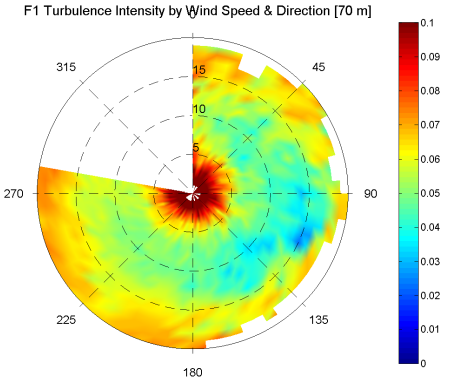
F1 Turbulence Intensity by Wind Speed & Direction [70 m]
0
45
90
135
180
225
270
315
5
10
15
0.1
0.09
0.08
0.07
0.06
0.05
0.04
0.03
0.02
0.01
0

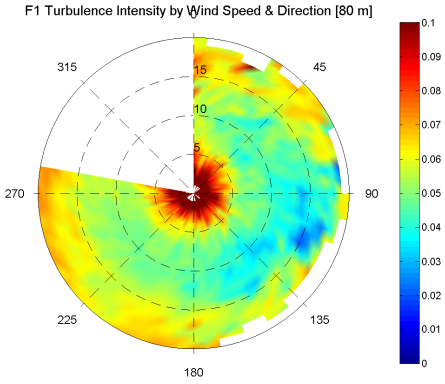
F1 Turbulence Intensity by Wind Speed & Direction [80 m]
0
45
90
135
180
225
270
315
5
10
15
0.1
0.09
0.08
0.07
0.06
0.05
0.04
0.03
0.02
0.01
0

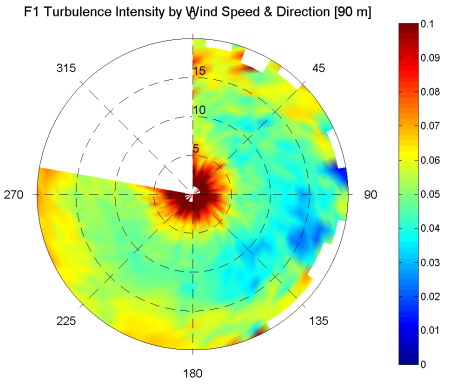
F1 Turbulence Intensity by Wind Speed & Direction [90 m]
0
45
90
135
180
225
270
315
5
10
15
0.1
0.09
0.08
0.07
0.06
0.05
0.04
0.03
0.02
0.01
0

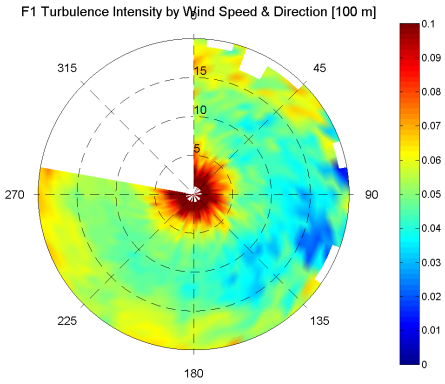
F1 Turbulence Intensity by Wind Speed & Direction [100 m]
0
45
90
135
180
225
270
315
5
10
15
0.1
0.09
0.08
0.07
0.06
0.05
0.04
0.03
0.02
0.01
0

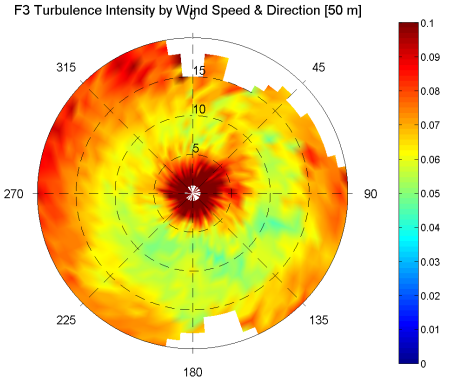
F3 Turbulence Intensity by Wind Speed & Direction [50 m]
0
45
90
135
180
225
270
315
5
10
15
0.1
0.09
0.08
0.07
0.06
0.05
0.04
0.03
0.02
0.01
0

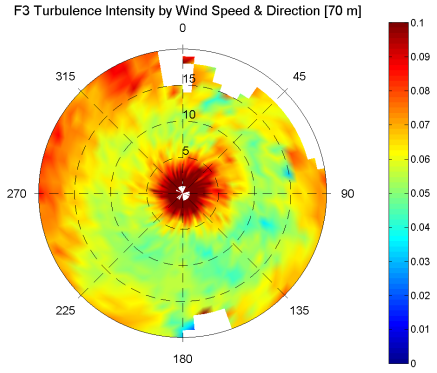
F3 Turbulence Intensity by Wind Speed & Direction [70 m]
0
45
90
135
180
225
270
315
5
10
15
0.1
0.09
0.08
0.07
0.06
0.05
0.04
0.03
0.02
0.01
0

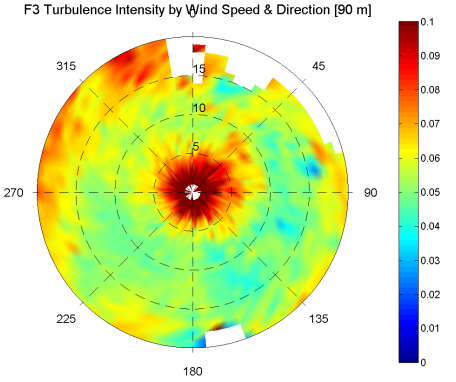
F3 Turbulence Intensity by Wind Speed & Direction [90 m]
0
45
90
135
180
225
270
315
5
10
15
0.1
0.09
0.08
0.07
0.06
0.05
0.04
0.03
0.02
0.01
0

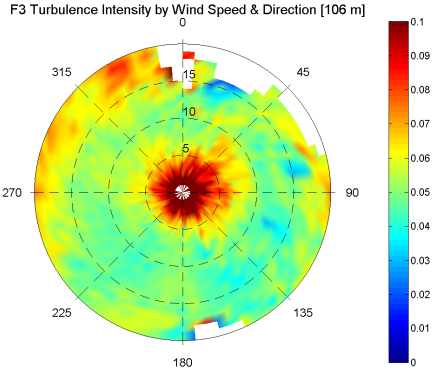
F3 Turbulence Intensity by Wind Speed & Direction [106 m]
0
45
90
135
180
225
270
315
5
10
15
0.1
0.09
0.08
0.07
0.06
0.05
0.04
0.03
0.02
0.01
0

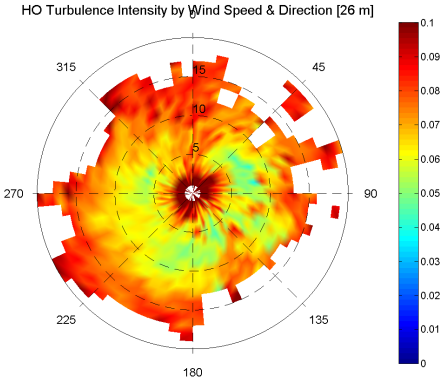
HO Turbulence Intensity by Wind Speed & Direction [26 m]
0
45
90
135
180
225
270
315
5
10
15
0.1
0.09
0.08
0.07
0.06
0.05
0.04
0.03
0.02
0.01
0

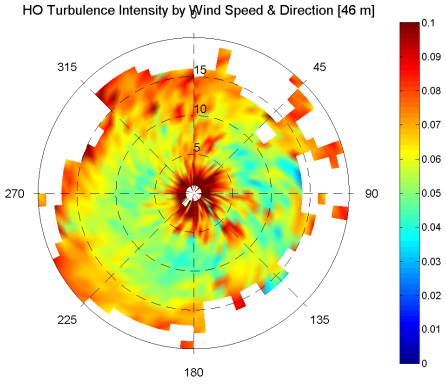
HO Turbulence Intensity by Wind Speed & Direction [46 m]
0
45
90
135
180
225
270
315
5
10
15
0.1
0.09
0.08
0.07
0.06
0.05
0.04
0.03
0.02
0.01
0

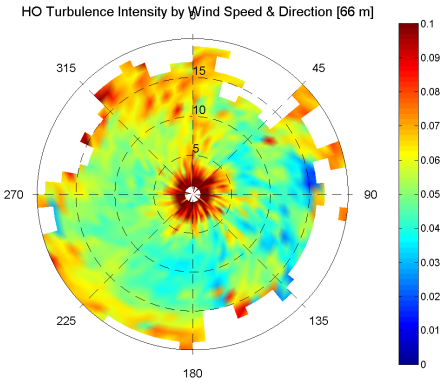
HO Turbulence Intensity by Wind Speed & Direction [66 m]
0
45
90
135
180
225
270
315
5
10
15
0.1
0.09
0.08
0.07
0.06
0.05
0.04
0.03
0.02
0.01
0

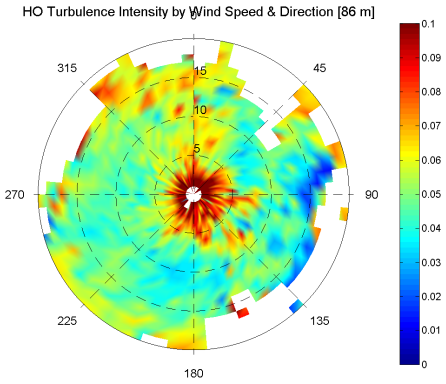
HO Turbulence Intensity by Wind Speed & Direction [86 m]
0
45
90
135
180
225
270
315
5
10
15
0.1
0.09
0.08
0.07
0.06
0.05
0.04
0.03
0.02
0.01
0

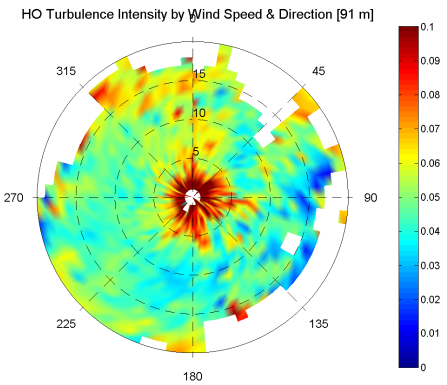
HO Turbulence Intensity by Wind Speed & Direction [91 m]
0
45
90
135
180
225
270
315
5
10
15
0.1
0.09
0.08
0.07
0.06
0.05
0.04
0.03
0.02
0.01
0

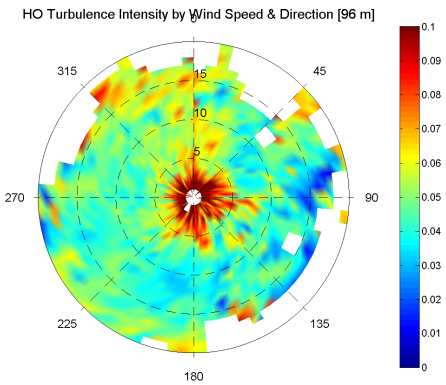
HO Turbulence Intensity by Wind Speed & Direction [96 m]
0
45
90
135
180
225
270
315
5
10
15
0.1
0.09
0.08
0.07
0.06
0.05
0.04
0.03
0.02
0.01
0

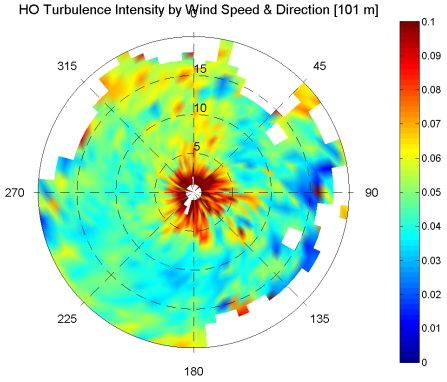
HO Turbulence Intensity by Wind Speed & Direction [101 m]
0
45
90
135
180
225
270
315
5
10
15
0.1
0.09
0.08
0.07
0.06
0.05
0.04
0.03
0.02
0.01
0

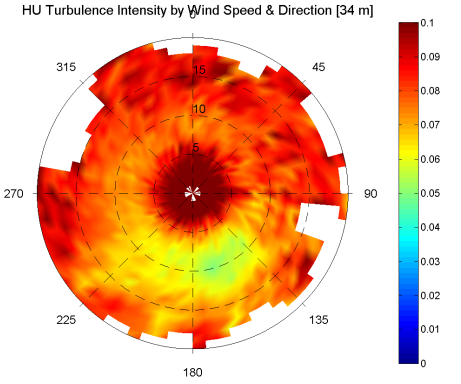
HU Turbulence Intensity by Wind Speed & Direction [34 m]
0
45
90
135
180
225
270
315
5
10
15
0.1
0.09
0.08
0.07
0.06
0.05
0.04
0.03
0.02
0.01
0

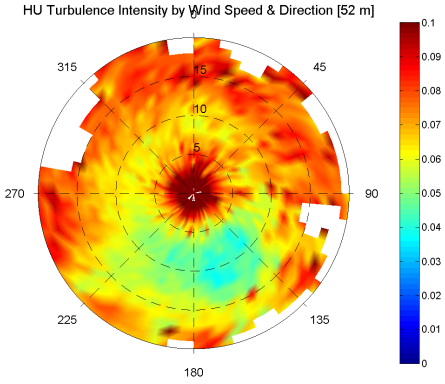
HU Turbulence Intensity by Wind Speed & Direction [52 m]
0
45
90
135
180
225
270
315
5
10
15
0.1
0.09
0.08
0.07
0.06
0.05
0.04
0.03
0.02
0.01
0

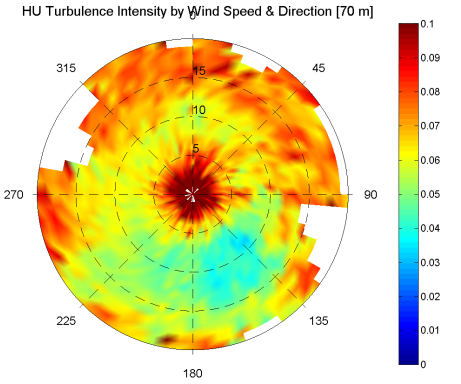
HU Turbulence Intensity by Wind Speed & Direction [70 m]
0
45
90
135
180
225
270
315
5
10
15
0.1
0.09
0.08
0.07
0.06
0.05
0.04
0.03
0.02
0.01
0

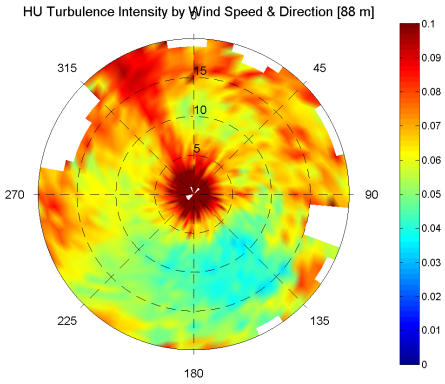
HU Turbulence Intensity by Wind Speed & Direction [88 m]
0
45
90
135
180
225
270
315
5
10
15
0.1
0.09
0.08
0.07
0.06
0.05
0.04
0.03
0.02
0.01
0

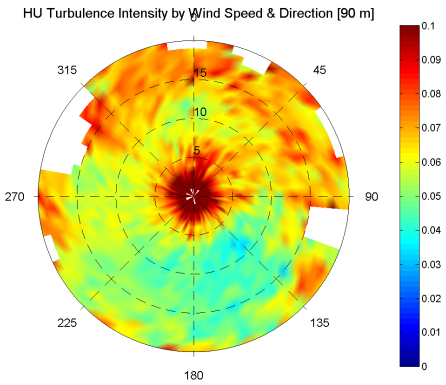
HU Turbulence Intensity by Wind Speed & Direction [90 m]
0
45
90
135
180
225
270
315
5
10
15
0.1
0.09
0.08
0.07
0.06
0.05
0.04
0.03
0.02
0.01
0

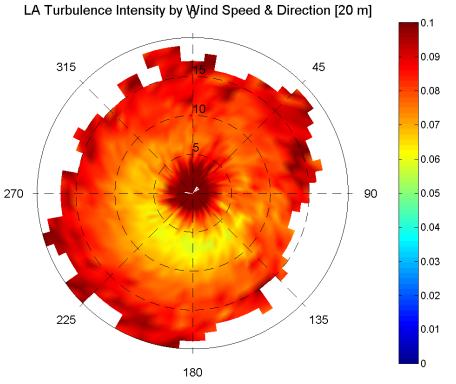
LA Turbulence Intensity by Wind Speed & Direction [20 m]
315
45
270
90
225
135
180
15
10
5
0.1
0.09
0.08
0.07
0.06
0.05
0.04
0.03
0.02
0.01
0

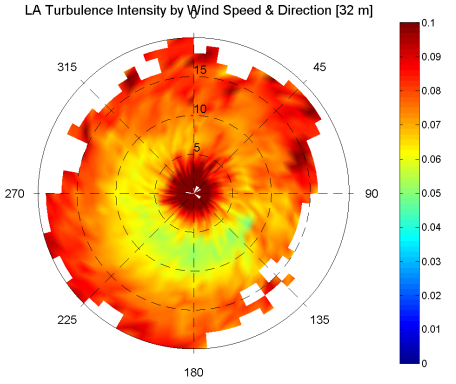
LA Turbulence Intensity by Wind Speed & Direction [32 m]
315
45
270
90
225
135
180
15
10
5
0.1
0.09
0.08
0.07
0.06
0.05
0.04
0.03
0.02
0.01
0

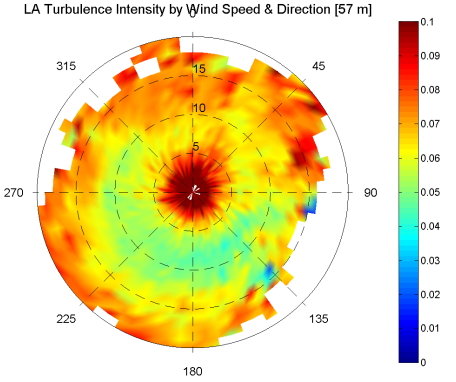
LA Turbulence Intensity by Wind Speed & Direction [57 m]
315
45
270
90
225
135
180
15
10
5
0.1
0.09
0.08
0.07
0.06
0.05
0.04
0.03
0.02
0.01
0

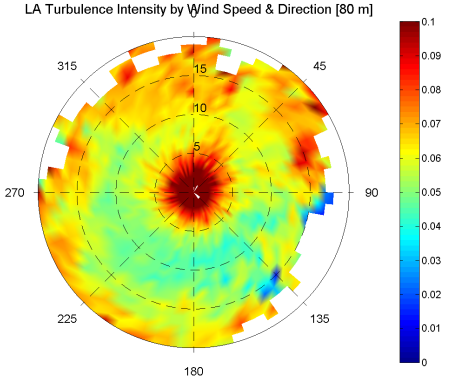
LA Turbulence Intensity by Wind Speed & Direction [80 m]
315
45
270
90
225
135
180
15
10
5
0.1
0.09
0.08
0.07
0.06
0.05
0.04
0.03
0.02
0.01
0

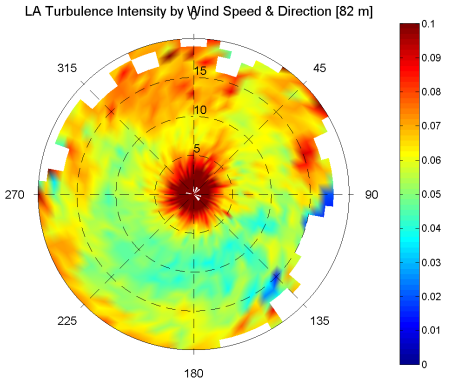
LA Turbulence Intensity by Wind Speed & Direction [82 m]
315
45
270
90
225
135
180
15
10
5
0.1
0.09
0.08
0.07
0.06
0.05
0.04
0.03
0.02
0.01
0

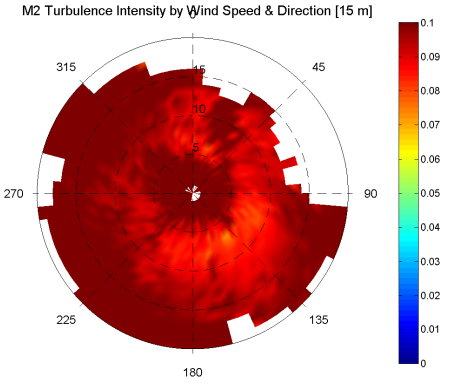
M2 Turbulence Intensity by Wind Speed & Direction [15 m]
0
45
90
135
180
225
270
315
5
10
15
0.1
0.09
0.08
0.07
0.06
0.05
0.04
0.03
0.02
0.01
0

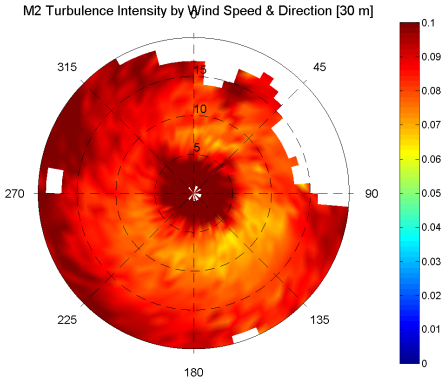
M2 Turbulence Intensity by Wind Speed & Direction [30 m]
0
45
90
135
180
225
270
315
5
10
15
0.1
0.09
0.08
0.07
0.06
0.05
0.04
0.03
0.02
0.01
0

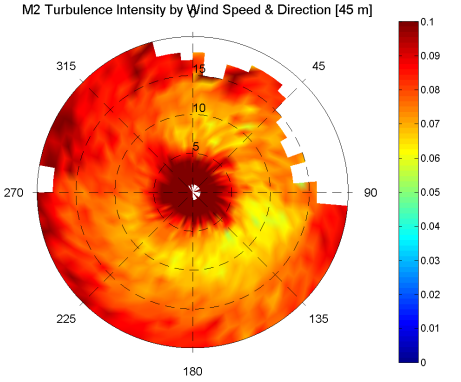
M2 Turbulence Intensity by Wind Speed & Direction [45 m]
0
45
90
135
180
225
270
315
5
10
15
0.1
0.09
0.08
0.07
0.06
0.05
0.04
0.03
0.02
0.01
0

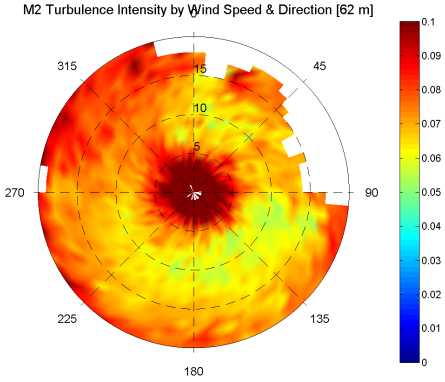
M2 Turbulence Intensity by Wind Speed & Direction [62 m]
0
45
90
135
180
225
270
315
5
10
15
0.1
0.09
0.08
0.07
0.06
0.05
0.04
0.03
0.02
0.01
0

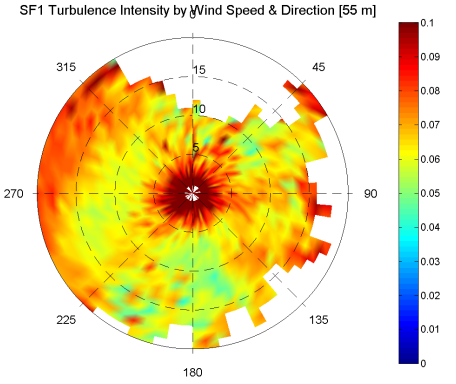
SF1 Turbulence Intensity by Wind Speed & Direction [55 m]
0
45
90
135
180
225
270
315
5
10
15
0.1
0.09
0.08
0.07
0.06
0.05
0.04
0.03
0.02
0.01
0

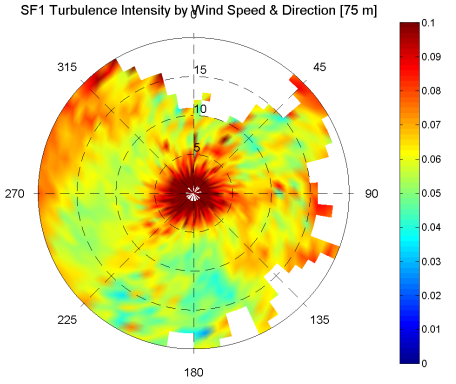
SF1 Turbulence Intensity by Wind Speed & Direction [75 m]
0
45
90
135
180
225
270
315
5
10
15
0.1
0.09
0.08
0.07
0.06
0.05
0.04
0.03
0.02
0.01
0

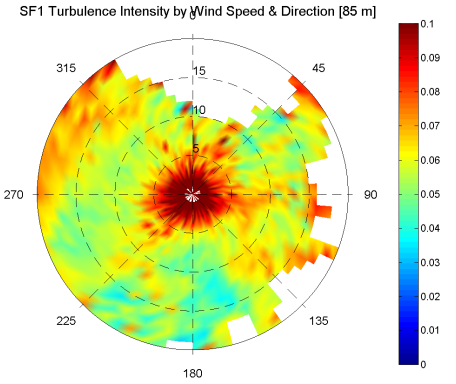
SF1 Turbulence Intensity by Wind Speed & Direction [85 m]
0
45
90
135
180
225
270
315
5
10
15
0.1
0.09
0.08
0.07
0.06
0.05
0.04
0.03
0.02
0.01
0

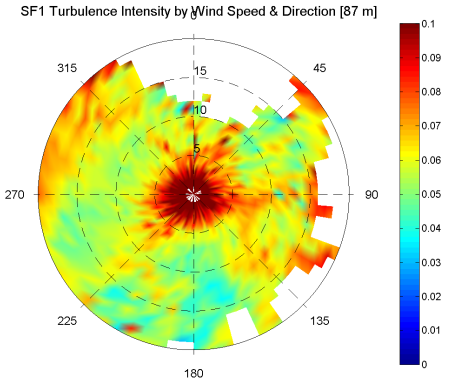
SF1 Turbulence Intensity by Wind Speed & Direction [87 m]
0
45
90
135
180
225
270
315
5
10
15
0.1
0.09
0.08
0.07
0.06
0.05
0.04
0.03
0.02
0.01
0

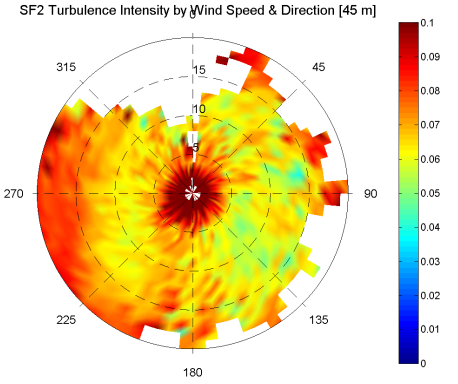
SF2 Turbulence Intensity by Wind Speed & Direction [45 m]
0
45
90
135
180
225
270
315
5
10
15
0.1
0.09
0.08
0.07
0.06
0.05
0.04
0.03
0.02
0.01
0

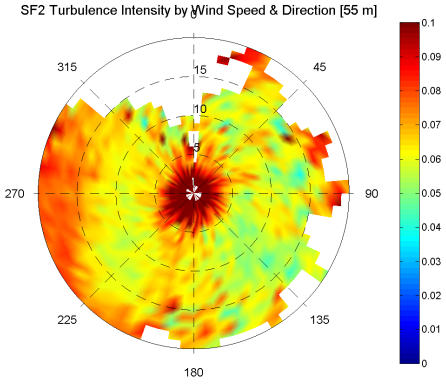
SF2 Turbulence Intensity by Wind Speed & Direction [55 m]
0
45
90
135
180
225
270
315
5
10
15
0.1
0.09
0.08
0.07
0.06
0.05
0.04
0.03
0.02
0.01
0

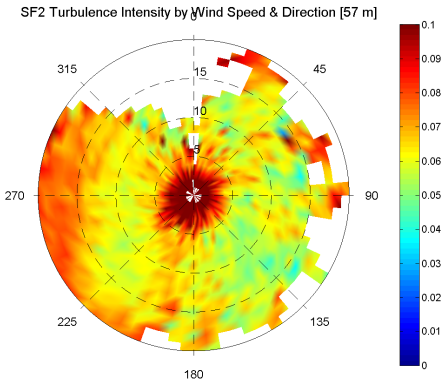
SF2 Turbulence Intensity by Wind Speed & Direction [57 m]
0
45
90
135
180
225
270
315
5
10
15
0.1
0.09
0.08
0.07
0.06
0.05
0.04
0.03
0.02
0.01
0